

SMC Bulletin

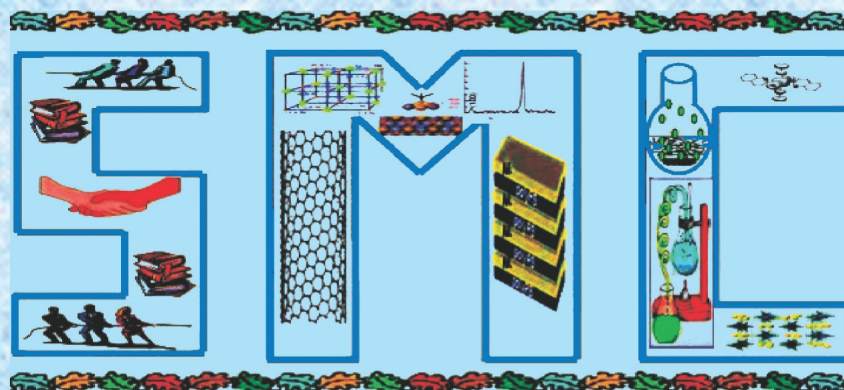
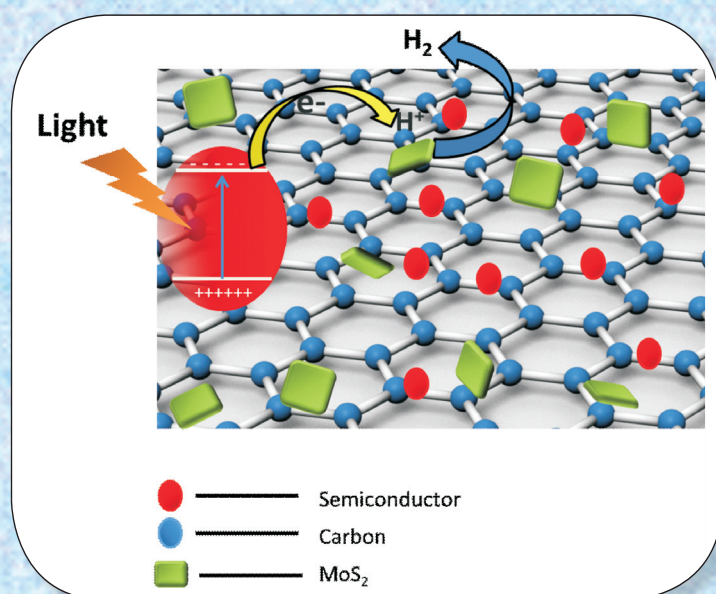
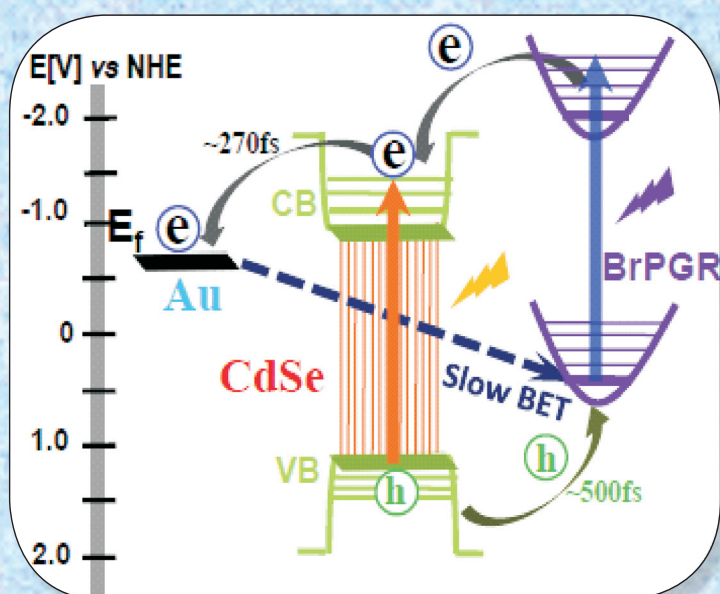
ISSN 2394-5087

A Publication of the Society for Materials Chemistry

Volume 6

No. 3

December 2015



SOCIETY FOR MATERIALS CHEMISTRY

Society for Materials Chemistry

Society for Materials Chemistry was mooted in 2007 with following aims and objectives:

- (a) to help the advancement, dissemination and application of the knowledge in the field of materials chemistry,
- (b) to promote active interaction among all material scientists, bodies, institutions and industries interested in achieving the advancement, dissemination and application of the knowledge of materials chemistry,
- (c) to disseminate information in the field of materials chemistry by publication of bulletins, reports, newsletters, journals.
- (d) to provide a common platform to young researchers and active scientists by arranging seminars, lectures, workshops, conferences on current research topics in the area of materials chemistry,
- (e) to provide financial and other assistance to needy deserving researchers for participation to present their work in symposia, conference, etc.
- (f) to provide an incentive by way of cash awards to researchers for best thesis, best paper published in journal/national/international conferences for the advancement of materials chemistry,
- (g) to undertake and execute all other acts as mentioned in the constitution of SMC.

Executive Committee

President

Dr. S. K. Sarkar
Bhabha Atomic Research Centre
Trombay, Mumbai, 400 085
sarkarsk@barc.gov.in

Vice-Presidents

Dr. V. K. Jain
Bhabha Atomic Research Centre
Trombay, Mumbai, 400 085
jainvk@barc.gov.in

Prof. Sandeep Verma

Indian Institute of Technology
Kanpur
sverma@iitk.ac.in

Secretary

Dr. P. A. Hassan
Bhabha Atomic Research Centre
Trombay, Mumbai, 400 085
hassan@barc.gov.in

Treasurer

Dr. Sandeep Nigam
Bhabha Atomic Research Centre
Trombay, Mumbai, 400 085
snigam@barc.gov.in

Members

Dr. K. Ananthasivan
Indira Gandhi Centre for Atomic Research
Kalpakkam, 603102

Dr. (Smt.) A. Banerjee
Bhabha Atomic Research Centre
Trombay, Mumbai-400085

Dr. K. Bhattacharyya
Bhabha Atomic Research Centre
Trombay, Mumbai-400085

Dr. D. Das
Bhabha Atomic Research Centre
Trombay, Mumbai-400085

Dr. G. K. Dey
Bhabha Atomic Research Centre
Trombay, Mumbai-400085

Dr. P. Sujata Devi
CSIR Central Glass & Ceramic Research
Institute, Kolkata-700032

Dr. C. P. Kaushik
Bhabha Atomic Research Centre
Trombay, Mumbai-400085

Dr. T. Mukherjee
Bhabha Atomic Research Centre
Trombay, Mumbai-400085

Dr. M. C. Rath
Bhabha Atomic Research Centre
Trombay, Mumbai-400085

Dr. (Smt.) S. S. Rayalu

CSIR National Environmental
Engineering Research Institute, Nagapur

Prof. S. D. Samant

Institute of Chemical Technology
Mumbai

Dr. A. K. Tyagi

Bhabha Atomic Research Centre
Trombay, Mumbai-400085

Dr. R. K. Vatsa

Bhabha Atomic Research Centre
Trombay, Mumbai-400085

Co-opted Members

Prof. A. Ajayaghosh
CSIR - National Institute for
Interdisciplinary Science and Technology
Thiruvananthapuram

Prof. A. K. Ganguli

Director, Institute for Nanoscience and
Technology

Prof. S. Ram

Indian Institute of Technology - Kharagpur

Dr. A. K. Tripathi

Bhabha Atomic Research Centre
Trombay, Mumbai-400085

Contact address

Society for Materials Chemistry

C/o Chemistry Division

Bhabha Atomic Research Centre, Trombay, Mumbai, 400 085, India

Tel: +91-22-25592001, E-mail: socmatchem@gmail.com

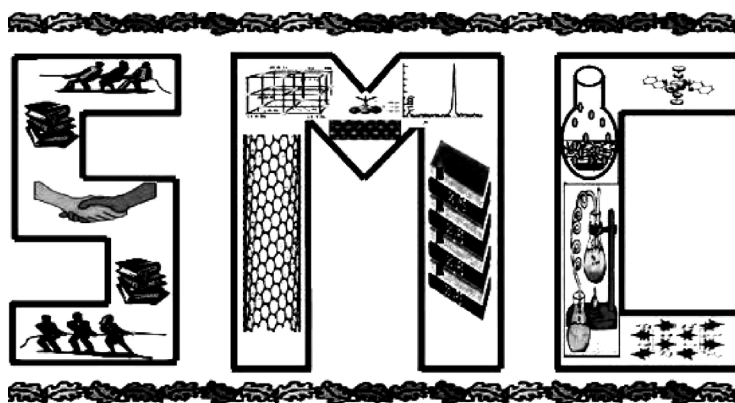
SMC Bulletin

A Publication of the Society for Materials Chemistry

Volume 6

No. 3

December 2015



SOCIETY FOR MATERIALS CHEMISTRY

SMC Bulletin

Vol. 6

No. 3

December 2015

Guest Editors

Dr. Kaustava Bhattacharyya
Chemistry Division,
Bhabha Atomic Research Centre
Trombay, Mumbai-400085
Email: kaustava@barc.gov.in

Dr. Atindra Mohan Banerjee
Chemistry Division,
Bhabha Atomic Research Centre
Trombay, Mumbai-400085
Email: atinmb@barc.gov.in

Editorial Board

Dr. Arvind Kumar Tripathi Chemistry Division, Bhabha Atomic Research Centre, Trombay, Mumbai 400085 e-mail: catal@barc.gov.in	Dr. Shyamal Bharadwaj Chemistry Division Bhabha Atomic Research Centre, Trombay, Mumbai 400085 e-mail: shyamla@barc.gov.in
Dr. Manidipa Basu Chemistry Division, Bhabha Atomic Research Centre, Trombay, Mumbai 400085 e-mail: deepa@barc.gov.in	Dr. Aparna Banerjee Product Development Division Bhabha Atomic Research Centre, Trombay, Mumbai 400085 e-mail: aparnab@barc.gov.in
Dr. Sandeep Nigam Chemistry Division, Bhabha Atomic Research Centre, Trombay, Mumbai 400085 e-mail: snigam@barc.gov.in	

About the Cover page graphic

Front cover shows schematic diagram of the electron hole transfer processes in CdSe(Au)/Br-PGR tri-composite along with H₂ generation in graphene - semiconductor - MoS₂ ternary nano composite.

Published by

Society for Materials Chemistry
C/o. Chemistry Division
Bhabha Atomic Research Centre, Trombay, Mumbai, 400 085
E-mail: socmatchem@gmail.com,
Tel: +91-22-25592001

Please note that the authors of the paper are alone responsible for the technical contents of papers and references cited therein

Guest Editorial



Kaustava Bhattacharyya



Atindra Mohan Banerjee

It has given us immense pleasure to be associated with this special issue of SMC bulletin on “Energy Materials”. Research on Energy Materials is a topic of enormous importance in the present energy scenario as future energy systems must provide a secure, sustainable, and environmentally acceptable energy supply. The need for sustainable and environment friendly clean energy system arises primarily due to two reasons. Firstly, in future the world will be facing a decline in production of conventional oil due to its limited resources, even though there will be a spurt in demand and secondly the serious Greenhouse Gas Emission (GHG) emissions accompanying their combustion. Thus, there is a growing scientific interest on investigations of alternate energy sources viz. solar energy, wind energy, nuclear energy, bioenergy as generation of power from these sources involve low carbon dioxide emissions and provide sustainable energy solutions.

In the current SMC bulletin we present contributions of studies on materials used in various forms of energy harvesting, conversion and storage. Topics ranging from material research on solar cells, bioenergy, Li-air batteries, photocatalytic and thermochemical hydrogen generation and thermoelectrics are included.

The editors sincerely thank all authors from different institutes for sharing their knowledge, expertise and scientific data in form of contributed articles in the present form. The articles will be beneficial to all those who are interested in materials solutions to the energy problem.



From the desks of the President and Secretary



Dr. Sisir K Sarkar
President



Dr. P. A. Hassan
Secretary

Dear Fellow members and Readers,
Greetings from the Executive Council of SMC.

At the outset wish you all a Happy & Prosperous New Year - 2016.

Looking back at the activities in 2015, we had a very successful meeting NWMC-2015 (OPT - MAT) to celebrate the International Year of Light (IYL 2015) during November 20-21, 2015. We organized a lecture under SMC Lecture series by Prof. Dr. Rainer Niewa, Institute for Inorganic Chemistry, University of Stuttgart, Germany titled "Chemistry of Ammonothermal Crystal Growth of Nitride Semiconductor Materials" on 7th November. We have published two theme based issues of SMC Bulletin on "High Purity Materials" and "Optical Materials". The present issue, the final one this year is based on the theme "Energy Materials", considering the thirst for new and innovative materials that can harness available energy sources.

As the worldwide debate continues, it is evident that managing energy use wisely in the 21st century will call for balancing three essential, but quite different, concerns: Resources, Responsibility and Security. Eventually we must devise ways to keep resources and consumption in sustainable equilibrium. The combustion of fossil fuels releases carbon dioxide into the atmosphere, and most climate scientists believe that the build-up of those gases is the primary cause of global warming in recent decades. Responsible stewardship of our planet demands that we find new ways to minimize or eliminate those effects.

Meeting all three of these energy concerns will be a long-term process with unknown outcomes. There is growing technical and financial interest in renewable and sustainable sources - such as advanced nuclear power, wind power, solar power, and certain biofuels - and in technologies that minimize carbon dioxide emissions and capture the gases in storage areas where they cannot reach the atmosphere. Much of the worldwide demand will be in developing nations - most notably China and India, which between them contain more than one-third of the planet's population - creating unprecedented competition for limited conventional resources.

Energy from renewable sources and solar power are some of the alternative sources that could meet the increased energy demands. If one can find materials that can efficiently harvest even one percent of the solar radiation falling on the planet earth will be sufficient to meet all our current and future demands. Developing different approaches and materials in harnessing solar power such as semiconducting materials, thin films, dye sensitized solar photovoltaics, quantum dots, solar hydrogen production etc remain an active area of research. Microbial fuel cells that can produce electrical energy through anaerobic oxidation of renewable organic matter provide an attractive route.

Development of efficient energy storage systems and materials for rechargeable batteries are also of great relevance in terms of energy materials. Mimicking the natural photosynthesis process by artificial molecular systems or nanostructured materials and photocatalytic production of hydrogen from water splitting are being explored as future sources. The list is long and is not possible to cover all of them in a single issue of the bulletin. Finally, we believe no one can afford to remain uninformed about the energy future because we all have a stake in its outcome.

Our Guest Editors, Dr. Kaustav Bhattacharya and Dr. Atindra Banerjee have taken keen interest to bring out articles that span some of the relevant areas. We put on record our sincere thanks and appreciation to the Guest Editors as well as the contributing authors for the timely publication of the issue. We express our gratitude to each and every members of SMC for their unstinted support and cooperation in the growth of the Society. Happy reading !!!

Dr. Sisir K Sarkar
President

Dr. P. A. Hassan
Secretary

CONTENTS

Sr No	Feature Article	Page No.
1	Bioenergy: A Review of Microbial Fuel Cells and the Nisargruna Biogas Technology <i>Reemadevi Singh, S. B. Ghosh and S. P. Kale</i>	1
2	Critical Challenges for Li-air Technology <i>Jishnu Bhattacharya</i>	8
3	Plasmon Induced Enhancement of Charge Separation in Epitaxial Metal- Semiconductor Nanohybrid Material Anchored with an Organic Molecule <i>Jayanta Dana and Hirendra N. Ghosh</i>	14
4	Artificial Photosynthesis Using Graphene-Based Nanomaterials <i>Suneel Kumar, Vipul Sharma, Venkata Krishnan</i>	20
5	Effect of Aliovalent Chlorine Doping on the Thermoelectric Properties of n-type $\text{AgBi}_{0.5}\text{Sb}_{0.5}\text{Se}_2$ <i>Satya N. Guin, Sohang Kundu and Kanishka Biswas</i>	30
6	Pt/Carbon Catalysts with Varying Porosity for Hydrogen Generation Reaction by HI Decomposition Reaction of S-I Thermochemical Cycle <i>Deepak Tyagi, Salil Varma, Shyamala R. Bharadwaj</i>	37



Bioenergy: A Review of Microbial Fuel Cells and the Nisargruna Biogas Technology

Reemadevi Singh, S. B. Ghosh* and S. P. Kale

Nuclear Agriculture & Biotechnology Division, Bhabha Atomic Research Centre, Trombay, Mumbai-400085.

Email: sbghosh@barc.gov.in

Introduction

The demand for energy, especially for liquid fuels is ever increasing. Exponentially increasing use of fossil fuel to meet this demand has undeniably damaged the world environment to a large extent. The need of the hour is to produce energy from renewable resources without a net carbon dioxide emission (Lovely, 2006, Davis and Higson, 2007). The advancements in the field of bioenergy i.e. renewable energy harnessed from biological sources, have great potential to provide relief to this energy conundrum. One such advancement is microbial fuel cells (MFCs) that convert the energy stored in chemical bonds in organic compounds to electrical energy. This is achieved through the catalytic reactions by microorganisms. Another important possibility is to convert organic compounds, including regular nutrient molecules like carbohydrate, proteins and fat to methane by anaerobic electron transport chain. Methane is a highly combustible molecule and can be considered a green energy when it is produced in a carbon neutral manner.

History of Microbial Fuel Cell

The concept of Microbial Fuel Cell (MFC) is derived from the natural process of cellular respiration. Cellular respiration is a collection of metabolic reactions, resulting in an overall exothermic redox reaction, which cells use to convert nutrients into common energy currency i.e. adenosine triphosphate (ATP) that fuels further cellular activity. All nutrient molecules (carbohydrates, proteins and lipids) while undergoing catabolic reactions, give rise to NADH as the major "energy" molecule along with small molecules including CO₂. Such catabolic processes mostly happen in the cytoplasm of all living cells. The NADH thus generated can donate its proton to a membrane bound proton acceptor which in turn can donate the newly acquired proton to the next member in a series of proton acceptor-donor combination spanning the width of the membrane. As a result of this downhill journey of the proton along an energy gradient the proton is released to the other side of the membrane creating a proton gradient across the membrane. When proton starts leaking from the proton rich side of the membrane to the proton deficient side through a proton pump, ATP is synthesized as ATP-synthase enzyme forms a part of the proton pump (Fig.1a).

The earliest instance of demonstration of the MFC concept was by M. C. Potter, botany professor at the University of Durham, in 1910 (Ieropoulos, 2005). He generated electrical energy from living cultures of *Escherichia coli* and *Saccharomyces* by using platinum electrodes (Potter, 1912). This work didn't receive much attention until it was discovered that mediators can be used to greatly enhance power output.

A classical MFC in general (Du et al. 2007) consist of an anodic and cathodic chamber divided by a proton (cation) selective membrane (Fig.1b). Microbes in the anodic compartment forms a biofilm on the surface of the electrode generating protons and electrons as the organic substrate is converted into energy. Microbes use and store this energy for their growth. While the electrons are transported from the anode to the cathode through an external circuit (wire) resulting measurable electric current, protons pass through the membrane, enter the cathode compartment and combine with oxygen to form water (Logan et al. 2006). A one compartment MFC eliminates the need for the cathodic chamber by exposing the cathode directly to the air. A typical two-compartment MFC has an anodic chamber and a cathodic chamber connected by a PEM (Proton exchange membrane), or sometimes a salt bridge, to allow protons to move across to the cathode while blocking the diffusion of oxygen in to the anode (Du et al. 2007).

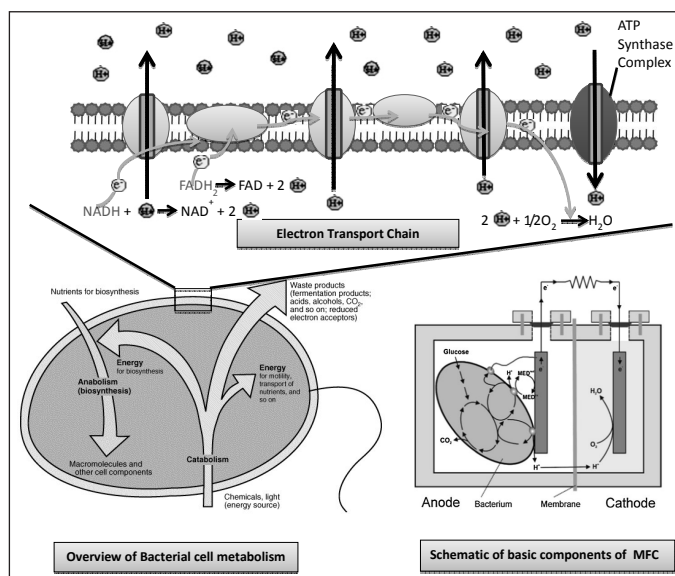


Fig. 1a

Fig.1b

The basic underlying challenge is to collect the electrons as the bacteria respire in the anodic chamber. Transferring electrons directly to the anode is not possible unless the species are anodophilic. Majority of the microbes have non-conductive lipid membranes, with peptidoglycans and lipopolysaccharides that hinder the direct transfer of electrons to the anode. Electron mediators accelerate the transfer of electrons from bacterial membrane to the anode (Davis and Higson, 2007). Instead of oxygen, an inorganic mediator functions as the terminal electron acceptor in the microbial electron transport chain. The mediator crosses the microbial membrane, captures electrons and exits the membrane in a reduced "electron-full" state. These electrons are released to the anode and the mediator becomes oxidized again in the bulk solution in the anodic chamber. Therefore good mediators should be able to grab electrons from the electron carriers of the electron transport chains, cross the cell membrane easily and deposit the electron to the anode (Ieropolus et al, 2005). It should also possess a high electrode reaction rate and have a good solubility in the anolyte without being toxic to the microbes. Some of the exogenous synthetic mediators that have been tried by researchers are dyes and metallorganics such as methylene blue (MB), neutral red (NR), thionine, meldola's blue (MelB), 2-hydroxy-1,4 -naphthoquinone (HNQ), Fe(III)EDTA and methyl violagen (Park and Zeikus, 2000; Tokuji and Kenji, 2003; Veag and Fernandez, 1987; Allen and Bennetto, 1993; Ieropolus et al., 2005). However these compounds are toxic and unstable during a prolonged period of usage, making their applications in MFCs limited. Some microbes can use naturally occurring compounds as mediators, such as microbial metabolites, called endogenous mediators. Endogenous mediators like humic acid, anthraquinone and the oxyanions of sulphur have the ability to transfer electrons from inside the cell membrane to the anode.

Exoelectrogens in Microbial Fuel Cells

Research by B. M. Kim et al in 1999, and Chaudhari and Lovely in 2003 provided a major breakthrough in the field in the form of mediator less MFCs. Such MFCs use exoelectrogens i.e. microbes that can transfer electrons directly to the anode. Exoelectrogens form a biofilm on the anode surface and transfer electrons directly by conductance through the membrane. *Shewanella putrefaciens* (Kim et al., 2002), *Geobacteraceae sulfurreducens* (Bond and Lovely, 2003), *Geobacter metallireducens* (Min et al., 2005) and *Rhodospirillum rubrum* (Chaudhari and Lovely, 2003) are some of the exoelectrogens used in the manner described above. In case of such anodic exoelectrogens, the final electron acceptors can be strong oxidizing agents in aqueous solutions or solid conductors. Two commonly

used acceptors are iron compounds (Fe(III) oxides) and manganese compounds (Mn(III/IV) oxides) (Hartshore R. et al., 2009; Baron D., 2009; Shi L. et al., 2006). Biofilms can also form on the cathode surface, affecting electron transfer between microbes and electrodes. For *Thiobacillus ferrooxidans* suspended in a catholyte in an MFC system that contains microbes in both anodic and cathodic chambers, the cathode serves as electron donor to the bacteria in cathode chamber. *G. metallireducens* and *G. sulfurreducens* (Gregory et al., 2004) or certain seawater biofilms (Bergel et al., 2005) can act as final electron acceptors by grabbing electrons from cathode. Mediator-less MFCs are advantageous in wastewater treatment and power generation since technologically it is easier to operate and the cost of mediators is eliminated. (Ieropolus et al., 2005). Marine sediment, soil, wastewater, freshwater sediment and activated sludge are rich sources for exoelectrogens (Niessen et al., 2006, Zhang et al., 2006).

The exact process in which cells reduce extracellular acceptors varies among exoelectrogens. However, research has shown the involvement of an oxidoreductase pathway that transports electrons to the surface of the cell membrane exposed to the external environment (Hartshore R. et al., 2009). The pathway splits off from the ETC pathway after Complex III (cytochrome bc₁ complex) is oxidized by c-type cytochromes, which moves electron towards the extracellular face located in outermost membrane. This is in contrast to typical ETC pathway, in which it moves towards Complex IV (cytochrome c oxidase). Examples of such c-type cytochromes are MtrC and OmcA which are found in the outer membrane of proteobacterium *Shewanella oniedensis* MR-1 (Hartshore R. et al., 2009; Baron D., 2009; Shi L. et al., 2006; Flynn J. et al., 2010; Lovely D., 2008).

MFC as Bio hydrogen producer

In the present day context of global warming and green house effect of many industrial emissions including emissions from thermal power stations, hydrogen is considered the cleanest fuel possible. While burning in air it combines with oxygen and produces water and energy without any emission. Calorific value of hydrogen (approx 28000 KCal/Kg) is much higher than common fuel gasses e.g 12000 KCal/Kg of Methane or 11000 KCal/Kg of LPG. While electricity cannot be stored effectively for a long time, hydrogen can be stored for a long time and can be transported through pipeline over a long distance. Because of these properties hydrogen is being considered as the fuel of future. MFCs can be modified to produce hydrogen instead of electricity. In a typical MFC, protons generated by the anodic reaction, travel towards the cathode to combine

with oxygen to form water. As an alternative concept, the migrated protons in the cathodic chamber may combine with electrons reaching the cathode and thereby produce Hydrogen. However, hydrogen generation from the protons and the electrons produced by the metabolism of microbes in an MFC is thermodynamically unfavorable. To overcome this thermodynamic barrier an external potential can be applied to increase the cathode potential in an MFC circuit enabling hydrogen production (Liu et al. 2005). In this mode, protons and electrons produced by the anodic reaction are combined at the cathode to form hydrogen. The required external potential for an MFC is theoretically 110mV, much lower than the 1210mV required for direct electrolysis of water at neutral pH because some energy comes from the biomass oxidation process in the anodic chamber. MFCs can potentially produce about 8-9mol H₂/mol glucose compared to the typical 4mol H₂/mol glucose achieved in conventional fermentation (Liu et al.,2005). In bio hydrogen production using MFCs, oxygen is no longer needed in the cathodic chamber. Since oxygen leak to the anodic chamber is not a concern, H₂ generation using MFC is more efficient.

MFC for waste water treatment

Municipal wastewater contains a multitude of organic compounds that can be used as fuel for MFCs. (Habermann and Pommer,1991). The amount of power generated by MFCs in the wastewater treatment process can reduce the electricity needed to halve in a conventional treatment process that consumes a lot of electric power while aerating activated sludges (Holzman, 2005). Furthermore, organic molecules such as acetate, propionate, butyrate can be thoroughly broken down to CO₂ and H₂O. A consortium can provide great result as it will be able to degrade variety of organics. MFCs using certain microbes have a special ability to remove sulfides as required in waste water treatment (Rabaey et al., 2006). Continuous flow, single compartment membrane-less MFCs are favored for waste water treatment due to ease in scale-up in such architecture compared to two compartment batch process (Jang et al., 2004; Moon et al., 2005; He et al., 2005). Sanitary wastes, food processing wastewater, swine wastewater and corn stover are all great biomass sources for MFCs because they are rich in organic matters (Suzuki et al.,1978; Liu et al.,2004; Oh and Logan, 2005; Minetal., 2005; Zuoetal.,2006).

Use of MFC in Biogas plant

Biogas plant

The anaerobic fermentation of biomass in the presence of water produces Biogas. It is a mixture of methane (CH₄), carbon dioxide (CO₂), hydrogen (H₂) and hydrogen

sulphide (H₂S). The chief constituent of biogas is methane and the content varies from 50% to 80% depending on the feed and technology used for biogas generation. While initiating a biogas plant cattle dung is mixed with an equal quantity of water to form slurry. This slurry is then fed into the digester through an inlet chamber. When the digester is more than half but less than three fourth filled, the introduction of slurry is stopped and the plant is left undisturbed for about two months. This is the way a conventional biogas plant is initiated and anaerobic culture is developed in situ. During the first couple of weeks of this period the anaerobic bacteria present in the cattle dung multiplies and establishes itself in the main digester chamber. Subsequently it decomposes or ferments the biomass in the presence of water. As a result of anaerobic fermentation, biogas is formed, which starts accumulating in the dome of the digester. As more and more biogas starts collecting, the pressure exerted by the biogas forces the spent slurry into the outlet chamber. This pressure induced slurry movement is facilitated by gravitational gradient or level difference between the inlet and out outlet of the main digester. From the outlet chamber, the spent slurry overflows into a series of manure tanks depending on the usage pattern of the spent slurry. The spent slurry can be manually removed from the manure tank and used directly as manure for crop plants or can be allowed to dry in a series of manure pits for a future use. The gas valve connected to a system of pipelines is opened when a supply of biogas is required. After the initial establishment of anaerobic culture, to obtain a continuous supply of biogas, a functioning plant can be fed continuously with the prepared slurry. The maximum amount of cattle manure that can be fed into the system is a function of the volume of the main digester.

Various examples of MFCs powered by waste used in biogas plant

Cow dung, rice washing water, drain water and slurry can be used in microbial fuel cells to generate electricity (Pranav K Barua., 2010). Wang et al (2009) used domestic waste water of concentration of 600mg/L for his two chambered mediator less MFC having graphite electrodes. The device generated a current density of 0.06 mW/cm². Oh and Logan (2005) used food processing waste water for a two chamber MFC, having graphite electrode and generated a current density of 0.05 mW/cm². Lee et al. (2011) made two different MFCs to treat solid waste that includes cow manure and was run in the batch mode. One was of single compartment type and other one of twin compartment type. They produced electricity at rates of 9.2 and 24.3 mW/kg of dry manure in single compartment

type and twin compartment type respectively. Electrodes used had 20% platinum catalyst and Nafion 117 was used as proton exchange membrane.

It can be concluded that from a biogas plant of higher capacity, sufficient amount of electricity can be generated which can be used for various small domestic needs. With modification in the electrode design and the biogas plant design, there is a good prospect of tapping unconventional energy source from biogas plant. By including certain natural organic waste in the slurry of biogas plant, there is possibility of enhancing the voltage output, which would add to the economy of biogas plant and increase the fertilizer property of exhaust slurry. Studies of the anode bio-film community composition of MFC would throw the door open for exploration of efficient way of harvesting electrical energy from the biogas plant as a new method for renewable and sustainable energy production. The waste generated from MFC can further be processed to produce manure and white coal. (Dinesh P. J., Alam J. 2013)

Nisargruna Biogas technology

Nisargruna, a Sanskrit word, which literally means 'the loan of Nature' is a solid waste management technology developed at Bhabha Atomic Research Centre, Mumbai, India for treating all sorts of biodegradable wastes including kitchen wastes. As opposed to a single anaerobic digester based conventional biogas plant, primarily meant for cattle dung as described above, Nisargruna introduced many concepts and differentiating factors that made this biogas technology universally amenable to all biodegradable wastes. It has two digesters - an aerobic digester is followed by an anaerobic digester. The aerobic digestion is carried out by a group of thermophilic bacteria and it is enabled by hot water addition using a solar water heater. It also has a provision for water recycling. Effluent water can be reused for waste processing (Shubhada N., Ph.D. thesis 2008).

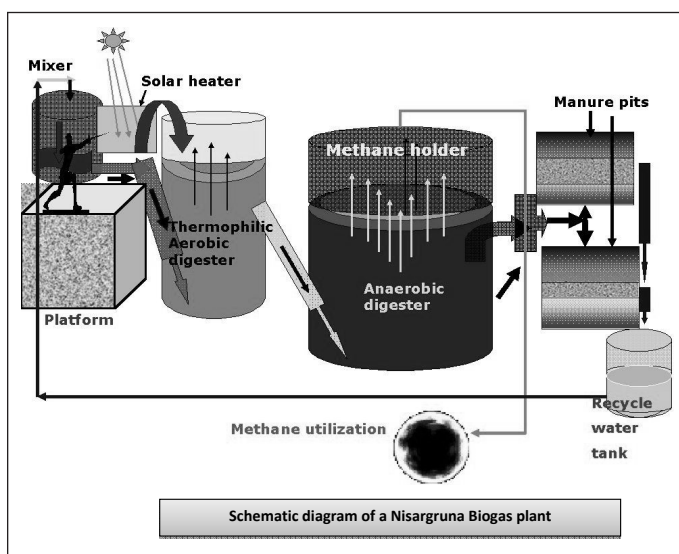
In *Nisargruna* biogas process the waste is first homogenized in an industrial mixer grinder by addition of water at 1:2 ratio w/w. Manual separation of impurities like glass, metals and plastics is done prior to grinding of waste. Homogenization reduces the particle size of material and thus facilitates degradation by bacteria. The slurry is then passed on to the aerobic pre-digester tank. Hot water at 65 °C heated using solar energy, is added in the ratio 1:2 to enable thermophilic predigestion and also to obtain optimum dilution and flow ability of the slurry and hence achieve easy operation. Wastes with small particle size and high moisture content are best suited for fermentation.

Conventional anaerobic digestion process takes place in three steps. In the first step hydrolysis and acidification takes place. During this step, biopolymers that are mostly water-insoluble, such as carbohydrates, proteins and lipids are decomposed by extracellular enzymes produced by the microorganisms to water soluble monomers [e.g. monosaccharides, amino acids, glycerol, fatty acids etc.] and thus made accessible to further degradation. The products of hydrolysis are converted into mixture of volatile fatty acids like acetic acid, formic acid, butyric acid and propionic acid, alcohols, hydrogen and carbon dioxide. In the second step acetogenesis occurs. In this process the anaerobic acetogenic bacteria convert the volatile fatty acids other than acetic acid and alcohol into acetic acid, hydrogen and carbon dioxide. In the final degradation step or methanogenesis, methanogenic bacteria utilize acetic acid, formic acid, CO₂ and H₂ to produce methane rich biogas.

The above three steps in conversion of biodegradable organic material to CH₄ and CO₂ are facilitated by three major groups of bacteria. The first group is of the fermentative bacteria which break down the complex biopolymers into respective soluble monomers through hydrolysis by extracellular enzymes. The hydrolyzed products are subsequently fermented intracellularly to short-chain fatty acids like- acetic acid, formic acid, propionic acid and butyric acid. Other products of the fermentation process are alcohols, CO₂ and H₂. Hydrolysis of carbohydrates is predominantly done by genera like *Bacteroides*, *Butyrivibrio*, *Ruminococcus*, *Acetivibrio* *Clostridium* and *Fibrobacter*. Hydrolysis of lipids is carried out more efficiently by *Clostridium* species & *Micrococcu*. While organisms belonging to the genera *Bacteroides*, *Butyrivibrio*, *Clostridium*, *Fusobacterium*, *Selenomonas*, and *Streptococcus* in the consortium improves proteins hydrolysis. The second group of bacteria is the acetogenic bacteria. The short-chain fatty acids that are longer than acetate are oxidized by the hydrogen producing acetogenic bacteria to H₂, acetic acid and CO₂. This acetogenesis and dehydrogenation is performed by *Syntrophobacter wolinii*, a propionate decomposer *Syntrophomonas wolfei*, a butyrate decomposer *Clostridium formicoaceticum*, *Acetobacterium woodii* and *Acetivibrio cellulolyticus*. (Shubhada N., Ph.D. thesis 2008) The third and last group consist of, the methanogenic bacteria. The end products from the fermenting and the acetogenic bacteria (formic acid, acetic acid, CO₂ and H₂) are converted to CH₄ and CO₂ by the methane-producing bacteria commonly known as methanogens. The methanogens belong to a large and diverse group who are the members of domain- Archaeobacteria. They are strict anaerobes requiring redox potential less than -330mV and form large

quantities of methane as the major product of their energy metabolism. Methanogens are commonly found in anoxic environments like-sediments of ponds, lakes, rivers and sea, geothermal springs, marshy swamps, intestinal tracts of animals, landfills, dental caries and sub gingival plaques and anaerobic digesters, where electron acceptors such as O_2 , NO_3^- , Fe^{3+} , and SO_4^{2-} are limiting.

In *Nisargruna* biogas plant, first step of hydrolysis and acidification is carried out in aerobic predigester, where the optimum preferred temperature is in the range of 40°C to 45°C. The predigester has two compartments- predigester 1 and 2 separated by a baffle wall at the centre. The raw slurry first comes to predigester 1 and then flows to predigester 2. After 72-96 hours in predigester, the pH of the slurry falls down to 4. The slurry then passes into anaerobic digester where the step two and three of the degradation process take place in the absence of oxygen.



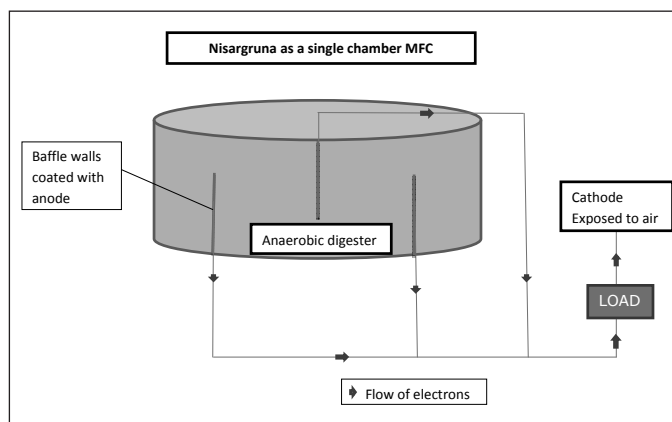
The output of the process is methane-rich biogas and chemically stabilized manure. The methane content can vary from 60-80%, remaining being CO_2 and moisture. This biogas can be directly used as fuel to substitute any conventional hydrocarbon or can be fed to a generator to produce electricity. Because of aerobic predigestion, most of the sulphur content in the waste material gets converted to SO_2 and escapes in the atmosphere. This results in negligible H_2S content in the produced biogas and this feature of *Nisargruna* is extremely useful for converting biogas to electricity using a generator. A single online scrubber is sufficient to take care of this negligible H_2S . After dewatering, and air-drying, the manure can be used as an excellent soil conditioner. The wastewater generated is recirculated into the pretreatment unit to adjust the

water content or can also be used directly to farmland as a liquid fertilizer.

A *Nisargruna* biogas plant that can process 1 metric ton biodegradable waste daily, can produce 60 to 80 M^3 methane rich biogas and 80-100 kg manure every day. This amount of biogas can replace 1.5-2 domestic LPG cylinders. Due to incorporation of aerobic predigestion prior to anaerobic one, the hydraulic retention time has been brought down to 16-18 days as compared to 30 - 40 days in single phase conventional anaerobic digestion.

Nisargruna Biogas plant as an MFC

In *Nisargruna* biogas technology, the predigester serves mainly as hydrolysis cum acidification tank for the treatment of suspended solids. The second or the main digester serves as a methane fermentation tank. The feed that enters the predigester is hydrolyzed under aerobic condition and this results in the formation of organic acids which then enters into the main digester. The first part of the main digester that receives slurry from the predigester, is microaerophilic in nature while the rest of the digester is totally anaerobic. This microaerophilic zone contains those bacteria that thrive on the mixtures of organic acids and provide the substrates (H_2 , CO_2 , acetic acid) for the methanogens to form methane under strict anaerobic condition. *Nisargruna* plant can be modeled to function as an MFC by collecting the electrons generated during acetogenesis and methanogenesis phase. The anaerobic chamber is divided into four compartments by three baffle walls. These walls can be covered with electrode material to capture electrons during anaerobic fermentation. There are various options for anode electrode materials like plain carbon cloth, multiwall carbon nanotubes, a graphite fiber brush. (Cheng et al., 2006) It could be designed as a one chamber MFC where cathode is exposed to air. For two chamber MFC, hydrogen ions need to be collected for completing the MFC circuit. *Nisargruna* plant in future could also be used to produce bio hydrogen, this could be






done by incorporating system that can capture hydrogen ions.

Acknowledgement:

Ms Aditi Ghosh, project trainee in the laboratory and B.Tech (Comp.Sc) student at BITS Pilani, Hyderabad campus actively participated in the manuscript preparation.

References:

1. R.M. Allen, H.P. Bennetto, *Biotechnol.*, 1993, **39-40**, 27.
2. D. Baron, E. LaBelle, D. Coursolle, J. A. Gralnick, D. R. Bond, *J. Biol. Chem.*, 2009, **284**, 28865.
3. A. Bergel, D. Feron, A. Mollica, *Electrochem. Commun.*, 2005, **7**, 900.
4. D. R. Bond, D. R. Lovley, *Appl. Environ. Microbiol.*, 2003, **69**, 1548.
5. S. K. Chaudhuri, D. R. Lovley, *Nat. Biotechnol.*, 2003, **21**, 1229.
6. S. Cheng, H. Liu, B. E. Logan, *Environ. Sci. Technol.*, 2006, **40**, 2426.
7. F. Davis, S. P. J. Higson, *Biosens. Bioelectron.*, 2007, **22**, 1224.
8. P. J. Dinesh, J. Alam, *Int. J. Scientiresear. pub.*, 2013, **8**, 2250.
9. Z. Du, H. Li, Z. Gu, *Biotechnol. Advns.*, 2007, **25**, 464.
10. J. M. Flynn, D. E. Ross, K. A. Hunt, *M. Bio.*, 2010, **5**, 00190.
11. K. B. Gregory, D. R. Bond, D. R. Lovley, *Environ. Microbiol.*, 2004, **6**, 596.
12. W. Habermann, E. H. Pommer, *Appl. Microbiol. Biotechnol.*, 1991, **35**, 128.
13. R. S Hartshorne, C. L. Reardon, D. Ross, J. Nuester, T. A. Clarke, A. J. Gates, *Proc. Natl. Acad. Sci. U.S.A.*, 2009, **106**, 22169.
14. Z. He, S. D. Minter, L. Angenent, *Environ. Sci. Technol.*, 2005, **39**, 5262.
15. D. C. Holzman, *Environ. Health. Persp.*, 2005, **113**, 754.
16. I. A. Ieropoulos, J. Greenman, C. Melhuish, *J. Hart, Enzym. Microb. Tech.*, 2005, **37**, 238.
17. J. K. Jang, T. H. Pham, I. S. Chang, K. H. Kang, H. Moon, K. S. Cho, *Process. Biochem.* 2004, **39**, 1007.
18. B. H. Kim, H. J. Kim, M. S. Hyun, D. H. Park, *J. Microbiol. Biotechnol.*, 1999, **9**, 127.
19. H. J. Kim, H. S. Park, M. S. Hyun, I. S. Chang, M. Kim, B. H. Kim, *Enzym. Microb. Tech.*, 2002, **30**, 145.
20. Y. Lee, *Bioresour. Technol.*, 2011, **102**, 5831.
21. H. Liu, S. Grot, B. E. Logan, *Environ. Sci. Technol.*, 2005, **39**, 4317.
22. B. E. Logan, *Appl. Microbiol. Biotechnol.*, 2005, **80**, 349.
23. B. E. Logan, B. Hamelers, R. Rozendal, U. Schroder, J. Keller, S. Freguia, *Environ. Sci. Technol.*, 2006, **40**, 5181.
24. D. R. Lovley, *Curr. Opin. Biotech.*, 2008, **6**, 564
25. D. R. Lovley, *Curr. Opin. Biotech.*, 2006, **17**, 327.
26. B. Min, S. Cheng, B. E. Logan, *Water Res.*, 2005, **39**, 1675.
27. H. Moon, I. S. Chang, J. K. Jang, B. H. Kim, *Biochem. Eng. J.*, 2005, **27**, 59.
28. J. Niessen, U. Schroder, M. Rosenbaum, F. Scholz, *Electrochem. Commun.*, 2004, **6**, 571.
29. S. E. Oh, B. E. Logan, *Water Res.*, 2005, **39**, 4673.
30. D. H. Park, J. G. Zeikus, *Appl. Environ. Microb.*, 2000, **66**, 1292.
31. M. C. Potter, *Proc. R. Soc. Ser. B.*, 1912, **84**, 260.
32. K. Rabaey, K. Van De Sompel, L. Maignien, N. Boon, P. Aelterman, P. Clauwaert, *Environ. Sci. Technol.*, 2006, **40**, 5218.
33. L. Shi, B. Chen, Z. Wang, D. A. Elias, M. U. Mayer, Y. A. Gorby, *J. Bacteriol.*, 2006, **188**, 4705.
34. S. Nayak. Ph.D. thesis submitted to the University of Mumbai 2008
35. I. Tokuji, K. Kenji, *Biochim. Biophys. Acta.*, 2003, **1647**, 121.
36. C. A. Vega, I. Fernandez, *Bioelectrochem. Bioenerg.*, 1987, **17**, 217.
37. X. Wang et al., *Electrochem. Acta.*, 2009, **54**, 1109.
38. E. Zhang, W. Xu, G. Diao, C. Shuang, *J. Power Sources*, 2006, **161**, 820.

	<p>Dr. S.P. Kale Associate Director of Bioscience group and Head of Nuclear Agriculture & Biotechnology Division, Food Technology Division has been honoured with the Padma Shri Award by the Government of India on January 26, 2013 in the Discipline of Science and Engineering. He has developed the NISARGRUNA biogas technology for solid biodegradable waste resource management. This is a combination of aerobic and anaerobic processes for faster and better degradation of biodegradable waste resulting in methane enriched biogas and organic manure generation. He has been propagating the NISARGRUNA biogas concept for solid biodegradable waste resource management at various levels in the country. So far 160 Nisargruna projects have been installed all over the country. These plants are based on kitchen, market, poultry, dairy and abattoir biodegradable waste resources. His fields of interest include: Marine pollution, Agriculture Biotechnology, Computer applications, Bioenergy, production of metallic nanoparticles through biological route and creating Public awareness regarding sustainable environment.</p>
	<p>Dr. S. B. Ghosh did his Masters in Biotechnology from JNU, Delhi in the year 1994 and joined 38th batch of biology-radiobiology training school. He obtained his Ph.D. from Botany Dept of University of Mumbai for his work on coat protein gene mediated transgenic virus resistance against PVY. He worked as a visiting fellow at National Institute of Health, Bethesda, Maryland, USA from Sep, 2006 till Jan, 2009 in the area of Brd4 mediated transcription regulation in response to UV stress. Dr. Ghosh is currently involved in research on different aspects of Nisargruna biogas technology including the microbiology of Nisargruna. He is also actively involved in implementation of various Nisargruna projects all over the country.</p>
	<p>Reema Devi Singh Rajan Completed Masters in Biotechnology from M. S. University of Baroda in the year 2013. She joined as scientific officer C in BARC after completion of the one year OCES program from 57th training school batch of Biosciences in 2014. She is currently working in Nuclear agriculture and biotechnology division under Bioscience group. Her area of research includes methods to improve efficiency of Nisargruna Biogas plant, study of nutraceutical and biofuel potential of microalgae.</p>

Critical Challenges for Li-air Technology

Jishnu Bhattacharya

Mechanical Engineering Department, IIT Kanpur

Email: jishnu@iitk.ac.in

Context

Vehicles driven solely by the rechargeable batteries are on our roads. But statistically they are insignificant compared to the conventional cars driven by gasoline engines. While it is well known that the fleet of billion cars worldwide is causing irreversible damage to the environment and the gasoline-reserve is an unsustainable resource, battery cars are non-competitive simply because of being a high-cost technology. The immature technology of electric vehicles results in a high running cost and a shorter range for these vehicles. Batteries in the EVs (electric vehicle) play the role of the heart in the human body. The current state of the art for the energy-dense battery is the Li-ion battery which provides specific energy of ~160 Wh/kg compared to that of gasoline ~1700 Wh/kg (including tank to wheel efficiency).¹ The technology of Li-ion battery is now about four-decades old and all sorts of possibilities for improving its energy and power density are well explored. It is now well-accepted in the scientific community that in no wild stretch, Li-ion batteries can ever meet the requirement of making an electric vehicle competitive to the gasoline vehicles.

The concept of Li-air battery provides the crucial hope to the scientists that the electric vehicles can be made competitive in near future paving the path towards the green and sustainable world. It is estimated that Li-air batteries can provide very similar energy density to that

of gasoline.¹ The other essential criteria for EV propulsion battery are cost, driving range, cycle life and safety. All these aspects are yet unknown for this nascent technology. It is neither practical, nor fair to compare these secondary parameters for Li-air batteries to a century old (gasoline) or a few decades old (Li-ion) technology while Li-air batteries are still a concept that require many tests and modifications to get its matured shape. In the current article, we discuss the key challenges to the Li-air technology and the state of the art status of the individual components.

A schematic diagram of the Li-air battery is shown in Fig. 1. The anode is made of Li-metal. The cathode is separated from the anode through the electrolyte solution. The cathode is called 'air-cathode' because the reactant in the cathode reaction is oxygen from air. However to provide reaction interfaces between the lithium-ions in the electrolytes and the oxygen molecules in the air stream, a porous and non-reactive (in principle) structure is used. During discharge, Li metal at anode is consumed to produce Li⁺ ions and the resultant electron flows through the outer circuit to drive the electric vehicle. The Li⁺ ions move through the electrolyte to get recombined with the electron at the cathode through a reaction with the atmospheric O₂. The cathode reaction between the Li-ions, free electrons from the outer circuit and O₂ crucially depends on the composition of the electrolyte. When there is no water molecule present in the electrolyte and we assume the air to be dry, the following overall reaction is assumed to take place:



If water is present in the electrolyte, it participates in the cathode reaction and the following reaction takes place:



As the voltage, reversibility and products of the cathode reaction determine the performance parameters of the cell, the above two reactions lead to the major classification of the Li-air cell: non-aqueous (also called aprotic) and aqueous (protic). The aqueous or non-aqueous electrolytes in the Li-air cells show some unique and some common issues to tackle. We will discuss the challenges to make the above reactions produce sustainable power in the following sections.

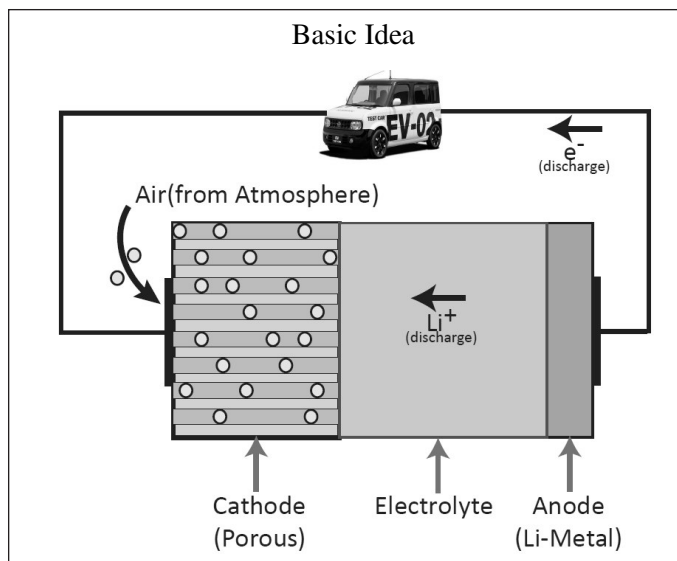


Fig. 1: A schematic diagram of Li-air battery.

Non-aqueous chemistry

Cathode

Understanding the cathode reaction

Cathode reaction is the most vital phenomenon in an electrochemical cell which dictates the cell voltage, capacity, rate capability and reversibility. In case of aprotic Li-air cell, this vital phenomenon is far from understood.

The reaction shown in eq. (1) is the proposed reaction for Li-air cells. The reversibility of this reaction is established through the success of the reverse reaction on charging.^{2,3} However, it is an open question whether lithium peroxide is the sole discharge product. Under slow enough discharge-rate, it has been shown that the Li_2O_2 is reduced further to form Li_2O , which increases the cathode capacity by a factor of 2 (twice as many Li ions consumed per O atom). This secondary reaction is not reversible though.⁴⁻⁷

There is a big voltage gap between the charge and discharge curve of a Li-air cell as shown in Fig. 2. The voltage gap indicates that the reactions on charging and discharging are not the same.

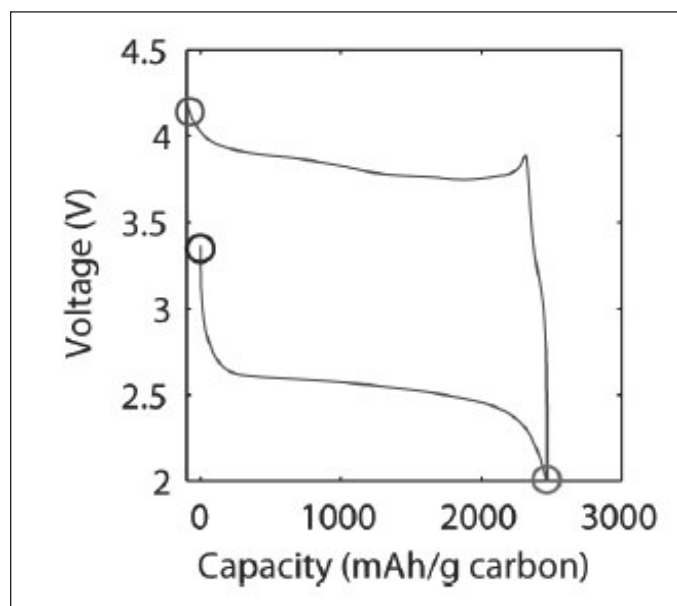


Fig. 2: Voltage gap during charging and discharging.⁸ Reproduced with permission from American Chemical Society.

The gap changes with different cathode catalysts. The electrolyte also plays a vital role in the cathode reaction. The organic carbonate electrolytes decompose on discharge^{9,10} which might lead to a separate cathode reaction on discharge. Hence the effects of catalysts and electrolytes on the cathode reaction need to be systematically analysed to identify the exact reactions that occur at cathode on

charge and discharge. The dependence of voltage on the catalysts^{11,12} also suggests that the chemical kinetics is a very important part of the understanding of the cathode. Understanding the cathode reactions in detail is the first and foremost area which needs to be resolved before the technology can progress further.

Finding suitable catalysts

Until 2010, catalysts for Li-air cell have been identified based upon the assumption that Li_2O_2 is the discharge product. However, Mizuno et al. showed that the discharge products of the carbonate based Li- O_2 battery are principally lithium carbonates. This shows that the catalysts developed for the decomposition of Li_2O_2 actually catalyse decomposition of the lithium carbonates. Porous carbon materials, transition metal oxides and both precious and non-precious metals were used as the electro-catalysts.¹³ The search for suitable catalysts for the Li_2O_2 -reduction reaction is an area of active research.

Protecting the cathode from the contaminants

The idea of Li-air cell for the application in EVs is so attractive because, it breathes air in and out during discharging and charging processes. The active cathode material is O_2 which needs not be to carried and hence the energy density of such cells are so high. However, the ambient air contains many other things along with oxygen. Ambient air will always contain certain degree of CO_2 and H_2O which leads to formation of Li_2CO_3 and LiOH at cathode. Both these products are insoluble (or have very low level of solubility in the electrolyte) making them get deposited on the porous cathode structure and blocking the air passage channels. Currently, the controlled experiments on Li-air cells assume the supply of pure and dry O_2 ^{14,15} which is a challenge in an actual cell. It is therefore important to use a O_2 -selective membrane which blocks the unwanted species from the ambient air. For separating out the O_2 , there might be several layers of membranes where different other contaminants are filtered. The multilayer porous membranes pose a hurdle for the continuous breathing of the cell especially at the higher rate.¹³

Maintaining cathode porosity and cell capacity

Not only the contaminants from air, but also the electrolyte composition (especially the organic carbonates) causes formation of insoluble products during the discharge reaction.

The insoluble discharge products clog the pores which hinders fresh O_2 coming into the cell. It has been shown that not all pores but the pores of the size 2-50 nm are the

effective pores which determine the capacity of the air-cathode. Ideally, the microstructure of the porous electrode should consist of large channels as major supply line for O_2 and mesoporous alleys of triple junctions of O_2 , electrolyte and carbon-substrate which acts as the reaction sites. Moreover the total weight and volume must be minimum so that the energy density is maximized. Currently several nano-scale structures and graphene based structures are being experimented with for the optimum cathode structure.¹⁶⁻¹⁸

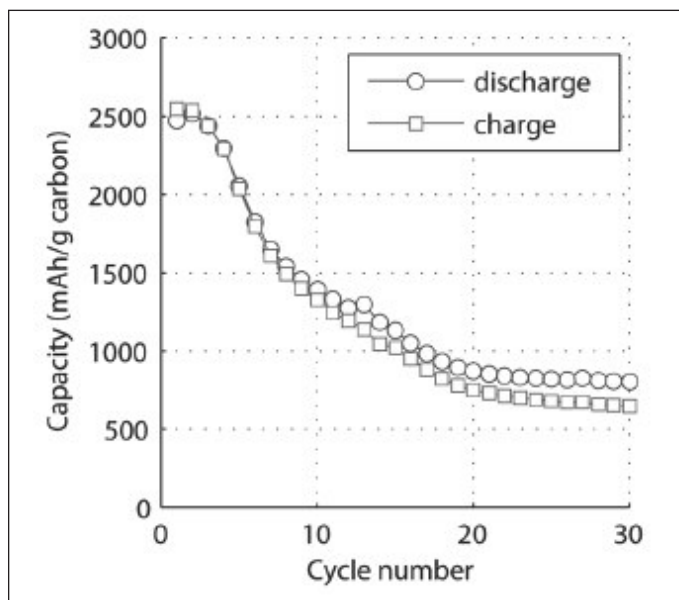


Fig. 3: Capacity loss with cycling. The Fig. is reproduced from ref. ⁸ with permission from American Chemical Society

Low cycle life of the current state of the art Li-air batteries is a major concern. The capacity drops very sharply within very few cycles as shown in Fig. 3. The reason behind the capacity loss can be multiple. One such reason is the loss of capacity of the cathode due to clogging of the pores. The irreversible side reactions also consume available lithium ions. The major discharge product, Li_2O_2 is a solid insulating material in bulk form. If the deposition happens as a film on the cathode surface, the product of the initial discharge process would hinder further reactions to proceed. Therefore it is important to control the microstructure of the discharge process.

Anode

Suppressing dendrite formation

It is well known that for any battery where lithium ions are the charge carriers, Li-metal anode would provide the maximum possible capacity as well as voltage. Therefore, when the concept of Li-air battery came into existence for the purpose of providing a major capacity leap required

for the EV application, the Li-metal anode was proposed along with it. However, Li-metal anodes form metallic dendrites on charging which may short-circuit the cell and hence pose a major safety hazard.^{19, 20}

The use of Li-metal as anode never succeeded for the Li-ion batteries for long-life batteries. Nonetheless, the discovery of solid lithium super-ionic conductors provides a strategy where we can use the mechanical strength of the solid electrolyte to stop the growth of the dendrites.²¹ There have been several efforts of using certain additives in the electrolytes to suppress the dendrite formations. However for Li-air batteries these additives and special electrolytes are not tested for their stability in an oxygen-rich environment. Special design of Li-metal anode with mechanical barriers and finding out suitable additives in the electrolyte are needed to make Li-metal to work as Li-air battery anodes for long cycle life.

Controlling SEI layer

Li-metal anodes show poor charge-discharge efficiency. The major reason behind it is the irreversible consumption of lithium in the SEI (solid-electrolyte interphase) layer that forms on the anode through various side reactions with the electrolyte.²² Lithium being a low potential electrode, the working potential of the cell allow many side reactions to happen while a higher potential anode (such as LTO)²³ suffers less from the formation of SEI layer. The SEI layer not only consumes lithium but also increases the impedance of the cell which causes further loss in coulombic efficiency. Therefore, controlling the growth of the SEI layer is key for successful use of Li-metal anode in a Li-air cell.

Minimizing excess Li

Due to irreversible consumption of Li-ions in both cathode and anode reactions, we need to use excess lithium in the anode to replenish the loss and keep the battery working for more number of cycles. The excess lithium causes big drop in capacity compared to the theoretical limit.¹¹ To harness the full potentiality of Li-air cell, the excess lithium has to be minimized which is indirectly linked with the progress in controlling the SEI layer and understanding the cathode reactions.

Electrolyte

Stabilizing the electrolyte

Electrolyte is the critical component of the Li-air batteries and poses significant challenges. An ideal electrolyte in any cell should be stable with the cathode and anode under different potentials. For a cell like Li-air which breathes air in each cycle of charge and discharge, the electrolyte needs to be non-evaporative as well. The

electrolyte in Li-air cell is required to be stable with respect to oxygen and the discharge products of the cathode reaction, i.e, lithium oxides. The surface of the porous cathode needs to be wet by the electrolyte to provide the triple junction of electrolyte, oxygen and cathode substrate. O₂ gas needs to be soluble in the electrolyte as well as easily diffusible to reach maximum reaction sites as the cathode substrate is flooded with the electrolyte. As in case of Li-ion cells, lithium ions should get transported very fast through the electrolyte to provide reasonable rate capability.

The obvious starting point for finding a suitable electrode is using the electrolytes for the Li-ion cells. Typically Li-ion electrolytes are based on organic carbonates which are susceptible to degradation on discharge of an Li-air cell as the major reaction at cathode becomes the formation of lithium carbonate.^{9, 10, 24} This continuous degradation of the electrolyte drastically reduces the cycle life of the cell. Ethers have been shown to be more stable with respect to the cathode and they show better cycling stability than the organic carbonates.^{25, 26} However they also show the sign of irreversible O₂ consumption leading to stability fading.²⁷

There have been few efforts in using solid electrolytes in the Li-air cells.²⁸⁻³¹ However, the solid electrolytes with fast ionic conduction for Li does not show fast transport for O₂ as well and it is always difficult to have enough solid-solid-gas triple junction in a all solid state lithium-air cell. The solid electrolytes also makes to difficult to adjust the volume change in individual components during charge and discharge. However, because of their higher stability, solid electrolytes can potentially provide significant improvement in the performance of the Li-air cells with proper material engineering.

Among all the issues discussed for the non-aqueous Li-air batteries, finding the optimum electrolyte material is the key for the progress of the technology and deserves the highest attention.

Aqueous chemistry

Many issues for the aqueous Li-air cells are common to what we have already discussed in case of aqueous cells. In this section, we will mention the challenges which are unique to the aqueous cells.

Cathode

Understanding the cathode reaction

Like aprotic cells, the gap between charging and discharging voltage exists in case of the protic cells which indicates that not one single reversible reaction (as in eq. 2) can explain cathode phenomena. Understanding the

cathode reaction and the chemical kinetics associated with it is essential.

Unlike the aprotic cell, the discharge reaction requires breaking of the O-O bond for the O₂ reduction into LiOH.¹¹ This makes the cathode reaction dependent on the catalysts.³²⁻³⁶ The catalysts developed for breaking O-O bonds in other reactions need to be tested for the cycle life in the aqueous Li-air cells.

Anode

Protecting from water

Lithium metal reacts vigorously with water. In current state, the Li metal anode is protected by a LISICON-type glass ceramic as shown by Visco et al.³⁷ Without this protection the lithium anode cannot work in aqueous cells. However, the glass ceramic and Li-metal are not stable with each other and some Li⁺-permeable membrane needs to be used between them. The LISICON-aqueous electrolyte suffers from degradation in acidic and basic condition. The lithium-LISICON combination for anode has not been tested for extensive cycling behaviour. The addition of multiple protection layers adds to the weight and volume of the cell decreasing the energy density. Therefore, effective protection for the lithium anode needs further attention.

Improving rate capability

The overall rate capability of the aqueous (as well as non aqueous) Li-air cells are very poor.¹³ The rate limiting reaction is not yet known. However, it is often conjectured that the anode reaction in these cells are slow and it leads to poor overall rate capability. For EV application, it is essential to improve the rate capability as not the energy density only, but the power density also which is crucial for such application.

Electrolyte

Handling insolubility of discharge product

In case of aqueous Li-air cells, the electrolyte actively participates in the cathode reaction. The chief discharge product is LiOH which has very low solubility limit in the electrolyte. The saturation happens corresponding to a capacity equivalent to a Li-ion cell^{11, 38} defeating the purpose of building a Li-air cell. Further progress of the cathode reaction leads to precipitation of the LiOH. The solid LiOH can block both anode and cathode surfaces to stop further reaction. One alternative approach is to employ a flow-cell design where electrolyte is continuously replenished to avoid the solubility limit is reached. The approach itself calls for huge storage for the electrolyte which results in drastic reduction in energy density. Therefore, a more

elegant method to handle the insolubility of the discharge product has to be designed.

Locking the water inside

Water in the electrolyte is not unwanted in the aqueous Li-air cells and it is an active component in the cell reaction. Hence, evaporation of water and removal of the same through the air breathing process can lead to significant change in the electrolyte composition and hence the cell chemistry. It is necessary to devise a mechanism to lock the water in the electrolyte for long cycle life of the aqueous Li-air batteries.

Concluding remarks

For future application in the electric vehicles, Li-air technology show enough promise. However, there are significant scientific and engineering challenges before this technology. The component-wise key issues are mentioned in the previous sections as a quick overview. Few key works in each area have been referred to which will lead to extensive literature on the individual research areas. There needs to be extensive research on this technology to unearth its real potential towards a sustainable world.

References

- G. Girishkumar, B. McCloskey, A. C. Luntz, S. Swanson and W. Wilcke, *Journal of Physical Chemistry Letters*, **1**, 2193-2203.
- T. Ogasawara, A. Debart, M. Holzapfel, P. Novak and P. G. Bruce, *Journal of the American Chemical Society*, 2006, **128**, 1390-1393.
- Z. Peng, S. A. Freunberger, L. J. Hardwick, Y. Chen, V. Giordani, F. Barde, P. Novak, D. Graham, J.-M. Tarascon and P. G. Bruce, *Angewandte Chemie-International Edition*, **50**, 6351-6355.
- S. S. Zhang, D. Foster and J. Read, *J. Power Sources*, **195**, 1235-1240.
- C. O. Laoire, S. Mukerjee, K. M. Abraham, E. J. Plichta and M. A. Hendrickson, *Journal of Physical Chemistry C*, 2009, **113**, 20127-20134.
- Y.-C. Lu, H. A. Gasteiger, M. C. Parent, V. Chiloyan and Y. Shao-Horn, *Electrochemical and Solid State Letters*, **13**, A69-A72.
- L. Trahey, C. S. Johnson, J. T. Vaughey, S. H. Kang, L. J. Hardwick, S. A. Freunberger, P. G. Bruce and M. M. Thackeray, *Electrochemical and Solid State Letters*, **14**, A64-A66.
- S. A. Freunberger, Y. Chen, Z. Peng, J. M. Griffin, L. J. Hardwick, F. Barde, P. Novak and P. G. Bruce, *Journal of the American Chemical Society*, **133**, 8040-8047.
- F. Mizuno, S. Nakanishi, Y. Kotani, S. Yokoishi and H. Iba, *Electrochemistry*, **78**, 403-405.
- W. Xu, V. V. Viswanathan, D. Wang, S. A. Towne, J. Xiao, Z. Nie, D. Hu and J.-G. Zhang, *J. Power Sources*, **196**, 3894-3899.
- P. G. Bruce, S. A. Freunberger, L. J. Hardwick and J.-M. Tarascon, *Nat. Mater.*, **11**, 19-29.
- V. Giordani, S. A. Freunberger, P. G. Bruce, J. M. Tarascon and D. Larcher, *Electrochemical and Solid State Letters*, **13**, A180-A183.
- Y. Shao, S. Park, J. Xiao, J.-G. Zhang, Y. Wang and J. Liu, *Acs Catalysis*, **2**, 844-857.
- J. Read, K. Mutolo, M. Ervin, W. Behl, J. Wolfenstine, A. Driedger and D. Foster, *J. Electrochem. Soc.*, 2003, **150**, A1351-A1356.
- J. Read, *J. Electrochem. Soc.*, 2002, **149**, A1190-A1195.
- J.-G. Zhang, D. Wang, W. Xu, J. Xiao and R. E. Williford, *J. Power Sources*, **195**, 4332-4337.
- J. Xiao, D. Mei, X. Li, W. Xu, D. Wang, G. L. Graff, W. D. Bennett, Z. Nie, L. V. Saraf, I. A. Aksay, J. Liu and J.-G. Zhang, *Nano Letters*, **11**, 5071-5078.
- R. R. Mitchell, B. M. Gallant, C. V. Thompson and Y. Shao-Horn, *Energy Environ. Sci.*, **4**, 2952-2958.
- D. Aurbach, E. Zinigrad, Y. Cohen and H. Teller, *Solid State Ion.*, 2002, **148**, 405-416.
- J. Yamaki, S. Tobishima, K. Hayashi, K. Saito, Y. Nemoto and M. Arakawa, *J. Power Sources*, 1998, **74**, 219-227.
- N. Kamaya, K. Homma, Y. Yamakawa, M. Hirayama, R. Kanno, M. Yonemura, T. Kamiyama, Y. Kato, S. Hama, K. Kawamoto and A. Mitsui, *Nat. Mater.*, **10**, 682-686.
- D. Aurbach, I. Weissman, A. Zaban and O. Chusid, *Electrochimica Acta*, 1994, **39**, 51-71.
- M. M. Thackeray, *J. Electrochem. Soc.*, 1995, **142**, 2558-2563.
- G. M. Veith, N. J. Dudney, J. Howe and J. Nanda, *Journal of Physical Chemistry C*, **115**, 14325-14333.
- C. O. Laoire, S. Mukerjee, K. M. Abraham, E. J. Plichta and M. A. Hendrickson, *Journal of Physical Chemistry C*, **114**, 9178-9186.
- C. O. Laoire, S. Mukerjee, E. J. Plichta, M. A. Hendrickson and K. M. Abraham, *J. Electrochem. Soc.*, **158**, A302-A308.
- W. Xu, J. Xiao, D. Wang, J. Zhang and J.-G. Zhang, *Electrochemical and Solid State Letters*, **13**, A48-A51.
- K. M. Abraham and Z. Jiang, *J. Electrochem. Soc.*, 1996, **143**, 1-5.
- J. Hassoun, F. Croce, M. Armand and B. Scrosati, *Angewandte Chemie-International Edition*, **50**, 2999-3002.
- B. Kumar, J. Kumar, R. Leese, J. P. Fellner, S. J. Rodrigues and K. M. Abraham, *J. Electrochem. Soc.*, **157**, A50-A54.
- P. Kichambare, J. Kumar, S. Rodrigues and B. Kumar, *J. Power Sources*, **196**, 3310-3316.
- Y. Wang and H. Zhou, *Chemical Communications*, **46**, 6305-6307.
- P. He, Y. Wang and H. Zhou, *Chemical Communications*, **47**, 10701-10703.
- E. Yoo and H. Zhou, *Acs Nano*, **5**, 3020-3026.
- F. Bidault, D. J. L. Brett, P. H. Middleton and N. P. Brandon, *J. Power Sources*, 2009, **187**, 39-48.

36. L. Jorissen, *J. Power Sources*, 2006, **155**, 23-32.
37. S. Visco, V. Nimon, A. Petrov, K. Pridatko, N. Goncharenko, E. Nimon, L. De Jonghe, Y. Volfkovich and D. Bograchev, *Journal of Solid State Electrochemistry*, **18**, 1443-1456.
38. T. Zhang, N. Imanishi, Y. Shimonishi, A. Hirano, J. Xie, Y. Takeda, O. Yamamoto and N. Sammes, *J. Electrochem. Soc.*, **157**, A214-A218.



Jishnu Bhattacharya received his PhD degree from University of Michigan, Ann Arbor in 2010. He had been associated with Northwestern University and IIT Kharagpur before he joined IIT Kanpur in 2014 where currently he is an assistant professor in mechanical engineering department. He works in the interdisciplinary area of energy storage systems which involves material chemistry as well as engineering aspects from mechanical and electrical engineering. He is interested in predicting and understanding ion transport in battery materials, thermal storage for solar energy, thermal management of battery packs in electric vehicles etc.

Plasmon Induced Enhancement of Charge Separation in Epitaxial Metal-Semiconductor Nanohybrid Material Anchored with an Organic Molecule

Jayanta Dana and Hirendra N. Ghosh*

Radiation and Photochemistry Division, Bhabha Atomic Research Centre, Mumbai, 400085, India.

E-mail: hngosh@barc.gov.in

Nanohybrid material composed of metals and semiconductors is a subject of great current interest in recent years due to their potential application in solar energy conversion, sensors and photo catalysis etc.¹⁻⁵ In quantum dot solar cell (QDSC), QDs are used as sensitizer. Now due to strong confinement of charge carriers there is significant enhancement of electron-hole Coulomb interaction in QD materials, which leads to multiple exciton generation (MEG),⁶ where a single photon can generate more than one exciton (electron-hole pair). However due to Auger recombination QD excitons lifetime decreased to tens of picoseconds.⁷

So to design and develop higher efficient QD solar cell extraction of charge carriers utmost important for efficient Auger recombination. In most of the nano-hybrid systems Fermi level of the metal lies below the conduction band of the semiconductor, as a result electron transfer from photo-excited QD to metal NP is thermodynamically viable. Now in nanohybrid material photo-excited electron from QD can be transferred to metal domain as Fermi level of the metal lies below the conduction band of the semiconductor, as a result Auger recombination can be minimized drastically. The electronic mixing between the electronic states of metal and semiconductor takes place very effectively in semiconductor-metal nanohybrid material as metal NPs are directly grown on the semiconductor surface without any spacer⁸, as a result the inter domain charge transfer can take place very efficiently from semiconductor domain to metal domain.⁹⁻¹¹

Dissociation of exciton through ultrafast electron and hole transfer processes in different QD/molecule systems have been extensively reported in literature.¹²⁻²⁰ Hot hole and thermalized hole extraction time was found to be 250 fs²⁰ and 500fs -1ps¹⁵⁻²⁰ respectively. Most of the reports available in literature for dissociation of exciton either by electron transfer or by hole extraction. However, not many reports are available literature except the report from our group²¹ where both electrons and holes are extracted from the photo-excited QD materials in the same time.

In the present article to demonstrate exciton dissociation simultaneously both by electron and hole extraction, CdSe{Au} hetero-structure (HS) materials was synthesized

and consequently sensitized by bromo-pyrogallol red (Br-PGR) molecule. Charge transfer reaction was monitored in CdSe{Au}/Br-PGR tri-composite system with the help of time-resolved emission and ultrafast transient absorption techniques. Energy level diagram in the tri-composite system suggests that photo-excited electron in QD can be transferred to gold domain and photo-excited hole can be captured by molecular adsorbate (Br-PGR) as both the processes are thermodynamically viable. Both electron and hole transfer dynamics was demonstrated in ultrafast time scale by femto-second transient absorption spectroscopy and discussed in detail.

For synthesizing of Au-CdSe heterostructure freshly prepared CdSe QD¹⁷ was used. The gold precursor was prepared by the mixing of 15 mg AuCl₃ (0.05mmol), 50 mg DDAB - Di Dodecyle Ammonium Bromide (0.1 mmol) and 90 mg (0.46 mmol) DDA - Dodecyle Amine in 4 mL toluene. The color of the solution becomes dark orange to light yellow. Now 20 mg synthesized CdSe is dissolved in 4 mL toluene under Ar Atmosphere. The gold precursor was added dropwise to the CdSe solution for a time period of 4 minutes under Ar atmosphere at room temperature. Gradually the color of the solution becomes dark brown. The DDAB stabilize the QD and DDAB acts as surfactant of Au NP. Finally the nanohybrid materials were precipitated in methanol. Then the precipitated nanohybrid materials were dissolved in chloroform for characterization and further use.

Fig. 1 HRTEM images of Au-CdSe nanohybrid and it is clearly seen that Au NP nicely coupled with CdSe QD, where size of Au NP can be determined to be 3-3.5 nm and size of CdSe QD found to be 4-4.5 nm. The TEM image clearly shows the homogeneous deposition of Au on the surface of CdSe QD with separate lattice images of both of them.

To characterize the CdSe{Au} hetero-structure (HS) optical absorption studies have also been carried out in chloroform solution and shown in Fig. 1. Fig. 1 a shows optical absorption spectra of CdSe QD with two excitonic absorption band at 560 nm and 450 nm which can be attributed to 1S(e)-1S_{3/2}(h) and 1P(e)-1P_{3/2}(h) transitions respectively. On the other hand Fig. 1 b shows the optical

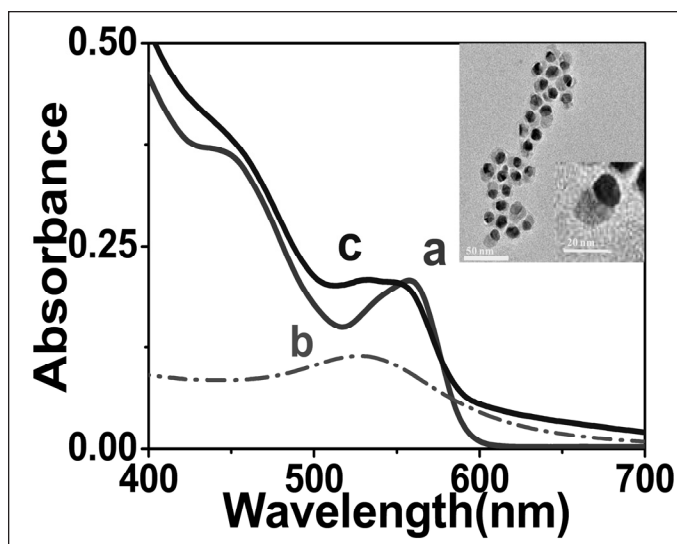


Fig. 1: Steady state optical absorption spectra of (a) CdSe quantum dot, (b) Au NP and (c) CdSe{Au} HS in chloroform. **Inset:** HR-TEM picture of CdSe{Au} HS material. (In Inset magnified image of Au/CdSe).

absorption due to plasmon band Au NP at 527 nm. Fig. 1c shows optical absorption spectra of CdSe{Au} HS where Au NP is grown on the surface of CdSe QD. Optical absorption studies clearly suggest that there is strong electronic interaction between plasmonic band of Au NP and excitonic band of CdSe QD.

Steady state and time-resolved emission studies have been carried out for both CdSe QD and CdSe{Au} HS to monitor the excited state properties of the hetero-structure. Fig. 2a shows the emission spectra of CdSe QD which shows emission band at 580 nm with emission quantum yield (QY) of 0.34. However no emission was observed

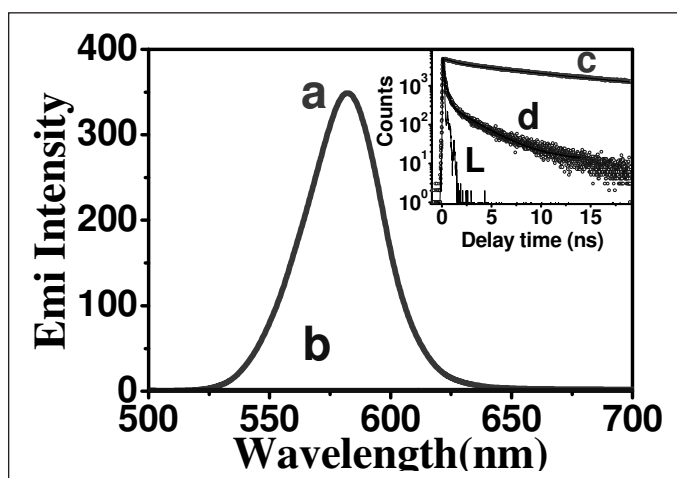


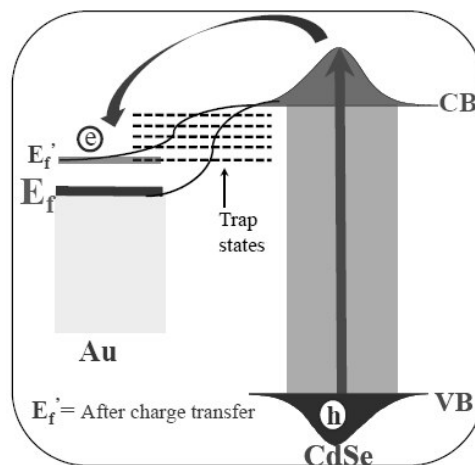
Fig. 2: Steady state photoluminescence spectra of (a) CdSe quantum dot (b) CdSe{Au} HS. **Inset:** Time resolved luminescence decay trace of (c) CdSe quantum dot and (d) CdSe{Au} HS at 580 nm after exciting the samples at 406nm. (L is the lamp profile of 406nm laser)

from CdSe{Au} HS (Fig. 2b). This quenching of emission can be attributed to transfer of electron from photo-excited CdSe QD to Au NP as shown in Scheme 1. It is clearly seen that Fermi level of Au NP lies below the conduction band of CdSe QD which makes the process thermodynamically viable.

Time-resolved luminescence measurements have also been carried out to reconfirm of electron transfer process. Fig. 2c and 2d shows the luminescence decay trace at 580 nm after exciting the sample at 406 nm for CdSe QD and CdSe{Au} HS respectively. The emission decay trace of CdSe QD found to follow bi-exponential decay with $\tau_{\text{avg}} = 11.66 (\pm 0.5)$ ns. Interestingly emission kinetics for CdSe{Au} HS found to decay much faster with $\tau_{\text{avg}} = 0.72 (\pm 0.05)$ ns. Now the observed decrease in lifetime can be attributed to electron transfer (ET) from CdSe QD to Au NP, then the ET rate constant can be determined through the following expression:

$$K_{\text{ET}} = 1/\tau_{\text{CdSe}\{\text{Au}\}} - 1/\tau_{\text{CdSe}} \quad (3)$$

Using the average lifetime values of 11.66 (± 0.5) ns (CdSe) and 0.72 (± 0.05) ns (CdSe{Au}) the electron transfer rate constant can be determined to be $1.39 \times 10^9 \text{ sec}^{-1}$.



Scheme 1: Schematic diagram showing electron transfer from semiconductor domain to the metal domain in CdSe{Au} nanohybrid material.

Time-resolved emission studies suggest that electron transfer process from CdSe QD to Au NP is too fast. Therefore, it is not easy to determine correctly the electron transfer time constant from time resolved emission study. Hence to determine the electron transfer time constant correctly, femtosecond transient absorption spectroscopic measurements have been carried by exciting both CdSe QD and specifically CdSe{Au} HS at 400 nm laser light and compared the transient data and shown in Fig. 3 which show transient spectra at different time delay.

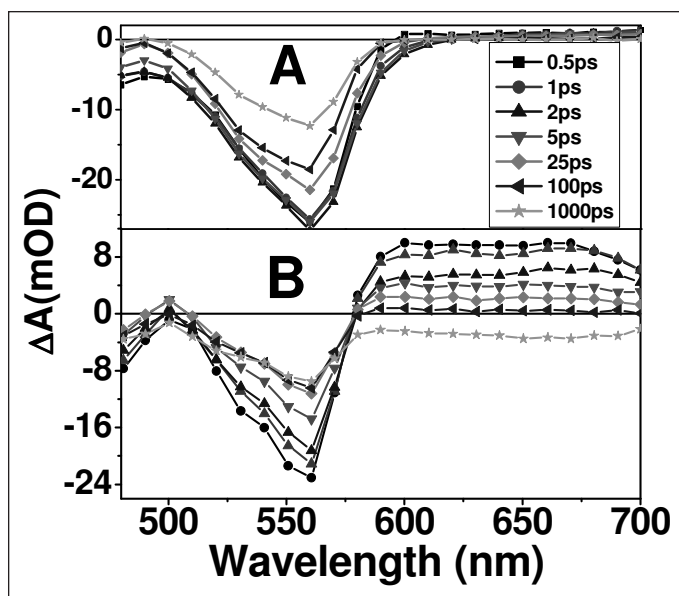


Fig. 3: Transient absorption spectrum of (A) CdSe quantum dot and (B) CdSe{Au} HS in chloroform solvent after exciting the samples at 400 nm.

Broad negative absorption band in both the transient absorption spectra which matches with the steady state optical absorption spectra can be attributed to excitonic bleach.

The transient bleach spectra of CdSe{Au} HS look quite similar to that pure CdSe QD but signature of plasmon bleach due to Au NP is completely absent. Earlier Zamkov *et. al.*²² reported suppression of surface plasmon of Au NP by the exciton of CdS nanorod in Au/CdS nanohybrid system. Interestingly in CdSe{Au} HS system positive absorption band appears in the red region of the spectra which can be attributed to the appearance of electron in

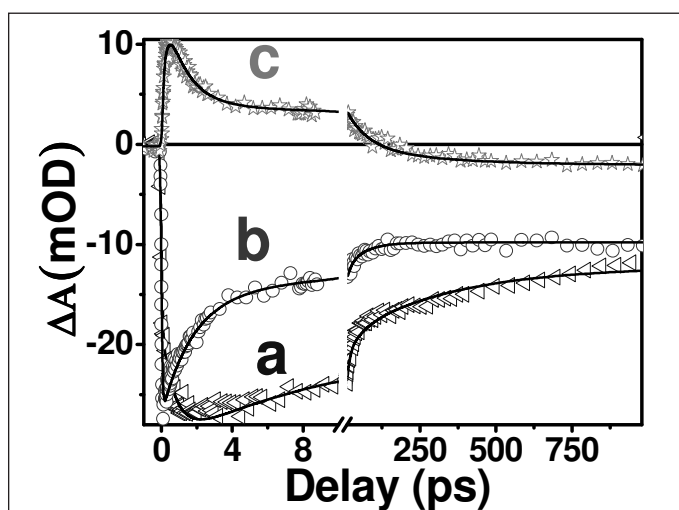


Fig. 4: Bleach recovery kinetics at 560 nm for (a) CdSe quantum dot and (b) CdSe{Au} HS; and (c) transient absorption kinetics at 650 nm for CdSe{Au} HS in chloroform after 400 nm laser excitation.

the Au NP^{22, 23} (in Fermi level) from the conduction band of CdSe QD which is thermodynamically viable process (Scheme 1). To monitor the charge carrier and transfer dynamics transient kinetics at different wavelengths for both CdSe QD and CdSe{Au} HS have been monitored and shown in Fig. 4. The bleach recovery kinetics at 560 nm for CdSe{Au} HS is much faster as compared to that of pure CdSe QD. This faster recovery kinetics in the excitonic bleach position of CdSe{Au} HS can be attributed to photoinduced electron transfer from the CB of CdSe QD to the fermi level of Au.

The transient kinetics at different wavelengths at different systems can be fitted multi-exponentially. However it's interesting to see that in presence of Au NP the bleach recovery kinetics drastically changes which can be attributed to ultrafast electron transfer from CdSe QD to Au NP. Its interesting to see that transient absorption band at 600-750 nm region appears only on photo-excitation of CdSe{Au} HS not pure CdSe QD. This transient signal can be attributed to the trapped of electron in the interface zone of metal and semiconductor which are transferred from photo-excited CdSe QD to Au NP. The faster decay component (1.2 ps) of the positive signal at 650 nm can be attributed to trapping of electron in the interface zone.

It is clearly seen in earlier section that on photoexcitation of CdSe{Au} HS photo-excited electrons are localized in Au NP and holes are localized in the valence band of CdSe QD (Scheme 1). To facilitate further charge separation process and slow down the charge recombination dynamics a molecular adsorbate namely bromo-pyrogallol red (Br-PGR) can be used whose HOMO levels lies above the valence band of CdSe QD (Scheme 2).

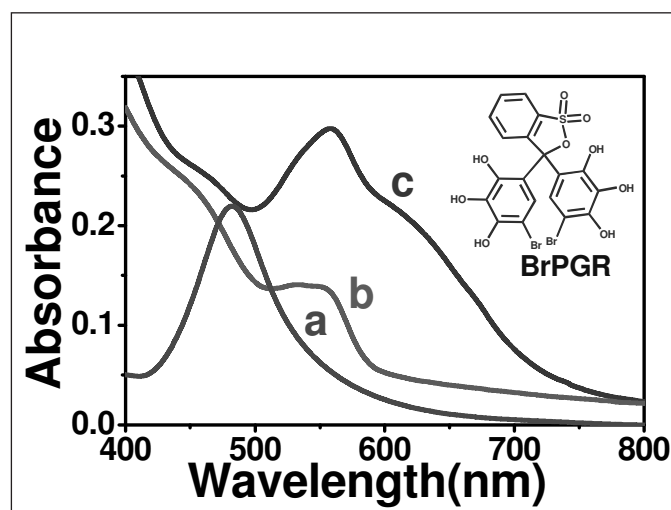


Fig. 5: Steady state optical absorption spectra of (a) Br-PGR dye (10μM) (b) CdSe{Au} HS and (c) Br-PGR sensitize CdSe{Au} HS in chloroform. Inset: Molecular structure of Br-PGR.

Steady state optical absorption studies have been carried out the CdSe{Au} HS sensitizing Br-PGR dye and shown in Fig. 5. It is interesting to see that optical absorption spectra of CdSe{Au}/Br-PGR (Fig. 5c) is completely different as compared to that of both Br-PGR (Fig. 5a) and CdSe{Au} HS (Fig. 5b). In the composite system a new hump appears in the absorption spectra at 620 nm which can be attributed to the formation of charge transfer complex between CdSe{Au} HS and BrPGR molecule.

Now to monitor charge separation dynamics in CdSe{Au}/Br-PGR tri-composite system in ultrafast time 400 nm laser light was exposed and transient spectra have been recorded at different time delay and are shown in Fig. 6, which shows a positive absorption band below 515 nm and a broad bleach in 515-715 nm region with a peak ~ 560 nm and a hump at 630 nm. Interestingly transient absorption spectra of the tri-composite materials is completely different as compared to both CdSe{Au} HS and Br-PGR. At longer time scale two negative absorption bands has been observed at 560 nm and 630 nm which can be attributed to the bleach due to excitonic absorption of CdSe QD and charge transfer complex respectively. The charge transfer processes in the tri-composite system are demonstrated clearly in Scheme 2.

On photo-excitation of CdSe QD, electrons will be excited to the conduction band and holes will be localized in the valence band. The photo-excited electrons are transferred to Au NP and holes are captured by Br-PGR. Again it is clearly seen in Scheme 2 also suggests that photo

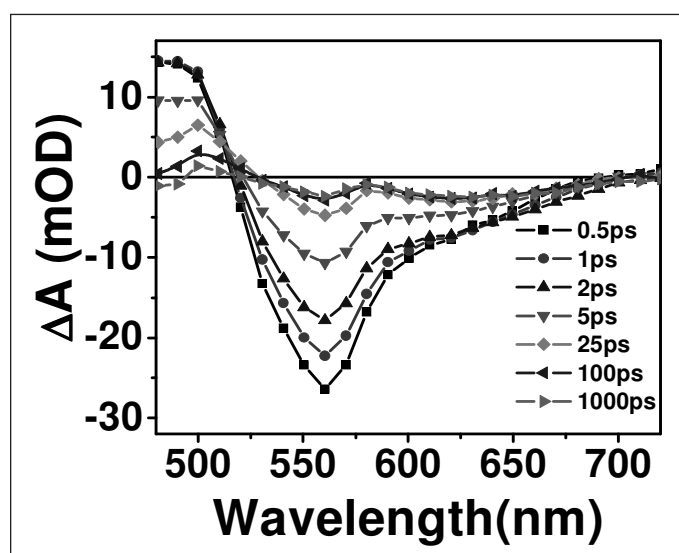
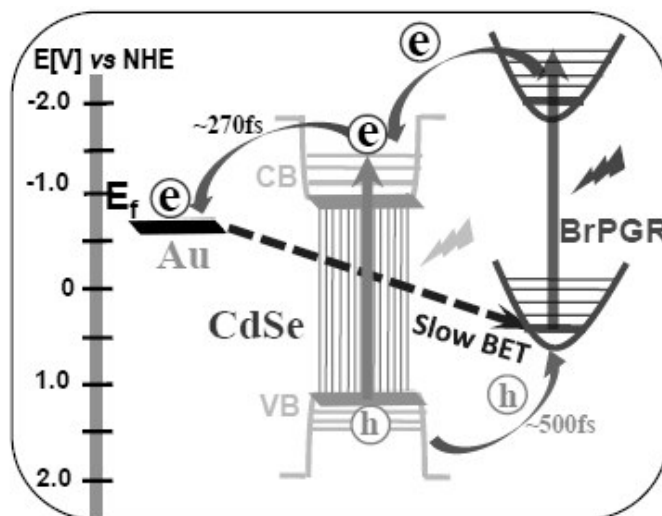


Fig. 6: The transient absorption spectra CdSe{Au}/Br-PGR tri-composite system at different time delay after exciting the samples at 400 nm in chloroform.



Scheme 2: Schematic diagram illustrating the electron and hole transfer processes in CdSe{Au}/Br-PGR tri-composite system. It shows photo-excitation of QD electron and hole are generated where electron is transferred to the Fermi level of Au NP and hole is captured by Br-PGR molecules. On the otherhand photo-excited Br-PGR injects electron into the CB of CdSe QD and finally transferred to AuNP. The dashed line indicates the charge recombination reaction between electron in Au NP and hole in Br-PGR.

excited Br-PGR can inject electron into the conduction band of CdSe QD which eventually transferred to Au NP. To find the effect of Au NP on charge recombination dynamics of CdSe{Au}/Br-PGR composite bleach recovery kinetics has been monitored at bleach due to CT complex position and shown in Fig. 7. It's very clear net charge recombination reaction found to be very slow due to localization of electron in Au NP and localization of hole

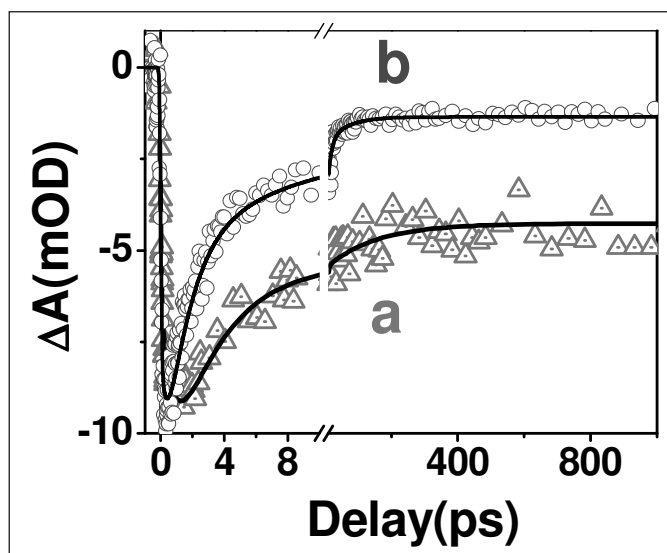


Fig. 7: Bleach recovery kinetics of (a) CdSe{Au}/Br-PGR tri-composite system and (b) CdSe/BrPGR system at 655nm.

in Br-PGR (Scheme 2) which are spatially separated and charge recombination is extremely slows down. For the first time in the literature we are reporting spatial charge separation dynamics in metal/semiconductor/ molecular adsorbate tri-composite system where electron is localized in Au NP and hole is localized in molecular adsorbate.

To reconfirm the above effect photodegradation of o Rhodamin-B (Rh-B) dye in presence of Au NP, CdSe QD, CdSe{Au} and Au/CdSe/Br-PGR nanohybrid materials have been carried out and shown in Fig. 8. It is clearly seen that Au/CdSe/Br-PGR tri-composite materials is the best material for photo reduction of Rh-B.

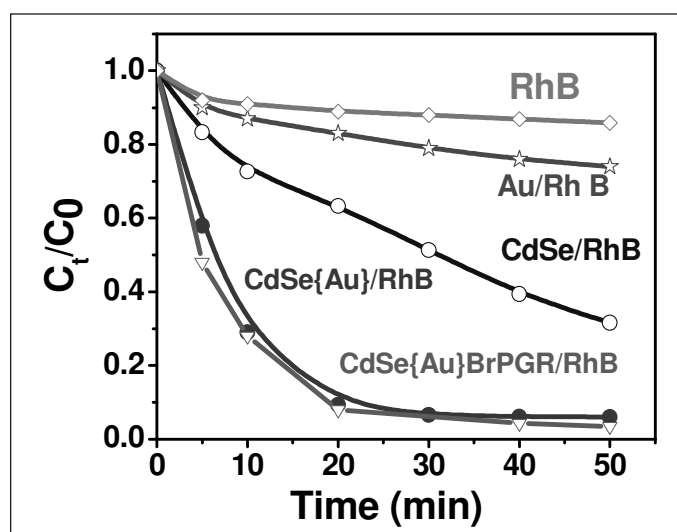


Fig. 8: Photodegradation of RhB in presence of Au, CdSe, CdSe{Au} and CdSe{Au}/BrPGR at different time after illumination of 350 nm light. The C_0 is the initial concentration of Rh B and C_t is the concentration after t time.

In conclusion CdSe{Au} hetero-structure (HS) has been successfully synthesized and characterized by steady state absorption and emission spectroscopy and HRTEM measurements. Surface plasmon of Au NP found to be suppressed in presence of CdSe QD due to strong exciton-Plasmon coupling between Au NP and CdSe QD. Photo-excited electron in CdSe QD is found to be transferred to the Au NP as monitored by both time-resolved emission and ultrafast transient absorption studies. Spectroscopic measurements have been carried out to study charge transfer dynamics after sensitizing CdSe{Au} HS with bromo-pyrogallol red (Br-PGR). Steady state optical absorption studies have confirmed formation of charge transfer complex between CdSe{Au} HS and Br-PGR. Charge separation in CdSe{Au}/Br-PGR tri-composite system found to take place in different pathways, like electron transfer from the CB of CdSe QD to Au NP, hole transfer from VB of CdSe QD to Br-PGR,

electron injection from photo-excited Br-PGR to the CB of CdSe QD. Spectroscopic investigations suggest that on photo-excitation CdSe{Au}/Br-PGR tri-composite system cascading electron transfer and hole transfer take place where all the electrons are localized in Au NP and all the holes are localized in Br-PGR. Electron and hole transfer time from photo-excited CdSe QD to Au NP and Br-PGR were found to be ~ 270 fs and ~ 500 fs respectively. Charge recombination reaction between electron in Au NP and hole in Br-PGR was found to be very slow due spatial separation of charges in CdSe{Au}/Br-PGR tri-composite system. Our experimental investigations clearly suggest that metal/semiconductor/molecular adsorbate tri-composite system can be the reality of multiple exciton dissociation and finally higher photoconversion efficiency in QDSCs.

Acknowledgement:

This work was supported by "DAE-SRC Outstanding Research Investigator Award" (Project/Scheme No.: DAE-SRC/2012/21/13-BRNS) granted to Dr. H. N. Ghosh. J.D. acknowledges CSIR for research fellowship.

References:

1. X. H. Huang, I. H. El-Sayed, W. Qian and M. A. El-Sayed, *J. Am. Chem. Soc.*, 2006, 128, 2115.
2. H. Song, *Acc. Chem. Res.*, 2015, 48, 491.
3. K. P. Acharya, R. S. Khayzer, T. O'Connor, G. Diederich, M. Kirsanova, A. Klinkova, D. Roth, E. Kinder, M. Imboden and M. Zamkov, *Nano Lett.*, 2011, 11, 2919.
4. K. Wu, H. Zhu, Z. Liu, W. Rodriguez-Córdoba and T. Lian, *J. Am. Chem. Soc.*, 2012, 134, 10337.
5. E. Elmaleh, A. E. Saunders, R. Costi, A. Salant and U. Banin, *Adv. Mater.*, 2008, 20, 4312.
6. J. A. McGuire, J. Joo, J. M. Pietryga, R. D. Schaller and V. I. Klimov, *Acc. Chem. Res.*, 2008, 41, 1810.
7. V. I. Klimov, A. A. Mikhailovsky, D. W. McBranch, C. A. Leatherdale and M. G. Bawendi, *Science*, 2000, 287, 1011.
8. D. Steiner, T. Mokari, U. Banin and O. Millo, *Phys. Rev. Lett.*, 2005, 95, 056805.
9. Y. Kobayashi, Y. Nonoguchi, L. Wang, T. Kawai and N. Tamai, *J. Phys. Chem. Lett.*, 2012, 3, 1111.
10. P. Guardia, K. Korobchevskaya, A. Casu, A. Genovese, L. Manna and A. Comin, *ACS Nano*, 2013, 7, 1045.
11. S. K. Dutta, S. K. Mehetor and N. Pradhan, *J. Phys. Chem. Lett.*, 2015, 6, 936.
12. J. Huang, Z. Huang, Y. Yang, H. Zhu and T. Lian, *J. Am. Chem. Soc.*, 2010, 132, 4858.
13. Y. Yang, W. Rodriguez-Córdoba, X. Xiang and T. Lian, *Nano Lett.*, 2012, 12, 303.
14. J. Huang, Z. Huang, S. Jin and T. Lian, *J. Phys. Chem. C*, 2008, 112, 19734.
15. P. Maity, T. Debnath and H. N. Ghosh, *J. Phys. Chem. Lett.*, 2013, 4, 4020.

16. P. Singhal and H. N. Ghosh, *J. Phys. Chem. C*, 2014, 118, 16358.
17. T. Debnath, P. Maity, S. Maiti and H. N. Ghosh, *J. Phys. Chem. Lett.*, 2014, 5, 2836.
18. T. Debnath, P. Maity and H. N. Ghosh, *Chem. Eur. J.*, 2014, 20, 13305.
19. P. Maity, T. Debnath, U. Chopra and H. N. Ghosh, *Nanoscale*, 2015, 7, 2698.
20. P. Singhal and H. N. Ghosh, *Chem. Eur. J.*, 2015, 21, 4405.
21. J. Dana, T. Debnath, P. Maity and H. N. Ghosh, *J. Phys. Chem. C*, 2015, 119, 22181.
22. E. Khon, A. Mereshchenko, A. N. Tarnovsky, K. Acharya, A. Klinkova, N. N. Hewa-Kasakarage, I. Nemitz and M. Zamkov, *Nano Lett.*, 2011, 11, 1792.
23. S. Lambright, E. Butaeva, N. Razgoniaeva, T. Hopkins, B. Smith, D. Perera, J. Corbin, E. Khon, R. Thomas, P. Moroz, A. Mereshchenko, A. Tarnovsky and M. Zamkov, *ACS Nano*, 2014, 8, 352.



Jayanta Dana is a senior research fellow in Bhabha Atomic Research Centre. He completed his B.Sc from Burdwan University and M.Sc from Banaras Hindu University in 2010 and 2012, respectively. His current research interest is to investigate the charge transfer dynamics in Metal Semiconductor heterostructure sensitised with molecular adsorbate by femtosecond Transient Absorption spectroscopy and application of these materials in solar cell and photo-catalysis.



Dr. Hirendra Nath Ghosh after obtaining his M. Sc. in Chemistry from IIT, Kharagpur, in 1989, joined Chemistry Division, BARC, in 1990, through BARC Training School Course (33rd batch, 1989-90). Dr. Ghosh obtained his Ph.D. degree in 1996 from Bombay University for his work on fast photochemical processes in liquid and microheterogeneous media. He did his Post-doctoral studies for the period of 1997-1998, at the Chemistry Department of Emory University, Atlanta, USA, in Femtosecond infrared spectroscopy. Dr. Ghosh also visited Max-Born Institute, Berlin Germany as a visiting scientist for one year (2007-2008) for scientific collaboration on vibrational spectroscopy. Dr. Ghosh has published more than **128** research papers in highly reputed International Journals, and his research papers have been cited more than **4700** by peers in the field (**h-index = 35**). He has developed Femtosecond laser spectrometer detecting both in visible and infrared (IR) region in Radiation & Photochemistry Division in Bhabha Atomic Research Centre first time in the country. His current research interest includes ultrafast interfacial electron transfer and charge carrier relaxation dynamics in semiconductor nanoparticles and quantum dot core-shell nano-structured materials and proton coupled electron transfer reaction (PCET) in solution phase using different ultrafast techniques. He is also involved in design and development of Quantum Dot Solar Cell (QDSC) and also mechanism to improve the efficiency of QDSC through ultrafast spectroscopic techniques. Currently he is also involved in developing Femtosecond Terahertz Spectrometer.

Awards received:

1. **INSA Medal for Young Scientists** in the year **1998** from Indian National Science Academy, New Delhi.
2. **A.K. Bose Memorial Award** in the year **2000** from Indian National Science Academy, New Delhi.
3. **APA-Prize for Young Scientist** in the year **2004** from The Asian and Oceanian Photochemistry Association.
4. **Fellow of National Academy of Science (F. N. A. Sc.)**, Allahabad, India on Dec, **2008**.
5. **Homi Bhabha Science & Technology Award** for the year **2010** from Department of Atomic Energy (DAE), India.
6. **CRSI Bronze Medal** in the year **2011** from Chemical Research Society of India, Bangalore.
7. **DAE-SRC Outstanding Investigator Award** for the year **2012** from Department of Atomic Energy (DAE), India.
8. **Fellow of Academy of Science (FASc.)**, Bangalore, India on Jan, **2013**.
9. **C. N. R. Rao National Prize for Chemical Research** in the year **2014** from Chemical Research Society of India, Bangalore.

Artificial Photosynthesis Using Graphene-Based Nanomaterials

Suneel Kumar, Vipul Sharma, Venkata Krishnan*

*School of Basic Sciences and Advanced Materials Research Center, Indian Institute of Technology Mandi,
Kamand, Mandi 175005, H.P., India.*

Email: vkn@iitmandi.ac.in

Abstract

In the pursuit towards efficient and environmentally sustainable energy conversion, artificial photosynthesis, involving hydrogen production from solar water splitting, has recently gained significant importance. Research in this field is aimed at solving the global energy crisis in an environmentally friendly way by using two of the most abundant natural resources, namely sunlight and water. Over the past few years, carbon based materials particularly graphene has attracted much attention as an interesting material in the field of artificial photosynthesis. Due to the exceptional physical properties, graphene based functional materials have made substantial contribution in the generation of clean, renewable and viable form of energy from light driven water splitting. This review article provides a comprehensive overview of the recent research progress in the field of artificial photosynthesis using graphene-based nanomaterials. It begins with a brief introduction to the field and the basic principles of solar water splitting for hydrogen generation followed by the properties of graphene and graphene based materials. Then, it presents the development of various graphene based nanomaterials for artificial photosynthesis, wherein graphene plays different roles including electron acceptor/transporter, cocatalyst, photocatalyst and photosensitizer. This review concludes by highlighting the advantages and challenges involved in the use of graphene based nanomaterials for solar water splitting. Finally, the future perspectives of research in this field are also briefly mentioned.

1. Introduction

Global energy demand is continuously increasing for the past several years and the scientific community is mainly working to develop an alternative for the depleting fossil fuel reserves to address effectively the energy crisis and other environmental issues.¹ Hydrogen seems to a promising solution to overcome this energy crisis.² Hydrogen is mainly present in the fossil fuels such as natural gas from where it can be mainly produced by the steam reforming but this method is mainly restricted due to carbon dioxide emission and high cost.³ As hydrogen is abundant element and present in nature in the form of water, therefore its production from water using solar energy is an area of interest for researchers currently and is the best alternative to overcome energy crisis.⁴ J. A. Turner has presented various methods for hydrogen production by solar water splitting.⁵ It has also been reported that thermochemical water splitting needs very high temperature up to 1000°C.⁶ Consequently more research has been focused on the photoelectrochemical (PEC) and photocatalytic water splitting because these methods are simple, convenient and reliable for hydrogen production.⁷

For the first time PEC hydrogen production was reported in 1972 by Fujishima and Honda on a TiO₂ anode and Pt cathode under ultraviolet (UV) light irradiation.⁸

After this, researchers' interest to explore semiconductors for hydrogen production has grown significantly and great progress has been made in this field in past several years.⁹⁻¹¹ TiO₂ is the most explored semiconductor in water splitting due to its non-toxic nature, chemical stability, low cost and wide abundance.¹² Subsequently, many other semiconductor materials were also explored in water splitting.¹³⁻¹⁵ But due to the wide band gap, most of these materials are active in the UV-light region which constitutes only 5% of the total solar spectrum. During recent years, many research groups explored materials having narrow band gaps such as metal sulphides (CdS),¹⁶ metal oxides (SrTiO₃),¹⁷ oxysulphides¹⁸ and oxynitrides,¹⁹ etc. These semiconductors are active in visible light and hence proved to be efficient for hydrogen generation as visible light constitute about 43% of the total solar spectrum²⁰. In addition to this, suitable PEC and photocatalytic cells are also constructed for water splitting.²¹

In last 25 years, the emergence of carbon based nanomaterials has opened new ways of harvesting solar energy and generation of clean energy in the form of hydrogen.^{4, 22-24} These materials serve as excellent support for various semiconductors,²⁵ noble metals²⁶ Graphene is one of the most promising carbon-based materials in nanotechnology. Ideally graphene is a single layer carbon sheet which consists of a two dimensional (2D) network of

the sp^2 hybridized carbon atoms with hexagonal packed lattice structure.²⁷ Graphene also possess the unique electronic, optical and mechanical properties such as high theoretical specific surface area ($2630 \text{ m}^2\text{g}^{-1}$),²⁸ chemical stability, high transparency and good thermal conductivity ($5000 \text{ Wm}^{-1}\text{K}^{-1}$).²⁹ Its optical transmittance is about 97.7% and possesses superior electron mobility ($200000 \text{ cm}^2\text{V}^{-1}\text{s}^{-1}$), which makes it an ideal material for photocatalyst support and for the construction of PEC electrodes.³⁰ Furthermore, graphene based nanomaterials are highly desirable in PEC and photocatalytic hydrogen generation because,

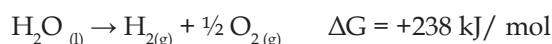
1. Single layer graphene sheets provide very good support to anchor the metal oxide/sulphide semiconductor nanoparticles which result in high performance photocatalysts.^{25, 31, 32}
2. Graphene acts as good electron acceptor and transporter and hence reduces the recombination of charge carriers in semiconductors by accepting the electrons from the conduction band of semiconductors and its transfer to the reaction site.³³
3. Graphene also acts as photocatalyst as band gap of reduced graphene oxide (RGO) can be tuned with the degree of reduction. Also CB of RGO has energy level of -0.52 eV which is more negative than $E_{\text{H}_2/\text{H}_2\text{O}} = 0$, hence it plays important role in hydrogen evolution from water.⁴
4. Due to high work function, graphene serves as promising cocatalyst in hydrogen generation and hence it can extract electrons from CB of semiconductor to reduce H^+ to H_2 molecule on its surface.³⁴

In this article, we will briefly discuss the basic principle of photoelectrochemical and photocatalytic hydrogen generation from water splitting. After that we will focus on synthesis and properties of graphene for hydrogen generation. Then we will present some graphene based binary/ternary systems which specify the role of graphene as electron acceptor/transporter, cocatalyst, photocatalyst and photosensitizer. Finally a brief summary of concluding remarks highlighting the advantages and challenges involved in the use of graphene based nanomaterials for water splitting will be presented. The future perspectives of research in this field are also briefly mentioned at the end.

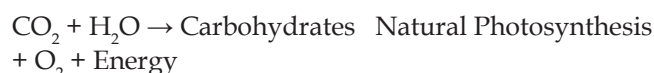
2. Basic Principles of Photoelectrochemical and Photocatalytic Hydrogen Generation

Water splitting reaction results in the conversion of solar energy to chemical energy and this reaction is accompanied by large positive change in the Gibbs free

energy ($\Delta G = +ve$). Hence overall water splitting reaction is an uphill reaction.



Photocatalytic water splitting reaction is quite similar to the process of photosynthesis which takes place in the green plants and hence it is known as artificial photosynthesis. Chemical reaction for both the parallel processes can be given as,



Hydrogen production through solar water splitting is widely explored as it has several advantages like raw material is easily available and combustion of hydrogen in the air produces water hence this method is environment friendly. Therefore this photocatalytic water splitting has been extensively studied using various semiconductor based material and many of the new semiconductor based photocatalyst have been discovered recently.

In 1972, Fujishima and Honda achieved photoelectrocatalytic water splitting using TiO_2 electrode. TiO_2 is irradiated with UV light and electrons and holes are generated in CB and VB respectively. TiO_2 electrode act as anode and is connected to Pt cathode through external bias. Photogenerated electrons reduce water to form H_2 on Pt electrode while holes oxidize water to form O_2 on TiO_2 electrode as illustrated in the Fig. 1a. After that semiconductor based material with suitable band gap has attracted much attention in this field. In order to make the utilization of solar energy efficiently many photoelectrochemical cells have been developed for hydrogen production and it was illustrated that band gap and stability plays important role in harvesting solar energy.^{10, 21}

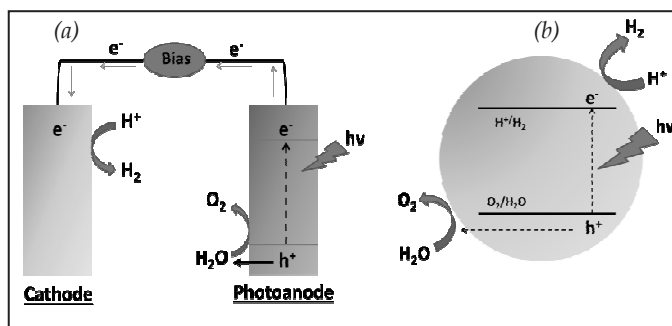


Fig. 1. a) Photoelectrochemical H_2 generation. b) Photocatalytic H_2 generation from water

Basically in the process of photocatalytic water splitting, photon of light having energy greater than band

gap energy of the chosen semiconductor material results in the formation of electron-hole pairs in conduction band (CB) and valence band (VB) respectively. These photo-generated electron-hole pairs are responsible for the reduction and oxidation reactions that is reduction of $H^+ \rightarrow H_2$ and oxidation of $H_2O \rightarrow O_2$ in CB and VB respectively as illustrated in Fig. 1b.

The most important point in achieving water splitting is the position of VB and CB in semiconductor materials. The bottom level of CB must be more negative than redox potential of $H^+ \rightarrow H_2$ (0V vs NHE), while the top level of VB must be more positive than oxidation potential of $H_2O \rightarrow O_2$ (1.23 V vs NHE). Therefore 1.23 eV is the minimum band gap for water splitting and this band gap correspond to the light of 1008 nm wavelength (near IR region). According to standard texts/literature⁹ wavelength and eV related to each other as,

Band gap $eV = 1240 / \lambda$ (nm). Hence a suitable band gap value plays crucial role in order to make them active in visible region of light to generate H_2 and O_2 by water splitting. Band gap of some semiconductor materials are summarized in Fig. 2.

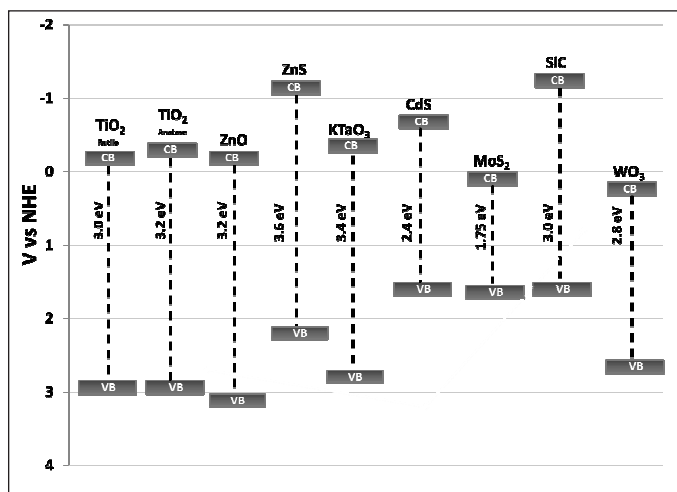


Fig. 2. Valence band and conduction band position of different semiconductors used for water splitting.⁹

As both band gap and wavelength are directly related to each other, therefore suitable band gap engineering is required to make photocatalyst active in the visible light region of spectrum. The overall water splitting reaction on the surface of semiconductor material occurs in three main steps,

1. Absorption of light
2. Charge separation
3. Redox reactions on the catalyst surface

The first step involves the absorption of light by photocatalyst and generation of electron-hole pairs in the CB and VB. Second step involves the charge separation and migration of charge carriers to the surface. Higher crystallinity and smaller size of particles plays a significant role in enhancing the photocatalytic activity by decreasing the recombination probability of photo-generated charge carriers.⁹ It is well known that higher is the crystallinity, lesser is the amount of defects and hence higher is the photocatalytic activity.³⁵ Finally the third step involves the reduction and oxidation of adsorbed species at the different reaction sites that is hydrogen production take place by the reduction of H^+ ions in CB. Hydrogen evolution by water splitting is promoted by the presence of cocatalysts such as (Pt, Rh, NiO, and RuO_2). These co-catalysts are mainly helpful to introduce the active sites on the photocatalyst surface and hence enhance the process of H_2 generation.

3. Synthesis of graphene and graphene based nanomaterials

Several chemical and physical methods have been developed for the synthesis of graphene and graphene based nanocomposites. The most important method for the graphene synthesis is Hummers method³⁶ which include chemical oxidation of graphite flakes to form graphene oxide (GO). GO contains carboxyl, epoxides and hydroxyl groups supported on the graphene sheet. This leads to the loss of electrical conductivity and limits the application of GO in many areas.³⁷ However the presence of polar functional groups in GO makes it hydrophilic in nature and is responsible for its easy dispersal in many solvents such as water which is helpful for the formation of various composites. The reduction of GO in various reducing conditions form reduced graphene Oxide (RGO) in which electrical conductivity is revived. This RGO is also known as chemical modified graphene or simply graphene.³⁸The composite formation of graphene mainly with semiconductor material has been reported by various methods such as hydrothermal/solvothermal, sol-gel, self-assembly, precipitation and photo-reduction. Some of these methods are elaborated below.

3.1. Hydrothermal/solvothermal method

Hydrothermal/solvothermal method involves the treatment in a confined volume of Teflon-lined autoclave at elevated temperature, wherein high pressure is generated. This method is very important for the synthesis of inorganic nanocrystals and gives rise to highly crystalline nanostructure and also reduces GO to RGO. As the name suggests water is main solvent in hydrothermal method and major advantage of water as solvent is its abundance in nature as well as its

nontoxic, noncarcinogenic and nonflammable nature. However other solvents like ethanol can be the main solvent in solvothermal method. Hence this method involves very simple and ecofriendly process for the synthesis of nanostructures. By controlling some other parameters of starting material such as concentration, the nanocomposites with various exposed crystal facets can be obtained by hydrothermal method.

3.2. Sol-gel method

Sol-gel method is another widely explored method for the synthesis of graphene based nanocomposites. This method is used in the in situ preparation of various semiconductor materials such as TiO₂ on GO sheets. The precursor material undergoes a series of reactions, mainly controlled hydrolysis and condensation, to form the desired photocatalyst. The major advantage of using sol-gel method is the in situ growth of nanostructures so that the various functional groups on the surface of GO sheets are available which provide reactive and anchoring sites for the growth of nanoparticles and hence the resultant photocatalytic materials are chemically bonded with each other.

3.3. Self-assembly

Self-assembly is very important method wherein micro and nanostructures assemble spontaneously by supramolecular interactions to form larger functional units.³⁹ This self-assembly of nanoparticles is very useful for various applications. In the surfactant assisted ternary self-assembly of metal oxides with functionalized graphene sheets, an anionic surfactant gets adsorbed on the surface of graphene sheets and helps in dispersion of graphene sheets. Then, the surfactant micelles with graphene sheets bind with metal cations and hence act as building block for self-assembly of metal oxides. Finally metal oxides get crystallized between alternating layers of graphene to form fine layered nanostructure.³⁶ Self-assembly is important method for constructing the new class of layered nanostructures with stable, ordered and crystalline structure. In layer-by-layer self-assembly of functionalized graphene nanoplatelets, the electrostatic interactions between graphene nanoplatelets are responsible for self-assembly of graphene sheets.

3.4. Other methods

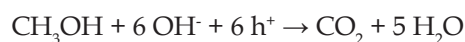
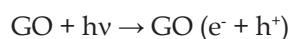
Beside the above mentioned methods, there are also other efficient methods for synthesis of graphene-metal oxide hybrid nanocomposites such as solution mixing⁴⁰ UV assisted reduction⁴¹ microwave irradiation⁴² etc.

4. Role of graphene and graphene based nanocomposites in watersplitting

4.1. Graphene as photocatalyst

Photocatalyst is a substance which shows the catalytic activity using energy from light without undergoing any change in itself⁴³. Photocatalytic activity depends on the generation of electron-hole pairs in the catalyst under the influence of light energy.⁴⁴ These photogenerated charge carriers then generate free radicals such as hydroxyl, superoxide, hydroperoxide which migrate to the surface of catalyst and undergo secondary reactions.⁴⁵ Yeh et al⁴⁶ demonstrated the graphite oxide as photocatalyst for hydrogen generation from water without using any noble metal as cocatalyst. They used the moderately oxidized GO with a band gap of 2.4-4.3 eV which can absorb visible light. Oxidation of graphite introduces many oxygen containing functional groups such as carboxyl, epoxides and hydroxyl groups on its surface which make GO hydrophilic. Thus GO is easily dispersible in water and because of this GO have more exposed area in aqueous solutions and effectively catalyzes the water splitting reaction.

The band gap of GO can be tuned with its oxidation level. Variation of band gap of GO with oxidation level has been illustrated in Fig. 3. Its electrical conductivity decreases with increasing oxidation level means fully oxidized GO acts as insulator and as semiconductor when it is partially oxidized.⁴⁷ Conduction band edge of GO is mainly formed by the anti-bonding π^* orbital which is having higher energy level - 0.52 eV. Thus due to more negative CB edge value which is needed for hydrogen generation, GO can act as photocatalyst. Also the VB edge of GO is mainly composed of O 2p orbitals may not be the positive enough to oxidize water but it varies with reduction degree. It has been observed that band gap of GO decreases with the reduction. It is well reported in the literatures that for GO with 12.5% of the oxygen atoms, top energy level of VB is not high enough to oxidize water for O₂ evolution but at the same time for GO having 25% coverage of oxygen atoms the energy level of CB is high enough for O₂ evolution from water.^{48, 49} Hence by tuning the electronic properties of GO, it can act as a promising material for H₂ generation from water without any co-catalyst. The possible mechanism of water splitting using methanol as scavenger can be summarized as,⁴⁶



Eda et al.⁵⁰ have investigated the insulator

→semiconductor→ semimetal transition in RGO with degree of reduction. Further they find that the energy gap even approaches zero with the extensive degree of reduction. Therefore this possibility of band gap engineering of RGO is always the area of interest for its implementation in various applications. Yeh et al.⁵¹ also demonstrated the photoactivity of GO in hydrogen and oxygen evolution from water with different oxidation levels. They showed that band gap energy of GO increases with increasing oxidation level of GO which limits the light absorption and responsible for the poor photocatalytic activity than GO having narrow band gap energy. It was also observed that during the photocatalytic reaction the H₂ evolution rate was constant but not the O₂ evolution rate. This is mainly because of the reason that GO band gap decreases during the reaction leading to the upward shift of VB. Tend and coworkers⁵² have shown the functionality engineering of GO for tuning its band gap by its treatment with ammonia and explored its photoactivity in water splitting in visible light. Ammonia modified GO (NGO) shows the n-type conductivity due to the introduction of nitrogen functionality. The band gap of NGO is narrowed due to the removal of various epoxy and carboxyl groups and it further act as the promising photocatalyst towards the H₂ and O₂ generation from water splitting.

4.2. Graphene as cocatalyst

Cocatalyst is a substance which assists the catalyst in a chemical reaction and hence enhances the activity of catalyst⁵³. Cocatalysts are generally loaded on the surface of semiconductors as a dispersion of nanoparticles and accelerate the photocatalytic rate by introducing more reaction sites and promoting charge separation in semiconductors⁵⁴. In water splitting reactions, generally noble metals (e.g. Pt, Rh) and some metal oxides (e.g. NiO) act as cocatalyst and these are loaded on the surface of photocatalysts to produce more reactive sites and reduce the activation energy for gas evolution. Cocatalyst also enhances the charge separation in photocatalytic materials because of their high work function. This high work function of noble metals and some metal oxides makes the transfer of electrons from CB of excited semiconductors to cocatalyst and results in the formation of Schottky barrier which efficiently decreases the recombination of charge carriers.⁴ Hence cocatalysts play crucial role in the enhancement of photocatalytic activity by providing abundant reaction sites for H₂ evolution, increasing interfacial charge transfer and reducing the recombination probability of photogenerated electron-hole pairs.⁵⁵ But high cost of noble metals limits their use as co-catalyst on

a large scale. Graphene seems to be best alternative for noble metals. Graphene acts as a promising cocatalyst in H₂ evolution reactions due to its high work function (4.42 eV)⁵⁶ and reduction potential of graphene/graphene \square is reported to be - 0.08 eV which is more negative than reduction potential of H⁺ → H₂.⁵⁷

Role of graphene as cocatalyst has been illustrated by various research groups. Peng et al.⁵⁸ reported on graphene oxide (GO)-CdS nanocomposites, where GO acts as supporting matrix for the CdS nanoparticles which are about 10 nm in size. Due to narrow band gap CdS is active in visible region and they observed the highest H₂ production rate of 314 μ mol/h for the composition having 5 wt% of GO. Herein GO functions as excellent electron acceptor and transporter from CB of excited CdS to reaction sites. Thus graphene reduces the recombination rate of photo generated charge carriers and improves the interfacial charge transfer process which is ultimately responsible for the enhanced activity of photocatalyst. General mechanism for this has been illustrated in Fig. 4a. A similar binary nanocomposite has been reported by Xiang et al.⁵⁹ consisting of graphene modified TiO₂ nanosheets. This composite shows excellent H₂ production rate of 736 μ mol/h with 1wt% of graphene content. Here also the cocatalytic activity of graphene plays key role in better H₂ production. Lv et al.³⁴ demonstrated the cocatalytic activity of doped graphene (Cu-doped graphene/TiO₂ composites). They found the H₂ generation efficiency of Cu-graphene cocatalyst is about 5 times higher than pure graphene cocatalyst. Recently many reports have been published on graphene based ternary composites which are used as cocatalysts for solar water splitting. Ye et al.⁵⁵ have reported CdS/MoS₂/graphene nanocomposites which is active in visible light for hydrogen generation. They reported the hydrogen evolution rate of 1.8 mmol/h in lactic acid solution at 420 nm which is much higher than that of Pt/CdS system in same solution. This high H₂ evolution rate was mainly achieved because of the higher cocatalytic activity of MoS₂/graphene which leads to the more number of reaction sites and fast charge transfer. Moreover in nanosized MoS₂, exposed S atoms have strong affinity to H⁺ ions in solution which are reduced to H₂ by transferred electrons from CB of CdS. The general mechanism for ternary composite has been illustrated in Fig. 4b. Similarly Yu et al.⁶⁰ have reported a noble metal free TiO₂/ MoS₂/graphene system for H₂ generation. This composite prepared by two step hydrothermal process and observed the hydrogen production rate of 165 μ mol/h for composition having 0.5 wt% of cocatalyst. Table 1 shows

Table 1. Different photocatalytic materials where graphene act as cocatalyst

Photocatalyst	Preparation Method	Co-catalyst	Graphene Content (wt %)	Light Source	H ₂ Evolution (μmol/h)	Reference
RGO-TiO ₂	Microwave Hydrothermal	Graphene	1	UV-visible (Xe)	736	[59]
GO-CdS	Precipitation	Graphene	5	λ≥420 nm (Xe)	314	[58]
GO-TNT	Hydrothermal	Graphene	1	λ≥420 nm (Xe)	12.1	[61]
RGO-Cu ₂ O	Precipitation	Graphene	~	λ≥420 nm (Xe)	~	[62]
Cu/GO-TiO ₂	Photodeposition Hydrothermal	Cu-Graphene	2	λ≥400 nm (Xe)	~	[34]
RGO-CdS-ZnO	Solid State	Graphene	1	Visible (TH)	751	[63]
RGO-MoS ₂ -TiO ₂	Hydrothermal	MoS ₂ -RGO	5	UV-visible (Xe)	165.3	[60]
RGO-Zn _x Cd _{1-x} S	Coprecipitation-Hydrothermal	Graphene	0.25	λ=420nm	1824	[57]
GR-MoS ₂ -ZnS	Hydrothermal	GR-MoS ₂	0.25	Xe lamp	2258	[31]
N/RGO-CdS	Solution mixing	N-RGO	2	λ≥400 nm (Xe)	210	[64]

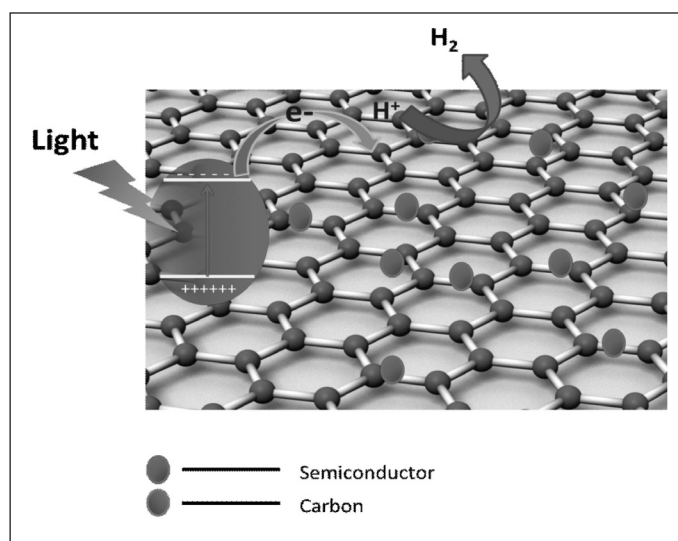


Fig. 4a. Schematic illustrating the cocatalytic activity of GO in graphene-semiconductor binary nanocomposite for H₂ generation.

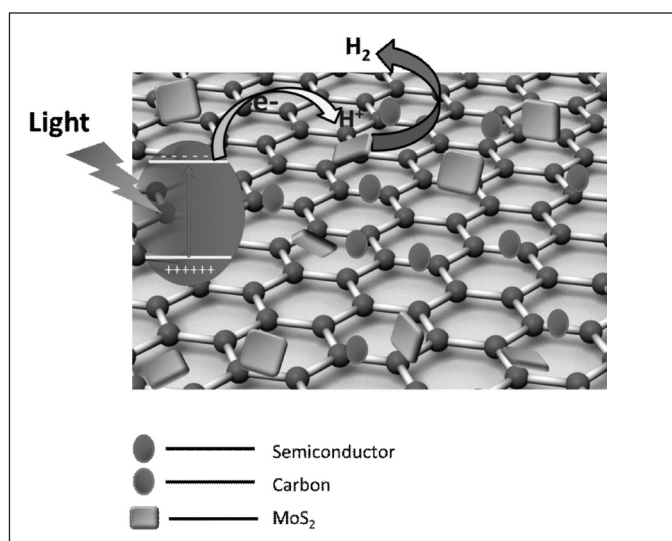


Fig. 4b. Schematic illustrating the cocatalytic activity of GO in graphene-semiconductor-MoS₂ ternary nanocomposite for H₂ generation.

different photocatalyst materials in which graphene act as cocatalyst for water splitting.

4.3. Graphene as photosensitizer

Photosensitizer is a light absorbing substance which mediates reactions either in living cells or in chemical systems.⁶⁵ Hence photosensitizer produces chemical change in another molecule in a photochemical process. So far graphene-semiconductor based composites have been widely explored for H₂ generation in which mainly graphene act as electron acceptor and transporter and

hence enhances the life span of photogenerated charge carriers which leads to the improved H₂ evolution. Besides this, graphene can act as excellent photosensitizer for semiconductors in nanocomposites.⁶⁶ Role of graphene as photosensitizer have been proved theoretically as well as experimentally.^{66, 67} Xu and coworkers⁶⁸ have demonstrated the role of graphene as photosensitizer by reporting graphene-ZnO nanocomposite which is active in visible light. Being a wide band gap semiconductor, ZnO is inactive in the visible light so they explained the photoactivity of this composite on the basis of photosensitizer role of graphene. Under the influence of visible light graphene is

photoexcited from ground state graphene to excited state graphene* to generate electrons which is then injected into the CB of ZnO to make this composite active in visible light. The authors concluded that for better sensitization there should be strong interfacial bonding between the graphene and semiconductor, and self-induced photosensitization such as organic dye sensitization should be avoided.

The photosensitizer role of graphene has been demonstrated in Fig. 5. Du et al.⁶⁶ reported the graphene/titania hybrid nanocomposite and explained the interfacial charge transfer by using density functional calculations. They demonstrated the formation of charge transfer complex at interface of graphene and titania due to work function difference of both material and on visible light irradiation, the electron in the upper VB of graphene can be excited to the CB of titania. As TiO₂ is inactive in visible light the photoactivity is mainly attributed to photosensitizer graphene which generate the charge carriers which is then transferred to reduce the absorbed species on the surface of photocatalyst. Zhang et al.⁶⁹ also explored the photosensitizer role of graphene by reporting the nanosized assembly of ZnS on GO sheets and the interfacial contact between ZnS and GO. They formulated a new photocatalytic mechanism for this visible light driven activity of this nanocomposite. As ZnS itself is not band gap excited and on visible light irradiation photogenerated electron from graphene is transferred to CB of ZnS and hence transform a wide band gap semiconductor to visible light active photocatalyst. Peng and coworkers⁷⁰ fabricated GO-TiO₂ binary nanocomposite by simple hydrothermal method and demonstrated the high visible light driven H₂ evolution from water. Herein they claimed graphene as photosensitizer and efficient interfacial charge transfer is observed on visible light irradiation. Hence on the basis of all above mentioned reports it can be concluded that besides acting as electron reservoir to capture and shuttle the electrons, graphene also act as photosensitizer and transform the UV active semiconductors into visible

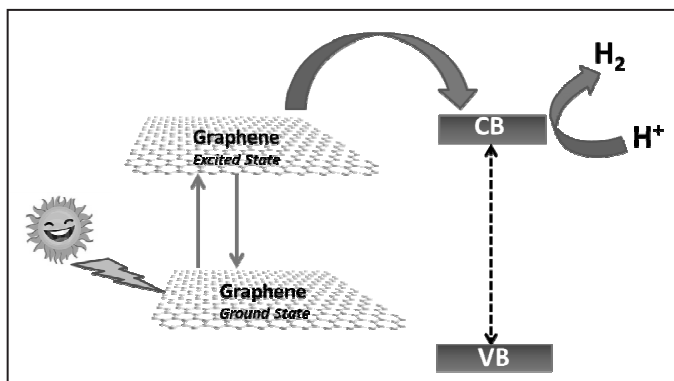


Fig. 5. Schematic illustrating the photosensitizer role of graphene.

light responsive. This photosensitization by graphene has opened many new paths in fabricating new graphene-semiconductor based nanocomposites to explore various photocatalytic applications.

5. Concluding Remarks and Outlook

The combination of excellent properties and the easy availability of graphene has made it one of the most promising material as catalyst for chemical, photochemical and electrochemical reactions. There are thousands of reports available in literature which are mainly devoted to the wide range applications of graphene based composites such as in lithium ion batteries⁷¹⁻⁷⁶, photocatalysts, fuel cells⁷⁷⁻⁸¹, Raman enhancement⁸²⁻⁸⁵, drug delivery⁸⁶⁻⁹⁰, supercapacitors^{79, 80, 91-93}, sensing applications⁹⁴⁻⁹⁸ and photovoltaics⁹⁹⁻¹⁰³. Solar energy harvesting for hydrogen evolution from water is one of the attractive and challenging field in photocatalysis. Due to the huge specific surface area graphene acts as excellent 2D supportive material for metals and metal oxides which results in the formation of some interesting photocatalysts. Tunable optical and electronic properties of graphene have made this a versatile material and it can act as cocatalyst, photocatalyst and photosensitizer, and even exhibit the property of hydrogen evolution by itself. Thus graphene based composites have shown promising results in hydrogen generation as compared to some conventional catalysts as we have described in this review articles.

Despite of all excellent results obtained with graphene and graphene based composites in hydrogen generation, there are some challenges for improving its use in photoelectrocatalytic and photocatalytic hydrogen evolution.

First of all the water splitting reaction is thermodynamically unfavourable reaction as the Gibbs free energy is positive for this reaction and hence to make this reaction feasible and prevent back reaction of hydrogen and oxygen to form water is a big challenge.

Oxidation of graphite flakes introduces various functional groups in graphene oxide which disrupt its electronic structure by several orders of magnitude as compared to pristine graphene. The conductivity is revived when graphene oxide is reduced but various defects remains. Thus fabrication of a novel graphene composite with improved catalytic performance is still a challenge.

The role of graphene as photocatalyst and photosensitizer is also complex in mechanistic way, because generally it has been reported that the enhanced photogenerated charge carriers separation and then charge transfer to CB of semiconductor is responsible

for the activity of the catalyst but many research groups have demonstrated that electron can be transferred from upper VB of graphene to semiconductor as graphene can act as photosensitizer. Such kind of mechanism is not fully understood till date and a detailed study is needed for this particularly interesting interfacial charge transfer in graphene composites.




Hydrogen storage is also a big issue in order to use it as fuel in combustion engines.

Although a huge number of photocatalysts have been explored for hydrogen generation by solar water splitting, but the significant breakthrough in harvesting solar energy still needs to be achieved.

References

- R. Ferroukhi, N. Ghazal-Aswad, S. Androulaki, D. Hawila, T. Mezher, *Int. J. Energy Sector Management*, 2013, **7**, 84.
- P. S. Chasek, D. L. Downie, J. Brown, "Global environmental politics", Westview Press, 2013.
- J. Dufour, D. P. Serrano, J. L. Gálvez, J. Moreno, A. González, *Energy & Fuels*, 2011, **25**, 2194.
- G. Xie, K. Zhang, B. Guo, Q. Liu, L. Fang, J. R. Gong, *Adv. Mater.*, 2013, **25**, 3820.
- J. A. Turner, *Science* 1999, **285**, 687.
- T. Pregger, D. Graf, W. Krewitt, C. Sattler, M. Roeb, S. Möller, *Int. J. of Hydrogen Energy*, 2009, **34**, 4256.
- M. G. Walter, E. L. Warren, J. R. McKone, S. W. Boettcher, Q. Mi, E. A. Santori, N. S. Lewis, *Chem. Rev.*, 2010, **110**, 6446.
- A. Fujishima, K. Honda, *Nature*, 1972, **238**, 37.
- A. Kudo, Y. Miseki, *Chem. Soc. Rev.*, 2009, **38**, 253.
- X. Chen, S. Shen, L. Guo, S. S. Mao, *Chem. Rev.*, 2010, **110**, 6503.
- K. Maeda, K. Domen, *J. Phys. Chem. Letters*, 2010, **1**, 2655.
- M. Ni, M. K. Leung, D. Y. Leung, K. Sumathy, *Renewable and Sustainable Energy Rev*, 2007, **11**, 401.
- K. Domen, A. Kudo, T. Onishi, *J. Catal.*, 1986, **102**, 92.
- A. Kudo, K. Omori, H. Kato, *J. Am. Chem. Soc.*, 1999, **121**, 11459.
- A. Kudo, H. Kato, I. Tsuji, *Chem. Letters*, 2004, **33**, 1534.
- M. Sathish, B. Viswanathan, R. Viswanath, *Int. J. Hydrogen Energy*, 2006, **31**, 891.
- K. Iwashina, A. Kudo, *J. Am. Chem. Soc.*, 2011, **133**, 13272.
- A. Ishikawa, T. Takata, T. Matsumura, J. N. Kondo, M. Hara, H. Kobayashi, K. Domen, *J. Phys. Chem. B*, 2004, **108**, 2637.
- K. Maeda, K. Teramura, N. Saito, Y. Inoue, H. Kobayashi, K. Domen, *Pure and App. Chem.*, 2006, **78**, 2267.
- Z. Zou, J. Ye, K. Sayama, H. Arakawa, *Nature*, 2001, **414**, 625.
- O. Khaselev, J. A. Turner, *Science*, 1998, **280**, 425.
- Q. Xiang, J. Yu, *J. Phys. Chem. Letters*, 2013, **4**, 753.
- M. S. Mauter, M. Elimelech, *Environmental Science & Technology*, 2008, **42**, 5843.
- P. V. Kamat, *Nano Today*, 2006, **1**, 20.
- Q. Xiang, J. Yu, M. Jaroniec, *Chem. Soc. Rev.*, 2012, **41**, 782.
- B. Xia, Y. Yan, X. Wang, X. W. D. Lou, *Materials Horizons*, 2014, **1**, 379.
- J. C. Meyer, A. K. Geim, M. Katsnelson, K. Novoselov, T. Booth, S. Roth, *Nature*, 2007, **446**, 60.
- W. Yuan, B. Li, L. Li, *App. Surface Sci.*, 2011, **257**, 10183.
- X. Huang, X. Qi, F. Boey, H. Zhang, *Chem. Soc. Rev.*, 2012, **41**, 666.
- X. An, C. Y. Jimmy, *RSC Adv.*, 2011, **1**, 1426.
- B. Zhu, B. Lin, Y. Zhou, P. Sun, Q. Yao, Y. Chen, B. Gao, *J. Mater. Chem. A*, 2014, **2**, 3819.
- S. Min, G. Lu, *J. Phys. Chem. C*, 2012, **116**, 25415.
- H. Zhang, X. Lv, Y. Li, Y. Wang, J. Li, *ACS Nano*, 2009, **4**, 380.
- X.-J. Lv, S.-X. Zhou, C. Zhang, H.-X. Chang, Y. Chen, W.-F. Fu, *J. Mater. Chem.*, 2012, **22**, 18542.
- B. Ohtani, Y. Ogawa, S.-i. Nishimoto, *J. Phys. Chem. B*, 1997, **101**, 3746.
- W. Hummers, R. Offeman, *J. Am. Chem. Soc.*, 1958, **80**, 1339.
- S. Stankovich, D. A. Dikin, R. D. Piner, K. A. Kohlhaas, A. Kleinhammes, Y. Jia, Y. Wu, S. T. Nguyen, R. S. Ruoff, *Carbon*, 2007, **45**, 1558.
- C. Gómez-Navarro, R. T. Weitz, A. M. Bittner, M. Scolari, A. Mews, M. Burghard, K. Kern, *Nano letters*, 2007, **7**, 3499.
- N. Stephanopoulos, J. H. Ortony, S. I. Stupp, *Acta Materialia*, 2013, **61**, 912.
- H.-i. Kim, G.-h. Moon, D. Monllor-Satoca, Y. Park, W. Choi, *J. Phys. Chem. C*, 2011, **116**, 1535.
- W. Fan, Q. Lai, Q. Zhang, Y. Wang, *J. Phys. Chem. C*, 2011, **115**, 10694.
- K. Ullah, Z. Lei, S. Ye, A. Ali, W.-C. Oh, *RSC Adv.*, 2015, **5**, 18841.
- K. Maeda, K. Teramura, D. Lu, T. Takata, N. Saito, Y. Inoue, K. Domen, *Nature*, 2006, **440**, 295.
- O. Carp, C. L. Huisman, A. Reller, *Progress in Solid State Chem.*, 2004, **32**, 33.
- S. Banerjee, S. C. Pillai, P. Falaras, K. E. O'shea, J. A. Byrne, D. D. Dionysiou, *J Phys. Chem. Lett.*, 2014, **5**, 2543.
- T. F. Yeh, J. M. Syu, C. Cheng, T. H. Chang, H. Teng, *Adv. Functional Mater.*, 2010, **20**, 2255.
- R. Lahaye, H. Jeong, C. Park, Y. Lee, *Phys. Rev. B*, 2009, **79**, 125435.
- M. Shishkin, G. Kresse, *Phys. Rev. B*, 2006, **74**, 035101.
- M. Shishkin, G. Kresse, *Phys. Rev. B*, 2007, **75**, 235102.
- G. Eda, C. Mattevi, H. Yamaguchi, H. Kim, M. Chhowalla, *J. Phys. Chem. C*, 2009, **113**, 15768.
- T.-F. Yeh, F.-F. Chan, C.-T. Hsieh, H. Teng, *J. Phys. Chem. C*, 2011, **115**, 22587.
- T.-F. Yeh, S.-J. Chen, C.-S. Yeh, H. Teng, *J. Phys. Chem. C*, 2013, **117**, 6516.
- X. Zong, H. Yan, G. Wu, G. Ma, F. Wen, L. Wang, C. Li, *J. Am. Chem. Soc.*, 2008, **130**, 7176.
- J. Yang, D. Wang, H. Han, C. Li, *Acc. of Chem. Res.*, 2013, **46**,

- 1900.
55. K. Chang, Z. Mei, T. Wang, Q. Kang, S. Ouyang, J. Ye, *ACS Nano*, 2014, **8**, 7078.
 56. X. Wang, L. Zhi, K. Müllen, *Nano letters*, 2008, **8**, 323.
 57. J. Zhang, J. Yu, M. Jaroniec, J. R. Gong, *Nano letters*, 2012, **12**, 4584.
 58. T. Peng, K. Li, P. Zeng, Q. Zhang, X. Zhang, *J. Phys. Chem. C*, 2012, **116**, 22720.
 59. Q. Xiang, J. Yu, M. Jaroniec, *Nanoscale*, 2011, **3**, 3670.
 60. Q. Xiang, J. Yu, M. Jaroniec, *J. Am. Chem. Soc.*, 2012, **134**, 6575.
 61. H. Dang, X. Dong, Y. Dong, J. Huang, *Int. J. Hydrogen Energy*, 2013, **38**, 9178.
 62. P. D. Tran, S. K. Batabyal, S. S. Pramana, J. Barber, L. H. Wong, S. C. J. Loo, *Nanoscale*, 2012, **4**, 3875.
 63. Z. Khan, T. R. Chetia, A. K. Vardhaman, D. Barpuzary, C. V. Sastri, M. Qureshi, *RSC Adv*, 2012, **2**, 12122.
 64. L. Jia, D.-H. Wang, Y.-X. Huang, A.-W. Xu, H.-Q. Yu, *J. Phys. Chem. C*, 2011, **115**, 11466.
 65. P. Zhang, W. Steelant, M. Kumar, M. Scholfield, *J. Am. Chem. Soc.*, 2007, **129**, 4526.
 66. A. Du, Y. H. Ng, N. J. Bell, Z. Zhu, R. Amal, S. C. Smith, *J. Phys. Chem. Letters*, 2011, **2**, 894.
 67. K. K. Manga, Y. Zhou, Y. Yan, K. P. Loh, *Adv. Functional Mater*, 2009, **19**, 3638.
 68. M.-Q. Yang, Y.-J. Xu, *J. Phys. Chem. C*, 2013, **117**, 21724.
 69. Y. Zhang, N. Zhang, Z.-R. Tang, Y.-J. Xu, *ACS Nano*, 2012, **6**, 9777.
 70. P. Zeng, Q. Zhang, X. Zhang, T. Peng, *J. Alloys and Compounds*, 2012, **516**, 85.
 71. H. Wang, L.-F. Cui, Y. Yang, H. Sanchez Casalongue, J. T. Robinson, Y. Liang, Y. Cui, H. Dai, *J. Am. Chem.Soc.*, 2010, **132**, 13978.
 72. Z.-S. Wu, W. Ren, L. Wen, L. Gao, J. Zhao, Z. Chen, G. Zhou, F. Li, H.-M. Cheng, *ACS Nano*, 2010, **4**, 3187.
 73. G. Zhou, D.-W. Wang, F. Li, L. Zhang, N. Li, Z.-S. Wu, L. Wen, G. Q. Lu, H.-M. Cheng, *Chem. of Mater.*, 2010, **22**, 5306.
 74. K. Chang, W. Chen, *ACS Nano*, 2011, **5**, 4720.
 75. B. Li, H. Cao, J. Shao, G. Li, M. Qu, G. Yin, *Inorg. Chem.*, 2011, **50**, 1628.
 76. J. Z. Wang, C. Zhong, D. Wexler, N. H. Idris, Z. X. Wang, L. Q. Chen, H. K. Liu, *Chem.-A European J.*, 2011, **17**, 661.
 77. B. Seger, P. V. Kamat, *J. Phys. Chem. C*, 2009, **113**, 7990.
 78. H. Huang, H. Chen, D. Sun, X. Wang, *J. Power Sources*, 2012, **204**, 46.
 79. J. Hou, Y. Shao, M. W. Ellis, R. B. Moore, B. Yi, *Phys. Chem. Chem. Phys.*, 2011, **13**, 15384.
 80. H.-J. Choi, S.-M. Jung, J.-M. Seo, D. W. Chang, L. Dai, J.-B. Baek, *Nano Energy*, 2012, **1**, 534.
 81. Y.-C. Yong, X.-C. Dong, M. B. Chan-Park, H. Song, P. Chen, *ACS Nano*, 2012, **6**, 2394.
 82. K. Jasuja, V. Berry, *ACS Nano*, 2009, **3**, 2358.
 83. Z. Zhang, F. Xu, W. Yang, M. Guo, X. Wang, B. Zhang, J. Tang, *Chem. Comm.*, 2011, **47**, 6440.
 84. J. Huang, L. Zhang, B. Chen, N. Ji, F. Chen, Y. Zhang, *Nanoscale*, 2010, **2**, 2733.
 85. S. Murphy, L. Huang, P. V. Kamat, *J. Phys. Chem. C*, 2013, **117**, 4740.
 86. X. Sun, Z. Liu, K. Welsher, J. T. Robinson, A. Goodwin, S. Zaric, H. Dai, *Nano Research*, 2008, **1**, 203.
 87. X. Li, X. Huang, D. Liu, X. Wang, S. Song, L. Zhou, H. Zhang, *J. Phys. Chem. C*, 2011, **115**, 21567.
 88. Z. Liu, J. T. Robinson, X. Sun, H. Dai, *J. Am. Chem.Soc.*, 2008, **130**, 10876.
 89. Y. Pan, H. Bao, N. G. Sahoo, T. Wu, L. Li, *Adv. Func.Mater.*, 2011, **21**, 2754.
 90. S. Goenka, V. Sant, S. Sant, *J. Controlled Release*, 2014, **173**, 75.
 91. Y. Wu, S. Liu, H. Wang, X. Wang, X. Zhang, G. Jin, *Electrochimica Acta*, 2013, **90**, 210.
 92. K. Zhang, L. L. Zhang, X. Zhao, J. Wu, *Chem.of Mater.*, 2010, **22**, 1392.
 93. Q. Wu, Y. Xu, Z. Yao, A. Liu, G. Shi, *ACS Nano*, 2010, **4**, 1963.
 94. W. Hong, H. Bai, Y. Xu, Z. Yao, Z. Gu, G. Shi, *J. Phys. Chem. C*, 2010, **114**, 1822.
 95. X. An, C. Y. Jimmy, Y. Wang, Y. Hu, X. Yu, G. Zhang, *J. Mater. Chem.*, 2012, **22**, 8525.
 96. C. Shan, H. Yang, J. Song, D. Han, A. Ivaska, L. Niu, *Anal. Chem.*, 2009, **81**, 2378.
 97. Y. Shao, J. Wang, H. Wu, J. Liu, I. A. Aksay, Y. Lin, *Electroanalysis*, 2010, **22**, 1027.
 98. S. Guo, D. Wen, Y. Zhai, S. Dong, E. Wang, *ACS Nano*, 2010, **4**, 3959.
 99. Z. Liu, Q. Liu, Y. Huang, Y. Ma, S. Yin, X. Zhang, W. Sun, Y. Chen, *Adv. Mater.*, 2008, **20**, 3924.
 100. Z. Peining, A. S. Nair, P. Shengjie, Y. Shengyuan, S. Ramakrishna, *ACS App. Mater. & Interfaces*, 2012, **4**, 581.
 101. Q. Liu, Z. Liu, X. Zhang, L. Yang, N. Zhang, G. Pan, S. Yin, Y. Chen, J. Wei, *Adv. Functional Mater.*, 2009, **19**, 894.
 102. Y. H. Ng, I. V. Lightcap, K. Goodwin, M. Matsumura, P. V. Kamat, *J. Phys. Chem. Letters*, 2010, **1**, 2222.
 103. J. Fan, S. Liu, J. Yu, *J.Mater. Chem.*, 2012, **22**, 17027.

	<p>Mr. Suneel Kumar hails from Salooni in Himachal Pradesh and is currently a Ph.D. student at the Indian Institute of Technology Mandi working with Dr. Venkata Krishnan. Previously, he received his B.Sc. and M.Sc. degrees in chemistry from Himachal Pradesh University, Shimla in 2011 and 2013, respectively. His main research interest is in the field of semiconductor based photocatalysis and artificial photosynthesis, involving the design and development of efficient photocatalysts for water splitting applications based on biomimetic approaches.</p>
	<p>Mr. Vipul Sharma hails from Chamba in Himachal Pradesh and is currently a Ph.D. student at the Indian Institute of Technology Mandi working with Dr. Venkata Krishnan. Previously, he received his M.Tech. degree in nanoscience and nanotechnology from Amity University, Noida in 2012. His main research interest is in the field of fabrication and characterization of biomimetic functional surfaces for technological applications, including fog harvesting, surface enhanced Raman scattering (SERS), photocatalysis, etc.</p>
	<p>Dr. Venkata Krishnan is currently working as an assistant professor in the school of basic sciences at Indian Institute of Technology Mandi since April 2012. Dr. Krishnan did his B.Sc. and M.Sc. from P.S.G. College of Technology, Coimbatore, Tamil Nadu. Later he obtained his Ph.D. in physical chemistry in 2006 from the University of Stuttgart in Germany. Subsequently, he worked as a postdoctoral researcher from 2006 to 2010 at the University of Pennsylvania in U.S.A. and then as a research associate from 2010 to 2012 at the National Institute for Materials Science, Tsukuba, Japan. During his academic career, he has received several fellowships and awards including, DFG doctoral fellowship, DAAD fellowship, DOE postdoctoral fellowship and MANA research fellowship, in addition to proficiency award, best outgoing student award and best project award during his graduation period. He has also received the DST INSPIRE faculty award in chemical sciences in 2011 and IIT Mandi foundation day award for excellence in teaching in 2013. His main research interest is in the field of bioinspired functional materials including biomimetic approaches to artificial photosynthesis, biomimetic functional surfaces for technological applications, bioinspired materials for green catalysis and photovoltaics. He has published 33 research articles in reputed international journals, and has participated in several conferences and presented numerous posters and talks.</p>

Effect of Aliovalent Chlorine Doping on the Thermoelectric Properties of n -type $\text{AgBi}_{0.5}\text{Sb}_{0.5}\text{Se}_2$

Satya N. Guin, Sohang Kundu and Kanishka Biswas*

New Chemistry Unit, Jawaharlal Nehru Centre for Advanced Scientific Research (JNCASR),

Jakkur P.O., Bangalore 560064, India

Email: kanishka@jncasr.ac.in

Abstract:

Thermoelectric is an environment-friendly technology, enables the direct conversion of waste heat to electricity and can provide sustainable energy supply as the sources of non-renewable energy are rapidly dwindling. In the present paper we discuss the thermoelectric property of n -type $\text{AgBi}_{0.5}\text{Sb}_{0.5}\text{Se}_2$ system, which is a lead (Pb) and tellurium (Te)- free compound. We show that aliovalent chlorine can acts as an n -type dopant in the present system and increases the electrical conductivity, which results in an increase of the power factor ($S^2\sigma$) at high temperatures. High degree of anharmonicity in the bonding arrangements and presence of disordered cation sublattice effectively scatter heat carrying phonon and decreases the thermal conductivity. A maximum ZT of 0.45 at 708 K was achieved in n -type $\text{AgBi}_{0.5}\text{Sb}_{0.5}\text{Se}_{1.98}\text{Cl}_{0.2}$ crystalline ingot.

Introduction.

In the wake of the intransigent escalation in the depletion of non-renewable energy resources the world faces today, it is of dire need to find means of generating energy from nonpolluting and nonconventional sources.¹⁻⁸ The energy crisis issue has often found its answers in renewable energy resources such as tidal, solar, wind, geothermal and biomass etc. Apart from all these sources thermoelectric energy conversion form waste heat will play an important role for the future energy management.¹⁻⁵ In 1821, Baltic German scientist Thomas Johann Seebeck first discovered that a loop formed by two different metals when subjected to a difference in temperature across its two junctions can generate an electric potential difference.¹⁻³ This effect found its place in textbooks in the name of Seebeck effect.¹⁻⁶ This unique property of some materials to be able to convert a temperature gradient to a considerable potential gradient is a convincing remedy that might take us a step forward in reconciling the upset our earth finds itself in. These materials are hence called thermoelectric materials.¹⁻⁸

Over the past few years, there has been a steady growth in interest of the scientific community in this field of research and a library of compounds have proven their worth to be promising thermoelectric materials that could find their application in appliances and gadgets of the future. The efficiency of an intrinsic thermoelectric material is related to the well-known Carnot Efficiency by virtue of a dimensionless quantity called Thermoelectric Fig. of Merit, ZT . The efficiency (η) of this type of materials is given by the following relation.^{1,3,4}

$$\eta = \frac{\Delta T}{T_H} \frac{\sqrt{1 + (ZT)_{m,avg}} - 1}{\sqrt{1 + (ZT)_{m,avg}} + \frac{T_C}{T_H}}$$

where ZT is the thermoelectric Fig. of merit, T_{hot} and T_{cold} the respective temperatures of the hot and cold junctions and ΔT the difference between them. The dimensionless thermoelectric Fig. of merit (ZT) of thermoelectric materials can be expressed in terms of three very fundamental materials' properties as they are called

$$ZT = \sigma S^2 T / \kappa_{total}$$

where σ is the electrical conductivity, S the Seebeck coefficient, T the absolute temperature and κ_{total} the total thermal conductivity of the material under consideration. The quantity σS^2 , called the power factor together with the total thermal conductivity of the material given by $\kappa_{total} = \kappa_{el} + \kappa_{lat}$, where, κ_{el} and κ_{lat} being the electronic and lattice thermal conductivities of a material respectively.¹⁻⁸

Thermoelectric devices currently available have a ZT_{avg} of 1 and operate at an efficiency of $\sim 10\%$.² The only way out to make these materials more efficient is to devise a way to increase the ZT . The challenge to create high ZT thermoelectric materials lies in achieving simultaneously high electronic conductivity (σ), high thermopower (S) and low thermal conductivity (κ) in the same material.¹⁻⁶ This indeed is a challenging task, stemming from the fact that the desired material under consideration must have thermal conduction properties like glass, electronic transport properties like a metal, and a high Seebeck coefficient characteristic of semiconductors. In previous

years several new concepts have been implemented to get control over the carrier and phonon transport in the materials. Introduction of resonance levels,^{9,10} band convergence,¹¹ quantum confinement effects¹² and electron energy barrier filtering¹³ are some very well applied strategies to get control over carrier transport by the modification of electronic structure of materials. Lattice thermal conductivity (κ_{lat}) is independent of the electrical transport of the material via Weidemann Franz law, $\kappa_{\text{lat}} = \kappa_{\text{total}} - L\sigma T$; where L is Lorenz number. Thus, different approaches also been taken to reduce the κ_{lat} .¹⁻⁴ Some of the most effective ways are, solid solution alloying, second phase nanostructuring, and the all scale phonon scattering approach.^{7,14-16} By utilizing critical phase transitions or intrinsic low thermal conductivity value a high ZT value can be achieved in a single phase material.¹⁷

Thermoelectric research gained impetus around the last decade of the 20th century. For the power generation application purpose some of the well-known systems are PbTe,^{7,14} PbSe,^{18,19} SnTe,^{10,20,21,22} SnSe,⁸ AgSbTe₂,²³ AgSbSe₂,^{25,26,27,28,29} AgBiSe₂,^{30,31,32} Cu₂Se,³³ filled skutterudite,³⁴ hausler compounds³⁵. Moreover, Bi₂Te₃ based materials are well-known for their room temperature applications.^{16,36} Further research beyond these traditional well-known materials has brought into light, a family of I-V-VI₂ (where I = Cu, Ag, Au or alkali metal; V = As, Sb, Bi; and VI = Se, Te) system of semiconductors, which renowned for their intrinsically extremely low thermal conductivity finding its origin in the strong anharmonicity in the bonding patterns.^{25,37,38} Recent theoretical estimations and further calculations have showed that the lone pair on the Group V atom in these compounds is present in the stereochemically active ns orbital and hence leads to strong lattice deformation, thus lowering the thermal conductivity.^{37,38} Rosi *et al.*'s discovery, AgSbTe₂ proves to be the first of such compounds showing a ZT value of 1.3 at 720 K.²³ Further modifications of the compound have also met with success. Interestingly, alloy of AgSbTe₂ with GeTe (TAGS)³⁹ and PbTe (LAST-m)¹⁵ showed extraordinary ZT values of 1.5 at 750 K and 1.8 at 800 K, respectively. However, Te compounds prove to be toxic, highly expensive and of extremely low price stability owing to the low abundance of Te in the earth's crust.

The next obvious and overwhelmingly attractive alternative in terms of choice of materials seems to be Se, lying immediately above Te in the Periodic Table. Se being less toxic and cheaper with higher price stability as it is 50 times more abundant in the earth's crust, analogous compounds received attention. AgSbSe₂, an intrinsic p -type system, belongs to I-V-VI₂ class is a very promising

system. A ZT value more than unity has been reported for cation doped AgSbSe₂.^{25,26,27,28,29} Nanostructuring, carrier engineering and bond anharmonicity were found to synergistically boost the thermoelectric performance of p -type AgSbSe₂-ZnSe at 640K to provide a ZT value of 1.1.²⁶ More recently we have shown that Sb vacancy can also increase p -type carrier concentration in AgSbSe₂ and boost the thermoelectric performance. In recent times, ZT values as high as ~ 1 at temperature around 773 K has also been reported in n -type Nb doped and aliovalent anion doped bulk AgBiSe₂. Solution grown nanocrystalline AgBiSe₂ also boasts of a promising ZT value with an interesting p - n - p type conduction.

Silver bismuth selenide, AgBiSe₂, an n -type semiconductor in bulk phase, known to display temperature dependent structural phase transition (Fig. 1a). At room temperature AgBiSe₂ crystallize in a cento-symmetric ordered hexagonal phase (space group $Pm-31$) $a = 4.194 \text{ \AA}$, $c = 19.65 \text{ \AA}$.^{30,32} At 410 K it undergoes hexagonal-rhombohedral ($R-3m$ space group with lattice constant, $a = 7.022 \text{ \AA}$) structural and at 580 K rhombohedral-cubic (space group $Fm-3m$, $a = 5.832 \text{ \AA}$) transition takes place.^{30,32} The rhombohedral having ordered Ag and Bi atoms in distinguishable positions, while in the high temperature cubic phase, the Ag and Bi atoms are disordered in the lattice site. Due to this high degree of disorderness and presence of stereochemically active lone pair of electron in Bi atom cubic phase shows very low thermal conductivity.³⁰ It is also known that high symmetry in crystals structure results high band degeneracy in the electronic crystal structure and has an effect to increase the ZT value.³ Hence, stabilization of the high temperature phase cubic phase of AgBiSe₂ at room temperature is important to increase its working temperature range.

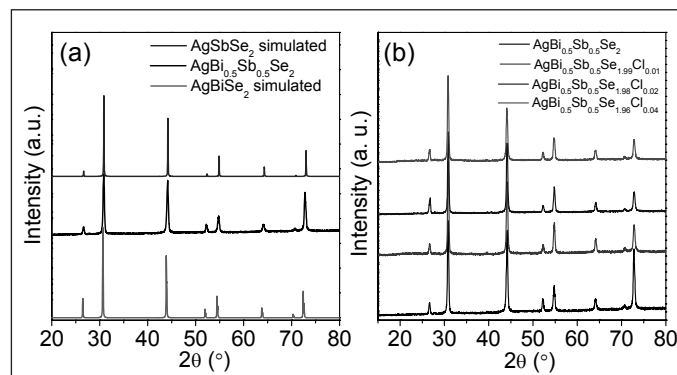


Fig. 1: Room temperature powder XRD (PXR) pattern of AgBi_{0.5}Sb_{0.5}Se₂ with cubic AgBiSe₂ and AgSbSe₂, (b) PXR pattern of AgBi_{0.5}Sb_{0.5}Se₂ and AgBi_{0.5}Sb_{0.5}Se_{2-x}Cl_x ($x = 0.01, 0.02$ and 0.04) samples.

The earlier observation has opened up an interest in the composition of $\text{AgBi}_x\text{Sb}_{1-x}\text{Se}_2$. $\text{AgBi}_x\text{Sb}_{1-x}\text{Se}_2$ is a solid solution of AgBiSe_2 and AgSbSe_2 .³² It has been shown that, with incorporation of Sb in Bi position of AgBiSe_2 , the crystal system changes towards cubic structure. In cubic $\text{AgBi}_x\text{Sb}_{1-x}\text{Se}_2$ system, Ag, Bi and Sb remains disordered in lattice site and similar to AgSbSe_2 , AgBiSe_2 , presence of $5s^2$ and $6s^2$ of Sb and Bi respectively lone pair creates high degree of anharmonicity in the bonding arrangement.³² Recently it has been shown *p*-type solid-solutioned homojunction nanoplates of $\text{AgBi}_{0.5}\text{Sb}_{0.5}\text{Se}_2$ shows a very promising *ZT* value of 1.1 at 550 K due to ultralow thermal conductivity.³² However, in literature no report discusses on the synthesis and thermoelectric property of bulk $\text{AgBi}_{0.5}\text{Sb}_{0.5}\text{Se}_2$.

Here, we report synthesis and thermoelectric property of high quality bulk crystalline ingots of *n*-type $\text{AgBi}_{0.5}\text{Sb}_{0.5}\text{Se}_2$. The electrical transport is moderate and hence the choice of various dopant systems to improve the thermoelectric Fig. of merit. We show that Cl acts as an effective *n*-type dopant and increases the electrical conductivity, which results in an increase of the power factor ($S^2\sigma$) of $\text{AgBi}_{0.5}\text{Sb}_{0.5}\text{Se}_2$. We could achieve a maximum *ZT* of 0.45 at 708 K in the case of *n*-type $\text{AgBi}_{0.5}\text{Sb}_{0.5}\text{Se}_{1.98}\text{Cl}_{0.02}$ crystalline ingot due to high power factor and intrinsically low thermal conductivity, which is significantly higher than pristine $\text{AgBi}_{0.5}\text{Sb}_{0.5}\text{Se}_2$ (*ZT* ~0.25 at 708 K).

Experimental section.

Materials. Elemental silver (Ag, 99.999%, metal basis), elemental bismuth (Bi, 99.9999%, metal basis), elemental antimony (Sb, 99.9999%, metal basis), elemental selenium (Se, 99.999%, metal basis), bismuth chloride (BiCl_3 , 99.999%), were purchased from Alfa Aesar and used as purchased.

Synthesis. Ingots (~7 g) of pristine $\text{AgBi}_{0.5}\text{Sb}_{0.5}\text{Se}_2$ and $\text{AgBi}_{0.5}\text{Sb}_{0.5}\text{Se}_{2-x}\text{Cl}_x$ ($x=2-4$ mol%) were synthesized by mixing appropriate ratios of high-purity starting materials of Ag, Bi, Sb BiCl_3 and Se in quartz tube. The tubes were sealed under high vacuum ($\sim 10^{-5}$ Torr) and slowly heated up to 673 K over 12 h, then heated up to 1123 K in 4 h, soaked for 10 h, and subsequently slow cooled to room temperature over a period of 12 hrs. For electrical and thermal transport measurements the samples were cut and polished in bar and disk shape. Bar-shaped sample is used for simultaneous electrical conductivity and Seebeck coefficient measurement, whereas disk-shaped sample is used for thermal conductivity measurement.

Powder X-ray diffraction. Powder X-ray diffraction for all the samples were recorded using a laboratory Bruker

D8 diffractometer with Cu K_α ($\lambda = 1.5406 \text{ \AA}$) radiation at room temperature.

Band gap. To probe optical energy gap, optical diffuse reflectance measurements has been performed on finely ground powders at room temperature. The spectra were recorded over the range of 500 nm to 2500 nm using a Perkin Elmer Lambda 900, UV/Vis/NIR spectrometer. Absorption (α/Λ) data was calculated from reflectance data using Kubelka-Munk equation: $\alpha/\Lambda = (1-R)^2/(2R)$, where *R* is the reflectance and α and Λ are the absorption and scattering coefficients, respectively.

Electrical transport. Electrical conductivity and Seebeck coefficient were measured simultaneously under helium atmosphere from room temperature to ~710 K on a ULVAC RIKO ZEM-3 instrument system. The typical sample for measurement has a rectangular shape with the approximate dimension of 2 mm × 2 mm × 8 mm. Heating and cooling cycles give repeatable electrical properties for a given sample.

Thermal transport. For thermal diffusivity, *D* measurement a Netzsch LFA-457 laser flash instrument used for measurement in the range 300-723 K under N_2 atmosphere. Coins with ~8 mm diameter and ~2 mm thickness were used for the measurement. Temperature dependent heat capacity, C_p , was derived using a standard sample (pyroceram) in LFA457. The total thermal conductivity, κ_{total} was calculated using the formula, $\kappa_{total} = DC_p\rho$, where ρ is the density of the sample, measured using sample dimension and mass. The density of the pellets is ~98 % of the theoretical density.

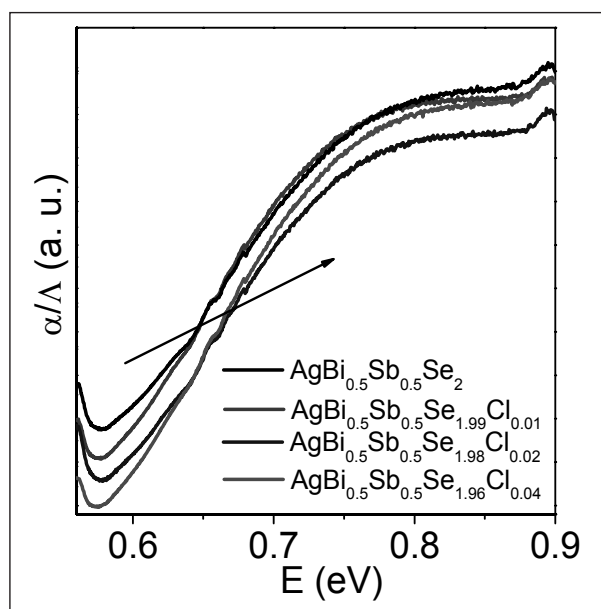


Fig. 2: Optical absorption spectra of $\text{AgBi}_{0.5}\text{Sb}_{0.5}\text{Se}_2$ and $\text{AgBi}_{0.5}\text{Sb}_{0.5}\text{Se}_{2-x}\text{Cl}_x$ ($x=0.01, 0.02$ and 0.04) samples.

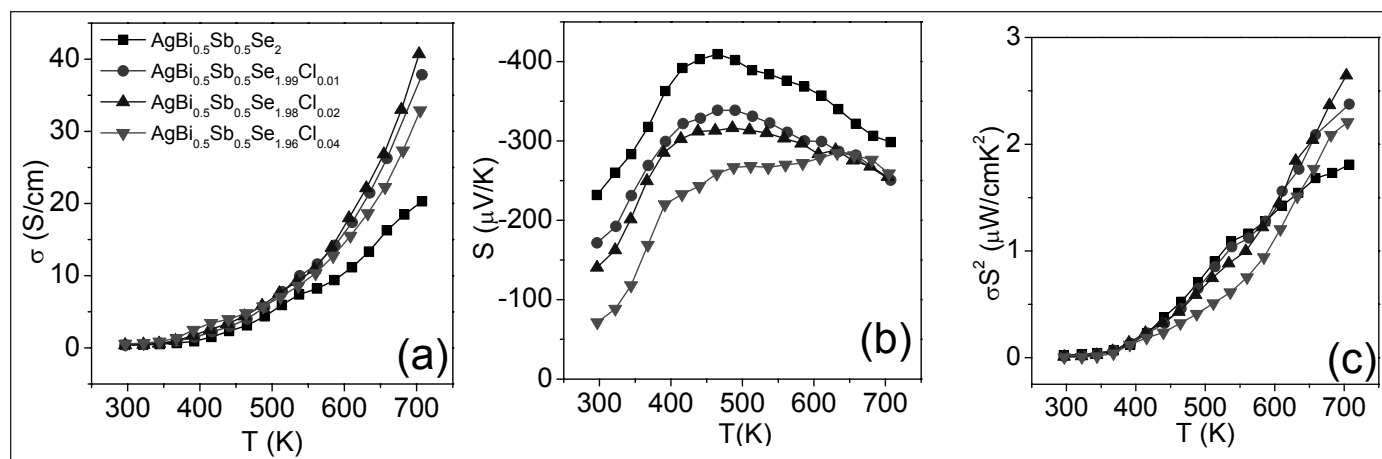


Fig. 3: Temperature dependent (a) electrical conductivity (σ), (b) Seebeck coefficient (S), and (c) power factor (σS^2) of $\text{AgBi}_{0.5}\text{Sb}_{0.5}\text{Se}_2$ and $\text{AgBi}_{0.5}\text{Sb}_{0.5}\text{Se}_{2-x}\text{Cl}_x$ ($x=0.01, 0.02$ and 0.04) samples.

Results and discussion.

Room temperature powder XRD pattern of pristine $\text{AgBi}_{0.5}\text{Sb}_{0.5}\text{Se}_2$ and $\text{AgBi}_{0.5}\text{Sb}_{0.5}\text{Se}_{2-x}\text{Cl}_x$ ($x=2-4$ mol%) samples presented in Fig. 1. It has been observed that the peaks for $\text{AgBi}_{0.5}\text{Sb}_{0.5}\text{Se}_2$ lie exactly in the middle of cubic phase of AgSbSe_2 and AgBiSe_2 , indicates perfect solid solution nature of the sample (Fig. 1a). No impurity phase being observed for $\text{AgBi}_{0.5}\text{Sb}_{0.5}\text{Se}_{2-x}\text{Cl}_x$ ($x=2-4$ mol%) samples within the detection limits of powder XRD indicates successful substitution of halogen in the Se site of $\text{AgBi}_{0.5}\text{Sb}_{0.5}\text{Se}_2$ (Fig. 1b).

In Fig. 2, we present room temperature optical absorption spectra of pristine $\text{AgBi}_{0.5}\text{Sb}_{0.5}\text{Se}_2$ and $\text{AgBi}_{0.5}\text{Sb}_{0.5}\text{Se}_{2-x}\text{Cl}_x$ (2-4 mol%) samples. The spectroscopically measured band gap of the pristine $\text{AgBi}_{0.5}\text{Sb}_{0.5}\text{Se}_2$ is ~ 0.56 eV. The band gap for $\text{AgBi}_{0.5}\text{Sb}_{0.5}\text{Se}_{2-x}\text{Cl}_x$ ($x=2-4$ mol%) are slightly blue shifted compared to that of for pristine sample. The higher band gap in chlorine doped samples is due to higher electronegativity of the chlorine ($\text{Cl} = 3.16$, in Pauling scale) than selenium (2.55 , in Pauling scale), which results higher ionic character of the metal-halogen bond than the metal-selenium bond. Increase of the ionic character in the bond results increase of the band gap for $\text{AgBi}_{0.5}\text{Sb}_{0.5}\text{Se}_{2-x}\text{Cl}_x$ ($x=2-4$ mol%). This result supports the successful substitution of chlorine in the Se site of $\text{AgBi}_{0.5}\text{Sb}_{0.5}\text{Se}_2$.

Temperature dependent electronic transport properties of pristine $\text{AgBi}_{0.5}\text{Sb}_{0.5}\text{Se}_2$ and $\text{AgBi}_{0.5}\text{Sb}_{0.5}\text{Se}_{2-x}\text{Cl}_x$ ($x=2-4$ mol%) samples have been presented in Fig. 3. In Fig. 3(a), we show temperature dependent electrical conductivity (σ) of $\text{AgBi}_{0.5}\text{Sb}_{0.5}\text{Se}_2$ and $\text{AgBi}_{0.5}\text{Sb}_{0.5}\text{Se}_{2-x}\text{Cl}_x$ ($x=2-4$ mol%). An σ value of ~ 0.4 S/cm has been measured at room temperature for pristine $\text{AgBi}_{0.5}\text{Sb}_{0.5}\text{Se}_2$, which increase to ~ 20 S/cm at 708 K. σ value for chlorine doped sample is remain almost same at room temperature, however at

elevated temperature is shows much higher value as that of for pristine sample. Typically, $\text{AgBi}_{0.5}\text{Sb}_{0.5}\text{Se}_{1.98}\text{Cl}_{0.02}$ sample shows a σ of ~ 40 S/cm at 708 K, Thus, the measured higher σ of $\text{AgBi}_{0.5}\text{Sb}_{0.5}\text{Se}_{2-x}\text{Cl}_x$ ($x=2-4$ mol%) samples is due to the substitution of Cl ion in Se^{2-} . Overall the results indicate that chlorine doping can enhance the electrical conductivity of $\text{AgBi}_{0.5}\text{Sb}_{0.5}\text{Se}_2$ by injecting electron in the conduction band of $\text{AgBi}_{0.5}\text{Sb}_{0.5}\text{Se}_2$.

The negative sign of the S indicates n -type conduction in all the samples (Fig. 3b). However, the conduction type for the nanocrystalline sample is p -type in nature. Formation of defects due to solution phase synthesis may be reasons for this difference. The S value for pristine $\text{AgBi}_{0.5}\text{Sb}_{0.5}\text{Se}_2$ is -231 $\mu\text{V/K}$ at room temperature, which increases to a value of -408 $\mu\text{V/K}$ at 468 K and reaches to a value of -296 $\mu\text{V/K}$ at ~ 710 K. Chlorine doping in $\text{AgBi}_{0.5}\text{Sb}_{0.5}\text{Se}_2$ has a significant effect on the temperature dependent seebeck coefficient. All the Chlorine doped samples show lower S values than that of for pristine $\text{AgBi}_{0.5}\text{Sb}_{0.5}\text{Se}_2$. The decrease in the Seebeck coefficient after halogen doping is due to increase in the carrier concentration in the system as, S is inversely related to the carrier concentration (n), $S \sim n^{-2/3}$. Typically, $\text{AgBi}_{0.5}\text{Sb}_{0.5}\text{Se}_{1.98}\text{Cl}_{0.02}$ sample shows an S value of -140 $\mu\text{V/K}$ at room temperature, which increase to value of -313 $\mu\text{V/K}$ at 465 K, then remains almost flat to a value of -255 $\mu\text{V/K}$ at 708 K.

Fig. 3(c) represents the temperature dependent power factors (σS^2) of $\text{AgBi}_{0.5}\text{Sb}_{0.5}\text{Se}_2$ and $\text{AgBi}_{0.5}\text{Sb}_{0.5}\text{Se}_{2-x}\text{Cl}_x$ ($x=2-4$ mol%). A maximum σS^2 of ~ 1.8 $\mu\text{W/cmK}^2$ have been achieved at ~ 708 K for pristine sample. All the chlorine doped samples show higher σS^2 at elevated temperature than that of for pristine sample. Typically, $\text{AgBi}_{0.5}\text{Sb}_{0.5}\text{Se}_{1.98}\text{Cl}_{0.02}$ sample shows a σS^2 value of ~ 2.64 $\mu\text{W/cmK}^2$ at 708 K. Superior electrical transports in the

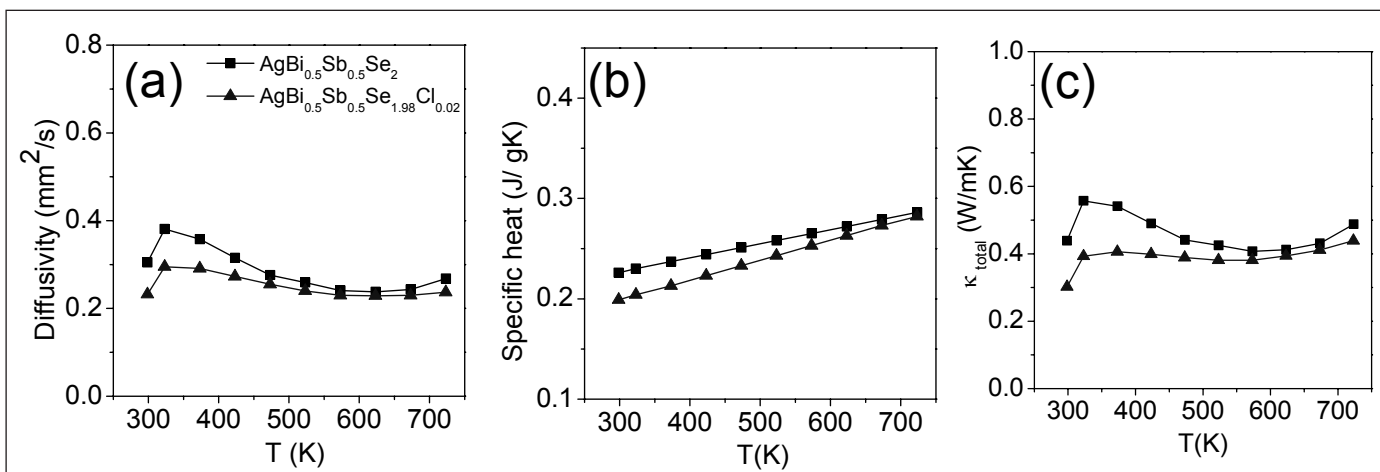


Fig. 4: Temperature dependent (a) thermal diffusivity (D), (b) specific heat (C_p), (c) total thermal conductivity (κ_{total}) of $\text{AgBi}_{0.5}\text{Sb}_{0.5}\text{Se}_2$ and $\text{AgBi}_{0.5}\text{Sb}_{0.5}\text{Se}_{1.98}\text{Cl}_{0.02}$ samples.

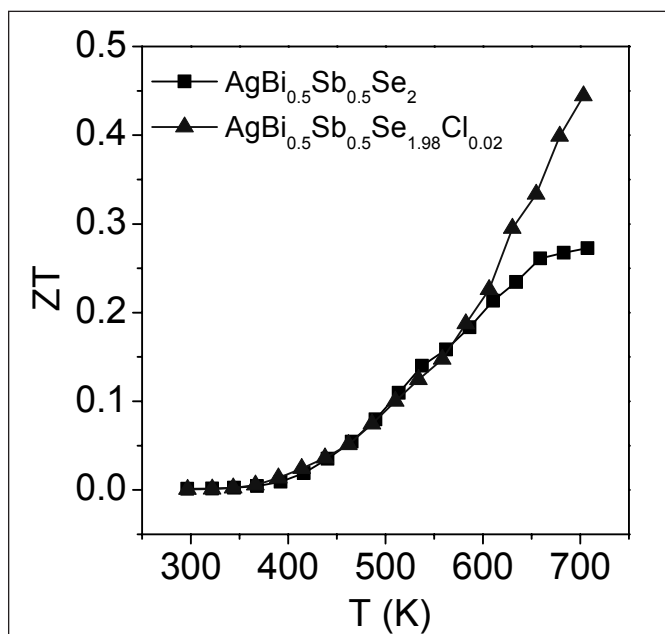


Fig. 5: Temperature dependent thermoelectric Fig. of merit (ZT) of $\text{AgBi}_{0.5}\text{Sb}_{0.5}\text{Se}_2$ and $\text{AgBi}_{0.5}\text{Sb}_{0.5}\text{Se}_{1.98}\text{Cl}_{0.02}$ samples.

chlorine doped samples result in the improvement in σ^2 value.

The total thermal conductivity, κ_{total} , of $\text{AgBi}_{0.5}\text{Sb}_{0.5}\text{Se}_2$ and $\text{AgBi}_{0.5}\text{Sb}_{0.5}\text{Se}_{1.98}\text{Cl}_{0.02}$ samples were estimated over 300-723 K temperature range using the formula, $\kappa_{total} = DC_p\rho$, where D is the thermal diffusivity, C_p is specific heat and ρ is density of the sample (Fig. 4). Temperature dependent D is measured using laser flash diffusivity technique over 300-723 K range (Fig. 4a). Temperature dependent C_p was derived during the diffusivity measurement in a LFA 457 instrument (Fig. 4b). At room temperature, a κ_{total} value of $\sim 0.44 \text{ Wm}^{-1}\text{K}^{-1}$ was measured for $\text{AgBi}_{0.5}\text{Sb}_{0.5}\text{Se}_2$,

which remains almost same value all over the measured temperature range and shows a value of $0.5 \text{ Wm}^{-1}\text{K}^{-1}$ at 723 K. We have observed similar trend in the temperature dependent κ_{total} for 2 mol% doped sample as well (Fig. 4c). However, κ_{total} value is lower than pristine sample. Creation of point defects due to chlorine doping result scattering of the heat carrying phonons which decreases the thermal conductivity to a further lower value.

Temperature dependent thermoelectric Fig. of merit, ZT , was estimated from the measured electrical and thermal transport data in temperature range of 300-708 K for pristine and $\text{AgBi}_{0.5}\text{Sb}_{0.5}\text{Se}_{1.98}\text{Cl}_{0.02}$ (Fig. 5). A peak ZT value ~ 0.27 at 708 K was achieved for pristine $\text{AgBi}_{0.5}\text{Sb}_{0.5}\text{Se}_2$. The ZT value for $\text{AgBi}_{0.5}\text{Sb}_{0.5}\text{Se}_{1.98}\text{Cl}_{0.02}$ sample follows almost same value as for pristine sample at low temperatures. However at high temperature the ZT value increases significantly. A peak ZT of ~ 0.45 at 708 K was achieved for $\text{AgBi}_{0.5}\text{Sb}_{0.5}\text{Se}_{1.98}\text{Cl}_{0.02}$.

Conclusions.

In summary, high quality crystalline ingots of n -type $\text{AgBi}_{0.5}\text{Sb}_{0.5}\text{Se}_2$ and $\text{AgBi}_{0.5}\text{Sb}_{0.5}\text{Se}_{2-x}\text{Cl}_x$ ($x=2-4$ mol%) were grown by simple melting of elemental metal and chalcogen followed by cooling to room temperature. Carrier concentrations in n -type $\text{AgBi}_{0.5}\text{Sb}_{0.5}\text{Se}_2$ can be tune by small amount aliovalent chlorine doing in the Se site to enhance the electrical conductivity compared to pristine sample. Chlorine aliovalently dope on the Se²⁻ sublattice and, from the simple valence electron counting, donates one n -type carrier in $\text{AgBi}_{0.5}\text{Sb}_{0.5}\text{Se}_2$, which gives rise to improved electronic transport property. High degree of anharmonicity in Bi-Se, Sb-Se bond and effective phonon scattering by the disordered Ag/Bi lattice give rise to ultra-low thermal conductivity in the cubic $\text{AgBi}_{0.5}\text{Sb}_{0.5}\text{Se}_2$. A peak




ZT of ~0.45 at 708 K was achieved for $\text{AgBi}_{0.5}\text{Sb}_{0.5}\text{Se}_{1.98}\text{Cl}_{0.02}$. Further improvement of the performance of $\text{AgBi}_{0.5}\text{Sb}_{0.5}\text{Se}_2$ could be achieved by either concurrent enhancement of Seebeck coefficient and electrical conductivity.

Acknowledgements

This work was supported by DAE-BRNS YSRA project (37(3)/01/2015/BRNS) and DST Ramanujan Fellowship.

References.

1. D. M. Rowe, *CRC handbook of thermoelectrics*; CRC Press: Boca Raton, FL, 1995.
2. L.D. Zhao, V. P. Dravid and M. G. Kanatzidis, *Energy Environ. Sci.*, 2014, **7**, 251-268.
3. J. Sootsman, D. Y. Chung and M. G. Kanatzidis, *Angew. Chem. Int. Ed.*, 2009, **48**, 8616-8639.
4. G. J. Snyder and E. S. Toberer, *Nat. Mater.* 2008, **7**, 105-114.
5. M. Zebarjadi, K. Esfarjani, M. S. Dresselhaus, Z. F. Ren and G. Chen, *Energy Environ. Sci.*, 2012, **5**, 5147-5162.
6. Y. Zhang and G. D. Stucky, *Chem. Mater.*, 2014, **26**, 837-848.
7. K. Biswas, J. He, I. D. Blum, C. I. Wu, T. P. Hogan, D. N. Seidman, V. P. Dravid and M. G. Kanatzidis, *Nature*, 2012, **489**, 414-418.
8. L. D. Zhao, S. H. Lo, Y. Zhang, H. Sun, G. Tan, C. Uher, C. Wolverton, V. P. Dravid, and M. G. Kanatzidis, *Nature*, 2014, **508**, 373-377.
9. J. P. Heremans, V. Jovovic, E. S. Toberer, A. Saramat, K. Kurosaki, A. Charoenphakdee, S. Yamanaka and G. J. Snyder, *Science*, 2008, **321**, 554-557.
10. A. Banik and K. Biswas, *J. Mater. Chem. A*, 2014, **2**, 9620-9625.
11. Y. Pei, X. Shi, A. La Londe, H. Wang, L. Chen and G. J. Snyder, *Nature* 2011, **473**, 66-69.
12. T. C. Harman, P. J. Taylor, M. P. Walsh and B. E. LaForge, *Science*, 2002, **297**, 2229-2232.
13. J. P. Heremans, C. M. Thrush and D. T. Morelli, *Phys. Rev. B*, 2004, **70**, 115334.
14. K. Biswas, J. He, Q. Zhang, G. Wang, C. Uher, V. P. Dravid and M. G. Kanatzidis, *Nat. Chem.*, 2011, **3**, 160-166.
15. K. F. Hsu, S. Loo, F. Guo, W. Chen, J. S. Dyck, C. Uher, T. Hogan, E. K. Polychroniadis and M. G. Kanatzidis, *Science*, 2004, **303**, 818-821.
16. B. Poudel, Q. Hao, Y. Ma, Y. Lan, A. Minnich, B. Yu, X. Yan, D. Wang, A. Muto, D. Vashaee, X. Chen, J. Liu, M. S. Dresselhaus, G. Chen and Z. Ren, *Science*, 2008, **320**, 634-638.
17. H. L. Liu, X. Yuan, P. Lu, X. Shi, F. F. Xu, Y. He, Y. S. Tang, S. Q. Bai, W. Q. Zhang, L. D. Chen, Y. Lin, L. Shi, H. Lin, X. Y. Gao, X. M. Zhang, H. Chi and C. Uher, *Adv. Mater.* 2013, **25**, 6607-6612.
18. J. Androulakis, I. Todorov, J. He, D. Y. Chung, V. Dravid, M. Kanatzidis, *J. Am. Chem. Soc.*, 2011, **133**, 10920-10927.
19. H. Wang, Y. Pei, A. D. Lalonde, G. J. Snyder, *Adv. Mater.*, 2011, **23**, 1366-1370.
20. A. Banik, U. S. Shenoy, S. Anand, U. V. Waghmare and K. Biswas, *Chem. Mater.*, 2015, **27**, 581-587.
21. G. Tan, F. Shi, S. Hao, H. Chi, L. -D. Zhao, C. Uher, C. Wolverton, V. P. Dravid and M. G. Kanatzidis *J. Am. Chem. Soc.*, 2015, **137**, 5100-5109.
22. G. Tan, F. Shi, J. W. Doak, H. Sun, L. -D. Zhao, P. Wang, C. Uher, C. Wolverton, V. P. Dravid and M. G. Kanatzidis, *Energy Environ. Sci.*, 2015, **8**, 267-277.
23. F. D. Rosi, E. F. Hockings and N. E. Lindenblad, *RCA Rev.*, 1961, **22**, 82-121.
24. B. Du, H. Li, J. Xu, X. Tang, and C. Uher, *Chem. Mater.*, 2010, **22**, 5521-5527.
25. S. N. Guin, A. Chatterjee, D. S. Negi, R. Datta and K. Biswas, *Energy Environ. Sci.*, 2013, **6**, 2603-2608.
26. S. N. Guin, D. S. Negi, R. Datta and K. Biswas, *J. Mater. Chem. A*, 2014, **2**, 4324-4331.
27. S. Cai, Z. Liu, J. Sun, R. Li, W. Fei and J. Sui, *Dalton Trans.*, 2015, **44**, 1046-1051.
28. D. Li, X. Y. Qin, T. H. Zou, J. Zhang, B. J. Ren, C. J. Song, Y. F. Liu, L. Wang, H. X. Xin and J. C. Li, *J. Alloys Compd.*, 2015, **635**, 87-91.
29. S. N. Guin, and K. Biswas, *J. Mater. Chem. C*, 2015, DOI: 10.1039/c5tc01429h
30. S. N. Guin, V. Srihari and K. Biswas, *J. Mater. Chem. A*, 2015, **3**, 648-655.
31. L. Pan, D. Berardan and N. Dragoe, *J. Am. Chem. Soc.*, 2013, **135**, 4914-4917.
32. C. Xiao, X. Qin, J. Zhang, R. An, J. Xu, K. Li, B. Cao, J. Yang, B. Ye and Y. Xie, *J. Am. Chem. Soc.*, 2012, **134**, 18460-18466.
33. H. Liu, X. Shi, F. Xu, L. Zhang, W. Zhang, L. Chen, Q. Li, C. Uher, T. Day and G. J. Snyder, *Nat. Mater.*, 2012, **11**, 422-425.
34. X. Shi, J. Yang, J. R. Salvador, M. Chi, J. Y. Cho, H. Wang, S. Bai, J. Yang, W. Zhang, and L. Chen, *J. Am. Chem. Soc.*, 2011, **133**, 7837-7846.
35. G. Joshi, R. He, M. Engber, G. Samsonidze, T. Pantha, E. Dahal, K. Dahal, J. Yang, Y. Lan, B. Kozinsky and Z. Ren, *Energy Environ. Sci.*, 2014, **7**, 4070-4076.
36. R. Venkatasubramanian, E. Siivola, T. Colpitts and B. O'Quinn, *Nature* 2001, **413**, 597-602.
37. D. T. Morelli, V. Jovovic and J. P. Heremans, *Phys. Rev. Lett.*, 2008, **101**, 035901.
38. M. D. Nielsen, V. Ozolins and J. P. Heremans, *Energy Environ. Sci.*, 2013, **6**, 570-578.
39. S. H. Yang, T. J. Zhu, T. Sun, J. He, S. N. Zhang and X. B. Zhao, *Nanotechnology*, 2008, **19**, 245707.

	<p>Kanishka Biswas obtained his MS and Ph.D degree from Solid State and Structural Chemistry Unit, Indian Institute of Science (2009) and did postdoctoral research from Department of Chemistry, Northwestern University (2009-2012). He is now an Assistant Professor in New Chemistry Unit, Jawaharlal Nehru Centre for Advanced Scientific Research (JNCASR), Bangalore. He is pursuing research in solid state chemistry of metal chalcogenides, thermoelectrics, topological insulators and intergrowth 2D nanosheets. He has published 63 research papers and 3 book chapters. He is also co-author of a book entitled "Essentials of inorganic materials synthesis" published by John Wiley and Sons, Inc. He is recipient of Ramanujan Fellowship from Department of Science and Technology, India. He is an Young Affiliate of The World Academy of Sciences (TWAS) and an Associate of Indian Academy of Science. He is also recipient of Young Scientist Research Award from Department of Atomic Energy, India and Young Scientist Platinum Jubilee award from The National Academy of Sciences (NASI), India.</p>
	<p>Satya Narayan Guin received his B.Sc. (2009) and M.Sc. (2011) degree in Chemistry from University of Kalyani, Kalyani, West Bengal, India. He is currently pursuing his Ph.D at New Chemistry Unit, Jawaharlal Nehru Centre for Advanced Scientific Research (JNCASR), Bangalore, India. His research topics focus on thermoelectric energy conversion based on metal chalcogenides. He is also a recipient of best poster award in "17th CRSI National Symposium in Chemistry" of CSIR, India.</p>
	<p>Sohag Kundu obtained a Project Oriented Chemical Education (POCE) diploma in 2014 from Jawaharlal Nehru Centre for Advanced Scientific Research (JNCASR), Bangalore, India. During his stay at JNCASR he worked as a visiting student under the supervision of Dr. Biswas. He received his B.Sc. (2015) in Chemistry from Presidency University, Kolkata. Currently he is pursuing a M.Sc. in Chemistry at Indian Institute of Technology, Bombay (IITB).</p>

Pt/Carbon Catalysts with Varying Porosity for Hydrogen Generation Reaction by HI Decomposition Reaction of S-I Thermochemical Cycle

Deepak Tyagi, Salil Varma*, Shyamala R. Bharadwaj

Chemistry Division, Bhabha Atomic Research Centre, Trombay, Mumbai 400085

Email: svarma@barc.gov.in

1. Introduction

Energy is key to social, economic, industrial and technological development of any society. There is continuous increase in energy demand worldwide due to increasing population and rising living standards. The need of the hour is research in the field of alternative energy sources that are CO₂ free.

CO₂ free energy systems are important basically due to the following two reasons: Firstly, the gap between energy demand and available energy sources will increase in future because the demand keeps on increasing due to increasing population, industrial growth etc but there is decline in production of conventional fossil fuels. Second reason for the increase in efforts and research for alternate energy sources is the concern for the environmental problems associated with the combustion of fossil fuels. Since fossil fuels are mainly hydrocarbons therefore their burning leads to CO₂ emission. Hence an increase in usage of these fossil fuels leads to increase in CO₂ emission. These increased CO₂ levels have huge impact on environment and climate since CO₂ is a greenhouse gas.

Some of the promising non-polluting renewable energy sources are nuclear, solar, wind, geothermal biomass etc. For some applications like transportation purpose where fossil fuels are extensively used, it is highly desirable to replace fossil fuels by a more environment friendly energy carrier. Hydrogen seems to be the most suitable option for this purpose due to its favorable properties, like no emission of pollutants or greenhouse gases, high energy density (140 MJ/kg) among all fuels etc.

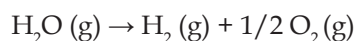
In spite of being the most abundant element on Earth, hydrogen is not available freely. It is present in the form of molecules in combination with other elements. It is present in form of water (with oxygen) or organic molecules (with carbon and other elements). Many methods are being used or can be used for hydrogen production from fossil fuels as well as from water. From fossil fuels, hydrogen can be produced by methods like steam reforming of natural gas or other light hydrocarbons, gasification of coal and other heavy hydrocarbons etc. From water it produced by methods like electrolysis, thermochemical cycles, photochemical methods etc.

Presently commercial hydrogen is mainly produced from fossil fuels based sources like coal, oil and natural gas (~96%) and only small fraction (~4%) comes from water electrolysis [1-4]. Main sources of hydrogen are shown below in Table 1.

Table 1: Present status of commercial hydrogen production from different sources.

Source	% Hydrogen production
Coal	18
Oil	30
Natural gas	48
Water Electrolysis	4

It is highly desirable to produce more hydrogen from water in an environment friendly manner. Hydrogen generation from water can be represented as:



But this reaction is highly endothermic ($\Delta H = 243 \text{ kJmol}^{-1}$ at 298 K) and very high temperatures (>2500 °C) are required for direct thermal decomposition or thermolysis of water. Energy required for decomposition can be provided by solar, nuclear, wind, electricity or combination of these. A large number of methods have been studied for producing hydrogen from water like Electrolysis (Alkaline electrolysis, PEM electrolysis and High temperature electrolysis), Photo-electrolysis (Photolysis), Photobiological (Biophotolysis), Photocatalysis, Thermal (Thermolysis), Thermochemical and Radiolysis.

Among these methods only electrolysis could be used at commercial level until now. But the cost of hydrogen production from electrolysis is high. Hence there is need as well as scope of improvement in efficiency and reduction of cost of hydrogen production. Thermochemical cycle is one such method which has potential for better efficiency. A thermochemical cycles can be defined as:

“A thermochemical cycle decomposes water into hydrogen and oxygen through a set of thermally driven reactions at much lower temperatures than that required for direct thermolysis of water.”

The heat required for a thermochemical cycle can be obtained either from a nuclear reactor [1-6], solar

concentrator [7,8] or by geothermal energy [9]. A thermochemical cycle can be schematically represented as shown in Fig 1.

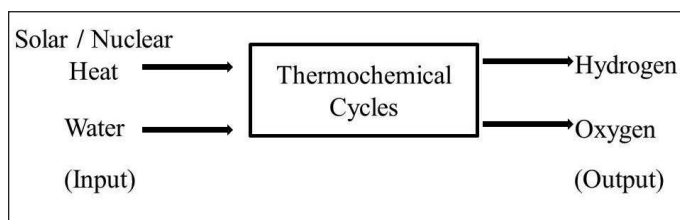
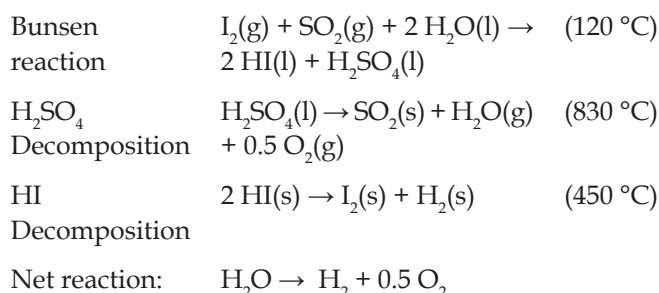
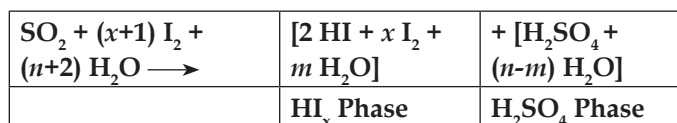


Fig. 1: A schematic of the concept of thermochemical cycles

More than 350 thermochemical cycles have been proposed and investigated worldwide. The main families are based on sulfur and halogens [10]. S-I cycle is one of the most studied cycle involving sulfur and iodine. This cycle was proposed and pursued by General Atomics in the USA, which made significant contributions to the process engineering and scaling up of the cycle [11,12]. It has potential for high efficiencies for hydrogen production [13]. The three reactions involved in S-I cycle are as follows:

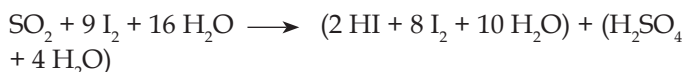


According to the reaction scheme of S-I thermochemical cycle, in Bunsen reaction one mole each of SO_2 and I_2 react in presence of two moles of water to produce two acids namely HI and H_2SO_4 . But from operation point of view, the conditions for Bunsen reaction are optimized by adding extra iodine and water. The excess iodine enhance the phase separation of the two acids and shifts Bunsen reaction equilibrium forward to produce more acids. Excess of water makes the reaction spontaneous and also causes the equilibrium to shift forward to produce more acids. This modified Bunsen reaction with extra iodine (x moles) and extra water (n Moles) can be written as follows.



The lower is the water excess n the lower is the operating cost and higher is the efficiency. While on the other hand lower iodine excess x is advantageous for the management of HI section [14]. Norman et al [11] have

reported the following optimum composition for the Bunsen reaction.

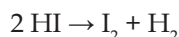


In case of S-I cycle, HI phase is containing excess iodine and water. Therefore production of hydrogen from this phase is highly energy consuming due the following two reasons:

- (i) The extraction of HI from the HI_x mixture is difficult because of the presence of an azeotrope in the mixture, so simple distillation is not possible.
- (ii) The extraction of HI from the HI_x mixture requires very large heat exchanges, due to the large heat capacity induced by the high water content of the mixture.

Hence various options have been tried to improve the overall efficiency of the process, like use of phosphoric acid for concentration of the HI solution [15], electro-electro dialysis concentration method [16,17], reactive distillation [18] and use of silica membrane reactor [19]. Reactive distillation has an advantage of combining reaction and separation in a single step leading to overall shift of equilibrium towards production of I_2 and H_2 [20].

HI Decomposition Reaction: As it can be seen from the above reaction scheme, HI decomposition reaction is the hydrogen producing step of the S-I cycle. In fact HI decomposition reaction is also integral part of some other iodine based cycles [21] for example Magnesium Iodine cycle [22] and Magnesium-Sulfur-Iodine cycle [23]. This reaction can be written as:



HI decomposition reaction has the following limitations:

- The decomposition reaction is incomplete (Equilibrium conversion is low).
- The decomposition reaction is slow.

Since hydrogen iodide (HI) decomposition is a thermodynamically limited reaction with low yields, therefore it requires considerable amount of energy for separation and recirculation of the unreacted species which in turn affects the overall efficiency of the thermochemical cycle. Therefore the efficiency of cycle depends on how efficiently HI is decomposed into hydrogen and iodine. It also requires a suitable catalyst for HI decomposition to achieve workable reaction rates by increasing the decomposition rate.

A wide range of catalysts have been used and studied for HI decomposition reaction. Several research groups

from around the globe are working in the field. Pt catalysts supported on different supports are the most studied systems like Pt/Carbon [24], Pt/Alumina [25], Pt/Ceria [26,27], Pt/Ceria-Zirconia [28] and bimetallic Pt-Ir catalysts [29] on carbon.

All the catalysts mentioned above have been employed for HI decomposition reaction in vapor phase at higher temperatures ($T > 450^\circ\text{C}$). Another approach which can be followed for HI decomposition is decomposition in liquid phase. In this case, dissolution of the I_2 formed at catalyst surface into the HI solution and continued intimate contact between HI and catalyst maintains high reactivity levels with generation of gaseous H_2 even in presence of I_2 . Very high conversion level as high as 50% is reported by O'Keefe et al [30]. In the present article, we present the work on development of platinum catalysts supported on various carbon supports for liquid phase HI decomposition reaction. Three different catalysts with 1% platinum loading were prepared with different carbon supports with different porosity.

2. Experimental

2.1 Synthesis of the Catalyst:

Different methods were used for preparation of catalysts. Nonporous carbon support was derived from graphitic carbon. Pt/Graphite catalyst supported on graphitic carbon was prepared by wet impregnation method which includes impregnation of the support (Colloidal Graphite) with a noble metal precursor followed by its reduction. While porous carbon support was prepared by hard templating method using porous silica templates. Microporous silica (fumed silica) resulted into microporous carbon and the catalyst prepared is named as Pt/FS-C, while mesoporous silica (MCM-41) resulted into mesoporous carbon and the catalyst is named as Pt/MCM-C. For preparation of catalysts, porous silica was impregnated with carbon source (sucrose) and platinum source (hexachloroplatinic acid), followed by carbonization by heating at 800°C for 3 h under N_2 atmosphere and reduction steps. Reduction in all three cases was carried out by heating the samples at 300°C for 3 h under flowing H_2 - N_2 mixture.

2.2 Characterization of the catalyst

The powder X-ray diffraction patterns were recorded on Philips analytical diffractometer (using Ni-filtered $\text{Cu K}\alpha$ radiation). The BET surface area of the catalysts was obtained from physical adsorption of N_2 at -196°C , on a Quantachrome Autosorb - 1 instrument. The prepared sample was characterized for carbon structure and hybridization, by spatially resolved Raman scattering

using micro/macro-Raman spectrometer (LABRAM-1, France) using a 488 nm line of an Ar^+ ion laser for excitation. The scattered Raman signal was collected using a single monochromator spectrometer equipped with a Peltier-cooled CCD detector in the backscattering geometry. The surface morphology was studied using JEOL JSM-6360. XPS studies for determining oxidation state of platinum and nature of carbon was studied using SPECS XPS system.

2.3 Activity and Stability of the Catalyst

All three catalysts were evaluated for their catalytic activity for liquid phase HI decomposition and noble metal leaching employing a reflux type batch reactor as shown in Fig. 2.

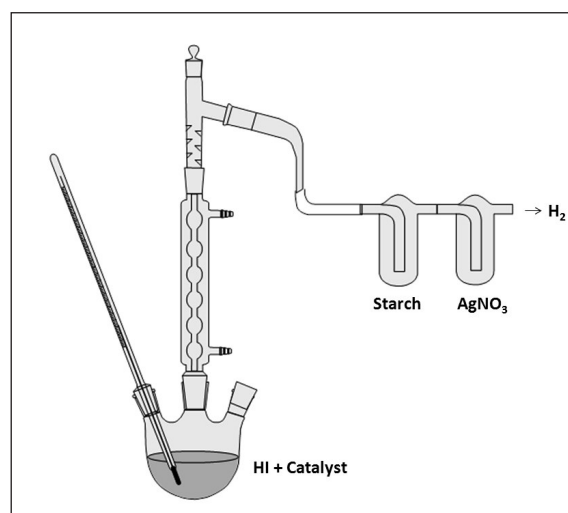


Fig.2: Block diagram of the experimental set up used for Hydriodic acid decomposition studies

For evaluation of catalytic activity and stability of the catalysts, 250 mg of catalyst was added to 50 ml of 27% hydriodic acid solution in 250 ml round bottom flask. The round bottom flask was fitted with a glass condenser at its top which is connected to two traps. Continuous evolution of bubbles is observed and it can be attributed to release of either hydrogen or the volatile species like hydriodic acid or iodine. The two traps having silver nitrate and starch solutions are employed to ensure that the gas coming out is neither HI nor I_2 . The bubbled gas does not result in appearance of blue color or yellow precipitate in starch and silver nitrate traps, respectively. Therefore, it can be inferred that refluxing of these compounds back into the reaction vessel is complete and the bubbles pertain only to the reaction product, i.e. hydrogen. After reaction, the vessel is allowed to cool and condenser washings are transferred to reaction bath and total volume was made up to 250 ml. After that % HI decomposition was measured

by means of titrating H⁺ and I⁻ ions using acid-base and iodometric titrations, respectively. The solution was filtered to separate the used catalyst and the eluent. The spent catalyst was characterized by XRD, Raman and SEM for their physical integrity and the eluent was analyzed using ICP-OES for the leached out platinum.

3 Results and Discussion

3.1 Characterization of the catalyst

3.1.1 XRD: The X-ray diffraction measurements were recorded in 10-60° 2θ range. Fig. 2 shows XRD patterns recorded for the three catalysts. XRD patterns of Pt/Gr shows sharp peak at 26.4° matching with JCPDS No. 26-1079, corresponding graphitic carbon, while the other two catalysts have a broad peak centring at 23 ° which corresponds to amorphous carbon. Pt/Gr does not show any distinct peak at 39.7°, pertaining to platinum metal (JCPDS No. 04-0802), while the other two have peaks pertaining to platinum metal. The reason for this may be that in case of hard templating method the catalysts see a high temperature during carbonization step which may cause the sintering of platinum particles which is otherwise in highly dispersed state in case of Pt/Gr catalyst.

3.1.2 Surface Morphology: Scanning electron microscopy was used to study the surface morphology of the platinum on carbon catalysts and the change in their morphology after using them for the HI decomposition reaction. SEM images of the three catalysts are shown in Fig. 4. Pt/Gr catalyst show a rough surface with few open pores and loose particles over it, similarly Pt/FS-C also presents rough surface morphology with some loose particles. There are no visible macro pore openings in both these case. Pt/MCM-C catalyst shows rough surface with lot of trough and crest like features but very few pore openings or particles.

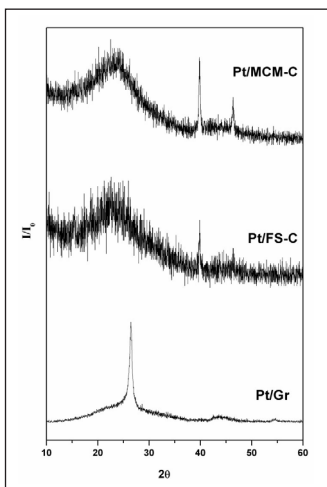


Fig.3: XRD patterns of the fresh catalysts

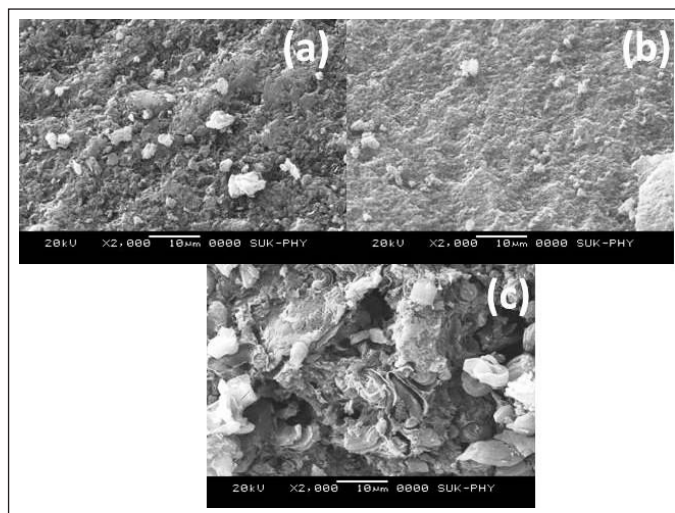


Fig.4: SEM images of the three catalyst samples (a) Pt/Gr (b) Pt/FS-C (c) Pt/MCM-C

3.1.3 Raman Spectroscopy: Raman spectroscopy is most powerful tool to characterize carbon systems. The Raman spectra of graphite carbon exhibit a single peak at ~1580 cm⁻¹ corresponding to the E_{2g} mode of vibration of sp² hybridized carbon (G band). Appearance of another peak at ~1350 cm⁻¹ is inevitably observed for sp³ hybridized carbon and some defects present in the carbon texture. This peak is known as D band [31].

The Raman spectra for the catalysts are shown in Fig. 5. It clearly shows that Pt/Graphite catalyst exhibits a sharp G band corresponding to the sp² hybridized carbon. Appearance of a broad D-band at 1350 cm⁻¹, suggests for the presence of sp³ hybridized carbon and some defects in the graphite structure either due to interaction with the noble metal or break in long range ordering. The other two catalysts shows less prominent G band along with broad D band, I_G/I_D ratio for these two catalysts was calculated and found to be equal to 1, which is expected for this type of porous carbon as reported in literature [32,33].

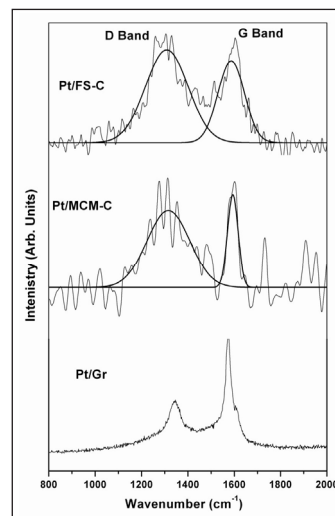


Fig.5: Raman spectra of the three catalyst samples

3.1.4 BET Surface area: BET Surface area of the Pt/Gr catalysts were evaluated using N₂ adsorption technique, Pt/Gr catalyst was found to exhibit very little porosity with major

contribution from intra-particle pores. Pt/FS-C show high surface area with microporous pore structure, while Pt/MCM-C show mesoporous pore structure identified by Type IV adsorption-desorption isotherms with a hysteresis loop as shown in Fig 6. The surface area and pore volume data for all the samples are given in Table 2.

Table 2: Surface area and pore volume data for different catalysts

Sr. No.	Catalyst	Surface Area (m ² g ⁻¹)	Pore Volume (cm ³ g ⁻¹)
1	Pt/Gr	80.0	0.390
2	Pt/FS-C	720.0	0.395
3	Pt/MCM-C	800.0	2.617

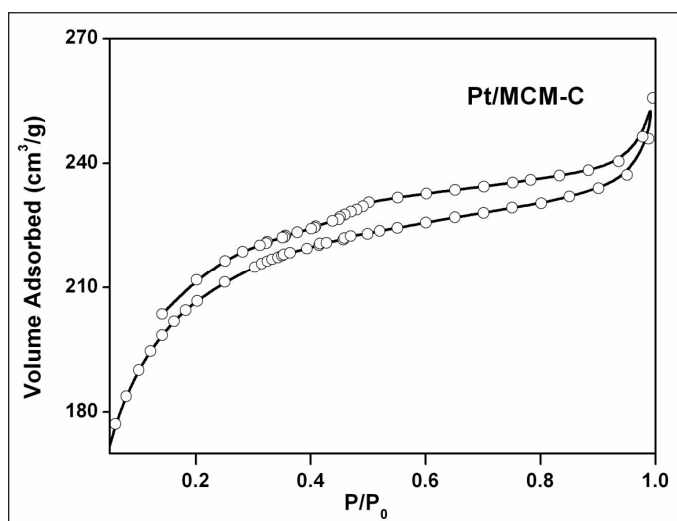


Fig. 6: Adsorption-Desorption isotherms for Pt/MCM-C catalyst

3.1.5 X-ray Photoelectron spectroscopy: Surface compositions of the catalysts were analyzed using X-ray photoelectron spectroscopy. The XPS measurements for Pt/C were carried out in constant analyzer energy mode using Al K_α radiation (1486.6 eV). The survey scan of the catalyst shows features corresponding to platinum, carbon and oxygen. Fig. 7 shows the intensity versus binding energy data obtained for the spectral region corresponding to Pt 4f of the three catalysts. It can be deconvoluted into only one doublet (4f_{5/2} and 4f_{7/2}) with respective binding energies of around 71.3 eV and 74.5 eV. These binding energy values correspond to the metallic state of platinum [34-35]. Thus XPS study reveals that platinum present here is in zero oxidation state which is essential for its catalytic activity.

Fig 8 shows the spectral region corresponding to C-1s; it can be fitted to three peaks with binding energies of 284.3, 285.4 and 287.9 eV. These peaks correspond

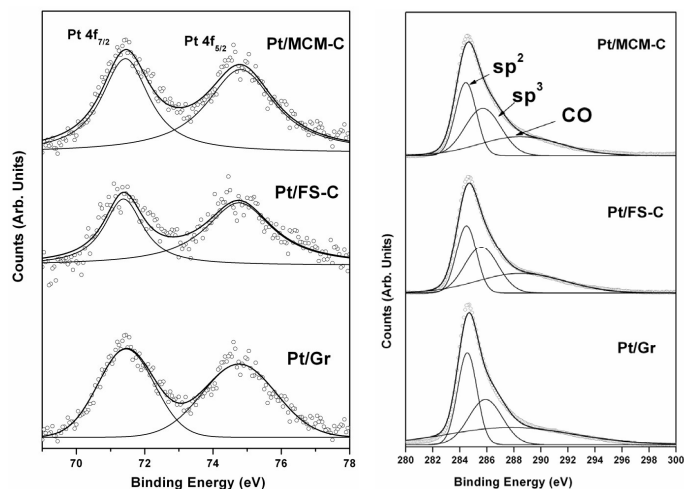


Fig. 7: XPS spectra of the catalysts in the spectral region corresponding to Pt-4f

Fig. 8: XPS spectra of the catalysts in the spectral region corresponding to C-1s

to sp², sp³ and CO (Carbon bonded to oxygen, C-O or C=O) types of carbon. Therefore the oxygen present is associated with carbon and not platinum. Also the presence of sp² hybridized carbon is in confirmation with the results of Raman. Carbon must be present in sp² hybridized state for the formation of this type of porous structure.

3.2 Catalytic Activity

The catalysts were evaluated for their activity for liquid phase HI decomposition reaction using a reflux type batch reactor. After the reaction, the extent of HI decomposition was measured by means of the change in H⁺, I⁻ and I₂ concentrations. The concentration of H⁺ and I⁻ was measured by potentiometric titrations using an Automatic Potentiometric Titrator, while that of iodine was measured by iodometric titration. For H⁺ ion, the solution was titrated against a standard NaOH solution using a glass electrode; the NaOH solution was standardized using KHP. On the other hand, I⁻ was titrated against a standard AgNO₃ solution using an Ag/AgCl electrode; the AgNO₃ solution was standardized using NaCl. The decrease in H⁺ and I⁻ ion concentration was the same and it was in accordance with the increase in iodine concentration in the solution. This change in concentration was used to calculate the percentage conversion.

Catalytic activity of the catalysts for liquid phase HI decomposition reaction was evaluated at 120 °C for 2 h reaction, and the % conversion values obtained for different platinum loadings are given in Table 3. From the Table, it can be seen that the % conversion increases significantly on using a catalyst (blank run gives only 2.9 % conversion).

Table 3: % Conversion in 2 hours at 120 °C for different catalysts

S. No.	Catalyst	% Conversion
1.	Blank	2.9 %
2.	Pt/Gr	17.5 %
3.	Pt/FS-C	17.0 %
4.	Pt/MCM-C	6.5 %

It is clear from the table that Pt/Gr catalyst shows highest activity which is comparable to that of mesoporous Pt/MCM-C catalyst. The catalytic activity of microporous Pt/FS-C is very low as compared to the other two. Hence, it appears that considering the large size of reactive moiety, HI, and the reaction product, I₂, the carbon support should either be mesoporous or planar.

3.3 Stability of the Catalyst

Stability of a catalyst is an important aspect especially in case of harsh reaction conditions. We have evaluated two aspects of the stability of the catalysts viz., (i) stability with respect to any change in structure and morphology and (ii) stability against noble metal leaching. For stability against structural and morphological changes, the used catalysts were analysed by XRD and SEM.

Fig.9 shows the XRD patterns of different used catalysts. The XRD pattern for the used Pt/Gr catalyst remain similar to original sample, with peak at ~26.4° 2θ value

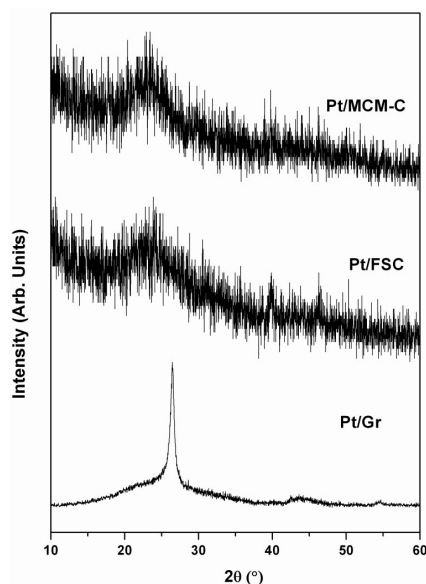


Fig. 9: XRD patterns of used catalysts

which corresponds to the graphitic carbon. There is no apparent difference in the XRD pattern of used catalyst as compared to the fresh one and also peak corresponding to platinum is not observed, which indicates that the Pt nanoparticles are not getting sintered. For Pt/MCM-C and Pt/FS-C, change is observed in the peak corresponding to platinum at ~39.6° value. This peak is drastically reduced for both the catalysts. Since platinum leaching is very low, therefore this reduction in peak intensity must be due to disintegration of larger particles into smaller entities and their redistribution over the carbon support.

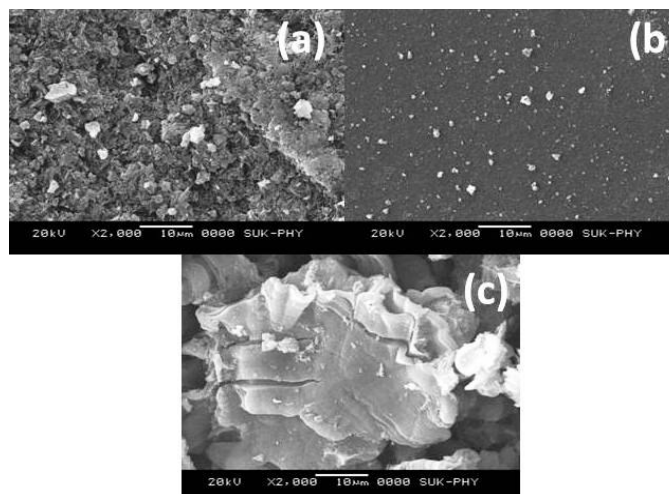


Fig. 10: SEM images of the used catalyst samples (a) Pt/Gr (b) Pt/FS-C (c) Pt/MCM-C

Fig. 10 shows SEM image of the used catalysts and it can be seen that there is no apparent difference in the morphology of the used catalysts as compared to fresh catalysts, even after using in harsh reaction environment.

The stability of the catalysts against noble metal leaching was studied by analyzing the eluent after a typical two hour reaction. The ICP AES analysis of the eluents showed presence of only few ppm of platinum (39, 39 and 65 ppm for Pt/Gr (b) Pt/FS-C (c) Pt/MCM-C). Therefore 0.23%, 0.39% and 0.68% of the original platinum loading is getting eluted out into the solution, indicating that the catalysts are having good stability against noble metal leaching in the harsh reaction environment.

4. Conclusion

Carbon supported platinum catalysts were prepared by different methods. These catalysts were found to be stable under liquid phase HI decomposition conditions. The efficiencies of these materials for HI decomposition reaction were found to be dependent on the structural nature of the porous carbon and their surface morphologies.

Catalyst prepared by using graphitic carbon support was giving maximum conversion and it was found to be stable also. The catalyst prepared using MCM-41 as template was found to be nearly equally effective for HI decomposition reaction and it was also found to be stable under the reported reaction conditions. While the catalyst prepared by using fumed silica as template was less active as compared to other two catalysts in spite of having high surface area.




5. Acknowledgements

The authors are thankful to Dr. P.S. Patil, Shivaji University, Kolhapur for providing SEM and Raman

facility and Dr. W. D. Einicke and Dr.R. Gläser, Institute of Chemical Technology, Universität Leipzig, Leipzig, Germany for N₂ adsorption measurements.

6. References

1. C.E. Bamberger and D.M. Richardson, *Cryogenics*, 1976, **16**,197.
2. J.E. Funk, *International Journal of Hydrogen Energy*,2001, **26**, 185.
3. S. Abandesand G. Flamant, *Solar Energy*, 2006, **80**, 1611.
4. I. Dincerand M.T. Balta, *International Journal of Energy Research*,2011, **35**,123.
5. R.R. Sadhankar, *International Journal of Energy Research*,2007, **31**, 1131.
6. M.A. Rosen, G.F. Natere, C.C. Chukwu, R. Sadhankarand S. Suppiah, *International Journal of Energy Research*,2012, **36**, 456.
7. Licht S. Thermochemical water Splitting. *Chemical Communications*, 2005,**37**, 4635.
8. A. Noglik, M. Roeb, C. SattlerandR. Pitz-Paal, *International Journal of Energy Research*,2011, **35**, 449.
9. M.T. Baltaand I. Dincer, *International Journal of Energy Research*, 2010, **34**, 757.
10. R.E.Chao, *I & EC Product Research Development*, 1974,**13**,94.
11. J.H. Norman, G.E. Besenbruch, L.C. Brown, D.R. O'Keefeand C.L. Allen, *Final Report for the Period February 1977 through December 31, 1981General Atomic Company Report GA-A16713*, 1981.
12. J.H. Norman, G.E. Besenbruch and D.R. O'Keefe. GRI-80/0105, 1981.
13. C. Forsberg, P.S. PickardandP. Peterson, *Nuclear News*, 2003, 30.
14. A. Giaconia, G. Caputo, A. Ceroli, M. Diamanti, V. Barbarossa, P. Tarquiniand S. Sau, *Int. J of Hydrogen Energy*, 2007, **32**, 531.
15. D. O'Keefe, C. Allen, G. Besenbruch, L. Brown, J. Normanand R. Sharp, *Int. J of Hydrogen Energy*, 1982, **7**, 381.
16. G. Arifal, G.J. Hwangand K. Onuki, *Journal of Membrane Science*, 2002, **210**, 39.
17. K. Onuki, G.J. Hwang, G. Arifaland S. Shimizu, *Journal of Membrane Science*, 2001, **192**,193.
18. B. Belaissaoui, R. Thery, X.M. Meyer, M. Meyer, V. Gerbaudand X. Joulia, *Chemical Engineering and Processing*, 2008, **47**, 396.
19. G.J. Hwangand K. Onuki, *Journal of Membrane Science*, 2001, **194**, 207.
20. M. Rothand K.F. Knoche, *Int. J of Hydrogen Energy*, 1989, **14**, 545.
21. C.E. Bamberger, *Cryogenics* ,1978, **18**, 170.
22. Y. Shindo, N. Ito, K. Haraya, T. HakutaandH. Yoshitome, *Int. J of Hydrogen Energy*,1983, **8**, 509.
23. T.Kumagai and S. Mizuta, *Industrial & Engineering Chemistry Process Design and Development*, 1985, **24**, **795**.
24. J.M. Kim, J.E. Park, Y.H. Kim, K.S. Kang, C.H. Kim, C.S. Parkand K.K. Bae, *Int J Hydrogen Energy*, 2008, **33**, 4974.
25. Z.C. Wang, L.J. Wang , P. Zhang, S.Z. Chen, J.M. Xuand J. Chen, *Chinese Chemical Letters*, 2009, **20**, 102.
26. Y.W. Zhang, J. Zhou, Z. Wang, J. Liuand K. Cen,*Int J Hydrogen Energy*, 2008,**33**,2211.
27. Y.W. Zhang, Z. Wang, J. Zhou, J. Liuand K. Cen,*Int J Hydrogen Energy*, 2008, **33**, 602.
28. Y. Chen, Z. Wang, Y. Zhang, J. Zhouand K. Cen,*Int J Hydrogen Energy*, 2010, **35**, 445.
29. Z. Wang, L. Wang, S. Chen, J. XuandJ. Chen, *Int J Hydrogen Energy*, 2010, **35**,8862.
30. D.R. O'keefe, J.H. Normanand D.G. Williamson,*Catalysis Reviews: Science and Engineering*, 1980, **22**,325.
31. Y. Wang, D.C. Alsmeyerand R.L. McCreery, *Chem. Mater.*,1990,**2**, 557.
32. A. Vinu, P. Srinivasu, M. Takahashi, T. Mori, V.V. Balasubramanianand K. Ariga, *Micro. Meso.Mat.*, 2007, **100**, 20.
33. M. Ignat, C.J. Van Oers, J. Vernimmen, M. Mertens, S.S. Potgieter-Vermaak, V. Meynen, E. Popoviciand P. Cool, *Carbon*, 2010, **48**, 1609.
34. A. K. Shukla, M. Neergat, P. Bera, V. JayaramandM.S. Hegde, *Journal ofElectroanalytical Chemistry*, 2001, **504** ,111.
35. J.J. Shao, Z.J. Li, C. Zhang, L.F. Zhang andQ.H. Yang, *Journal of Materials Chemistry A*, 2014, **2**,1940.

	<p>Mr. Deepak Tyagi joined BARC Training School in 2008 (52th Batch) after obtaining M.Sc. (Chemistry) from C.C.S. University, Meerut. After successfully completing one year orientation course in nuclear science and engineering, he joined Chemistry Division, BARC in 2009. Initially he was involved in research on development of catalysts for HI decomposition step of Sulphur - Iodine Thermochemical cycle for hydrogen production from water. His present research interests are development of catalysts for various DAE applications namely catalytic reduction of U^{6+} to U^{4+} and denitration reaction and development of materials for solid oxide fuel cells. He is one of the recipients of DAE Group achievement award 2010 and Group Achievement Award 2014 for his contributions in development of various catalysts for applications in DAE.</p>
	<p>Dr. Salil Varma joined BARC through Training School (40th Batch) in 1996. After working in WMPD for planning and commissioning of WIP Process Control Lab, he shifted to Chemistry group in 1999 and since has contributed to catalysis group for research on H_2 mitigation catalyst, mixed oxide catalysts for pollution abatement and for various TPD-MS/FTIR techniques for reaction mechanism studies. Passive Catalytic Recombiner Device based on hydrogen mitigation catalyst developed by him, was evaluated by NPCIL and approved for installation in Nuclear Power Plants in India. Technology for its commercial production has been transferred to ECIL, India. He was awarded PhD in 2004 by University of Mumbai and did his Post-doctoral research at University of Leipzig, as Alexander von Humboldt Fellow (2005-2006) on "Decomposition and selective catalytic reduction of nitrogen oxides on substituted rare earth orthovanadates". Currently he is involved in research on development of catalysts for HI decomposition step of Sulphur - Iodine Thermochemical cycle and ceramic materials for their application in SOFC. He has more than 35 papers in international journals of repute. He is recipient of DAE Group achievement award 2010, Special contribution award 2012 and Group Achievement Award 2014 for his contributions in development of various catalysts for applications in Department of Atomic Energy.</p>
	<p>Dr. Shyamala R. Bharadwaj is presently Head, Fuel Cell Materials & Catalysis Section, Chemistry Division, Bhabha Atomic Research Centre, Mumbai, India. She obtained her M.Sc. in Chemistry in 1981 and her Ph.D. in Physical Chemistry in 1991 from Mumbai University. Her main area of work during the past 38 years has been determination of thermodynamic properties of nuclear materials using various techniques such as vapour pressure measurements, thermogravimetry, isoperibol calorimeter etc. During 2000-2001, she worked as guest scientist at Juelich Research Centre, Juelich, Germany on Solid Oxide Fuel Cell (SOFC) materials. Her current interests are in the fields of Intermediate Temperature Solid Oxide Fuel Cells (ITSOFC) and Sulphur - Iodine thermochemical cycle for generation of hydrogen from water. She was awarded the NETZSCH -ITAS Award (2006) by the Indian Thermal Analysis Society in the year 2006 for her contributions in the field of thermal analysis. DAE Group Achievement Award for the year 2010 and 2014 was awarded to her Group for their work on catalysis. She is the Regional Editor for the Journal of Thermal Analysis and Calorimetry. She has more than 150 papers in refereed international journals and more than 150 papers in National and International Symposia. She has edited a book on "Thoria based fuels" along with her colleague Dr. D. Das and has contributed a chapter in that book (Published by Springer, 2013). She has also contributed chapters in other books and edited bulletins on Materials Chemistry and Thermal Analysis. She is Ph.D. guide of Mumbai University and HBNI and has guided about ten students for their Ph.D. Degree.</p>

Printed by:
Ebenezer Printing House
Unit No. 5 & 11, 2nd Floor, Hind Service Industries
Veer Savarkar Marg, Shivaji Park Sea-Face, Dadar (W), Mumbai - 400 028
Tel.: 2446 2632 / 2446 3872 Tel Fax: 2444 9765 E-mail: outworkeph@gmail.com

In this issue

	Feature Article	Page No.
1	Bioenergy: A Review of Microbial Fuel Cells and the Nisargruna Biogas Technology <i>Reemadevi Singh, S. B. Ghosh and S. P. Kale</i>	1
2	Critical Challenges for Li-air Technology <i>Jishnu Bhattacharya</i>	8
3	Plasmon Induced Enhancement of Charge Separation in Epitaxial Metal-Semiconductor Nanohybrid Material Anchored with an Organic Molecule <i>Jayanta Dana and Hirendra N. Ghosh</i>	14
4	Artificial Photosynthesis Using Graphene-Based Nanomaterials <i>Suneel Kumar, Vipul Sharma, Venkata Krishnan</i>	20
5	Effect of Aliovalent Chlorine Doping on the Thermoelectric Properties of n-type $\text{AgBi}_{0.5}\text{Sb}_{0.5}\text{Se}_2$ <i>Satya N. Guin, Sohang Kundu and Kanishka Biswas</i>	30
6	Pt/Carbon Catalysts with Varying Porosity for Hydrogen Generation Reaction by HI Decomposition Reaction of S-I Thermochemical Cycle <i>Deepak Tyagi, Salil Varma, Shyamala R. Bharadwaj</i>	37

Published by
Society for Materials Chemistry
C/o. Chemistry Division
Bhabha Atomic Research Centre, Trombay, Mumbai 40085
e-mail: socmatchem@gmail.com, Tel: 91-22-25592001